DEVELOPMENT OF ALUMINUM/STEEL HYBRID STRUCTURES BY SEMISOLID FORMING

A thesis submitted for the degree of

DOCTOR by Mondragon Unibertsitatea

ERIK ECHANIZ HERNANDEZ

Supervisors:

Dr. Iñaki Hurtado

Dr. Nuria Herrero-Dorca

Mechanical and Manufacturing Department

Mondragon Unibertsitatea

May 2016

PREFACE

Declaration

I hereby declare that this thesis is the result of my own work and that, to the best of my knowledge and belief, no part of this dissertation has previously been submitted for any similar qualification or degree.

Erik Echaniz

(May 2016)

ACKNOWLEDGMENTS

Quiero dar las gracias a todas las personas e instituciones que me han acompañado y que han hecho posible que esta tesis viera la luz.

A Elixabete, Xabier, Iñaki y Nuria por depositar su confianza en mí y acompañarme durante todo este camino.

A mi familia y amigos por escucharme y apoyarme.

Al resto de personas de marGUNE y MGEP por sus consejos y disposición ayudarme en todo momento.

A las instituciones que han apoyado económicamente esta tesis: CIC marGUNE, Mondragon Unibertsitatea, CIE Automotive y GOVA.

Eskerrik asko guztioi.

ABSTRACT

Weight reduction is the most cost-effective mean to improve fuel economy and greenhouse gas emissions from the transportation sector. Combining steel and aluminum in a hybrid structure will implement the integrated load-supporting of steel with the advantages of aluminum in weight reduction. However, due to the highly differing physical and mechanical properties, metallurgical bonds between these materials are difficult to achieve with traditional welding methods. These differences in properties lead to the formation of hard and brittle intermetallic compounds along the transition line which will significantly decrease the mechanical properties of the joining area.

Production of hybrid components by thixoformig of aluminum on steel is a promising method to manufacture near net shape components with good mechanical properties in a single process step. This process allows joining dissimilar materials in semisolid state at lower temperatures than traditional welding methods, causing a decrease in thickness of the intermetallic layer. In this work, the mount of the front cradle of the car was manufactured in different aluminum alloys and joined to a S355JH2 quality steel tube by thixo transverse forging method.

The first part of the dissertation focuses on design and simulation of an automotive hybrid structure and the development of a semi-industrial thixoforming cell. Influence of the main processing parameters such as, solid fraction, mold temperature, compaction time and punch speed are studied. In order to determine the optimum process parameters a thorough mechanical and metallographic analysis of the manufactured components is carried out. The second part of the dissertation deals with fundamental research on the formation and evolution of intermetallic phases when joining of AlSiMg alloys to raw and coated steel, at different joining temperatures in the semisolid range. The results reveal that quality hybrid components can be achieved with this forming method.

RESUMEN

La reducción de peso es lo más rentable para mejorar la economía de combustible y reducir las emisiones de gases de efecto invernadero procedentes del sector transporte. La unión de ambos materiales permite la creación de nuevas estructuras híbridas que combinan la dureza y resistencia al desgaste de los aceros con la baja densidad de las aleaciones de aluminio. Sin embargo, debido a las propiedades físicas y mecánicas dispares de estos metales, es difícil obtener uniones metalúrgicas con métodos de soldadura tradicionales. Estas diferencias en las propiedades conducen a la formación de compuestos intermetálicos en la intercara que por su naturaleza dura y frágil resultan perjudiciales para su aplicación final.

La producción de estructuras híbridas mediante tixoconformado de aluminio sobre acero en un único paso es un proceso prometedor para la fabricación de componentes funcionales con buenas propiedades mecánicas. Este proceso permite unir materiales disimilares en estado semisólido, de forma que la unión de los materiales ocurre a una temperatura inferior que en los métodos tradicionales de soldadura, provocando una disminución del espesor de la capa intermetálica. En el presente trabajo, se ha fabricado un componente real de automoción llamado brazo de la cuna delantera en diferentes aleaciones de aluminio y unido a un tubo de acero de calidad S355JH2.

La primera parte de la tesis se centra en el diseño y simulación de una estructura híbrida de automoción y el desarrollo de una célula de tixoconformado semi-industrial. También, se estudia la influencia de los principales parámetros de proceso tales como, fracción sólida, la temperatura del molde, el tiempo de compactación y la velocidad de conformado. Con el fin de determinar los parámetros de proceso óptimos se ha llevado a cabo un exhaustivo análisis mecánico y metalográfico de los componentes fabricados. La segunda parte de la tesis se ocupa de la investigación fundamental de la formación y evolución de las fases intermetálicas que surgen cuando se unen aleaciones AlSiMg con acero en bruto y revestido, a diferentes temperaturas de unión del rango semisólido. Los resultados revelan que es posible obtener componentes híbridos de calidad mediante este proceso de conformado.

LABURPENA

Ibilgailuen pisua murrizteak eragin nabarmena du erregai-ekonomian eta garraioaren sektoreko berotegi-efektuko emisioak gutxitzean. Bi material horien elkarteak egitura hibrido berriak sortzeko aukera ematen du, zeinak konbinatzen baitituzte altzairuen gogortasuna eta higadurarekiko erresistentzia aluminio-aleazioen dentsitate txikiarekin. Nolanahi ere, konplexua da material desberdinen arteko elkarteak sortzea, ezaugarri desberdinak baitituzte. Ohiko aluminio-altzairu soldaduren kasuan, aluminiotan aberatsak diren metal arteko konposatuak sortzen dira; baina gogorrak eta hauskorrak direnez, kaltegarriak dira azken aplikaziorako. Bestalde, halako elkarte-teknologiek muga handiak dituzte egitura mistoaren geometriari dagokionez.

Altzairuaren gaineko aluminiozko egitura hibridoak tixokonformazio bidez urrats bakarrean ekoiztea etorkizun handiko prozesua da propietate mekaniko onak dituzten osagarriak lortzeko. Prozesu honen bidez, material desberdinak elkartu daitezke bestelako soldadura-prozezuetan baino tenperatura baxuagoan eta, horrela, sortutako metalen arteko geruzaren lodiera murrizten da. Lan honetan, aluminiozko aleazio ezberdinen eta S355JH2 kalitatezko altzairuen arteko forja inguruko erdisolidoaren lotura-prozesuaren teknologia garatu da, automobil-industriarako prestazio handiko segurtasun-osagaien ekoizpenean erabili ahal izateko helburuarekin.

Tesiaren lehen atalaren ardatza izan da ibilgailuetarako egitura hibrido bat diseinatzea eta simulatzea, eta tixokonformazio erdiindustrialeko zelda bat garatzea. Halaber, prozesuko parametro nagusien eragina aztertu da; besteak beste, hauena: frakzio solidoa, moldearen tenperatura, trinkotze-denbora eta konformazio-abiadura. Prozesuko parametro optimoak zein diren zehazteko, ekoitzitako osagaien analisi mekaniko eta metalografiko sakona egin da. Tesiaren bigarren atalean, bestalde, AlSiMg aleazioak altzairu gordinarekin eta estalduradunarekin elkartzean sortzen diren fase intermetalikoen formazioaren eta eboluzioaren oinarrizko ikerketa egin da. Emaitzek agerian utzi dute posible dela kalitateko osagai hibridoak lortzea konformazio-prozesu honen bitartez.

CONTENTS

LIST OF TABLES

LIST OF FIGURES

CHAPTER 1

INTRODUCTION

In this chapter, an overall view of the current thesis is presented. First of all, the framework of the thesis and the motivation to carry out this research are described. Then, the research objectives of the thesis are presented followed by a brief presentation of the main stages of the thesis to accomplish its objectives.

1.1 Motivation and background

This dissertation concerns the development of hybrid structures by semisolid forming of aluminum on steel for automotive applications. This work lead to a better understanding of the mechanical properties (strength, fatigue...) and interface formed between aluminum-steel dissimilar joints in order to obtain high added value components. The first part of the dissertation is focused on the development of hybrid components including numerical modeling of semisolid process as well as the optimization of the main parameters of the thixoforming process. The second part deals with the set-up and the mechanical and microstructural characterization of the hybrid components.

In the last decades, transport has been the sector most resilient to efforts to reduce CO_2 emissions due to its strong dependence on fossil energy sources and its steady growth, offsetting the considerable vehicle efficiency gains made [Davis 2010]. Energy efficiency and effective transport demand management to substantially reduce emissions. Currently, the combustion of fossil fuels in the U.S. transportation sector accounts for one-third of all CO_2 emissions, three-quarters of those emissions are due to road transportation [U.S. Department of Energy 2015]. These economic and environmental concerns are constantly driving the automotive industry to lighten the structures and equipment without compromising the technical characteristics and safety operation of the vehicle.

Weight reduction is the most cost-effective mean to improve fuel economy and greenhouse gas (GHG) emissions from the transportation sector [Jeswiet 2008]. By reducing mass of the vehicle's main body and chassis structure, secondary weight and cost savings can be realized by downsizing subsystems through the mass decompounding effect. For instance, a lightweight vehicle body will result in smaller brakes, with reduced or even eliminated power braking booster componentry. Accelerating lighter vehicles cuts drive system output, reducing driveline-support structural needs. Smaller, reduced power drive components require smaller cooling systems with less coolant mass and smaller air inlets, reducing aerodynamic drag losses and thus reducing needed drive system energy and power, making those components even smaller and lighter [Malen 2007]. Figure 1 show the relationship between the curb weight and the fuel consumption of a vehicle:

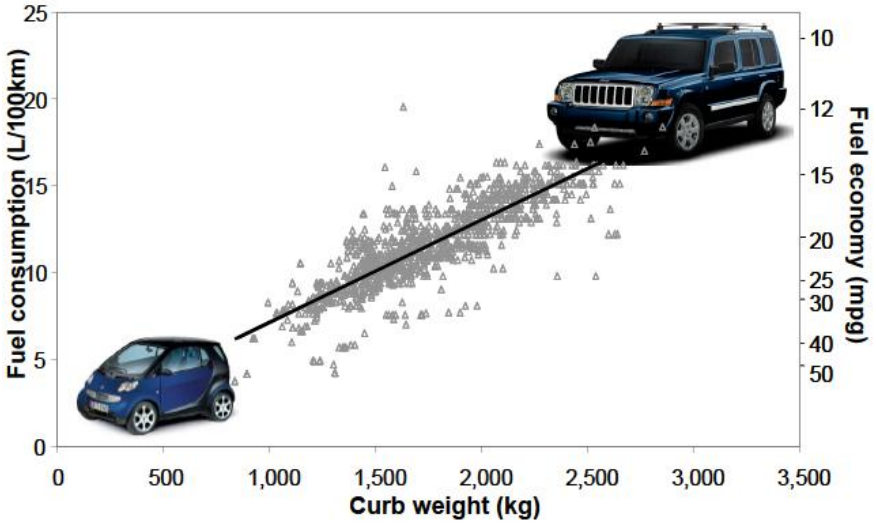

Figure 1 .Curb weight and fuel consumption of U.S. year 2005 model vehicles [Bandivadekar 2008].

Several studies have examined the distribution of mass within typical vehicles. Stodolsky *et al.* [Stodolsky 1995] showed a mass distribution in a passenger car (according to component groups) with the body, about 43% of the total vehicle mass, is the single heaviest group; followed by the powertrain and chassis, in almost equal proportions, at 27% and 26%, respectively. According to these studies, car body offers a high potential for lightweight construction, since it is nearly 40% of the car's total weight.

On the other hand it is estimated that every kilogram of weight reduced in a vehicle means about 20 kg of carbon dioxide reduction. In addition, fuel usage improves by 6-7% per 10% vehicle weight reduction [Quadrelli 2007].

Simple vehicle design changes can significantly reduce mass. These changes lie in removing unnecessary systems, such as heated power seating, to more aggressive part integration and optimization techniques. However, this is can be difficult, as market-driven demands for larger vehicles, has resulted in increases in the average size of vehicles year-after-year [El-Sayed 2011]. Other methods to reduce vehicle weight evolve around material substitution, where one material is replaced by another. Lightweight materials, such as high strength steel, aluminum, or glass fiber reinforced polymer composites are especially important for improving the efficiency and range of hybrid electric and electric vehicles because they offset the weight of power systems such as batteries and electric motors. However, due to the combined weight and mechanical properties demanded by the automotive industry material substitution is not always an easy task. To overcome this limitation, different strategies can be followed.

The first type implies the optimization in the design or/and in the production process. For example, the reduction of spot welds should reduce the body weight when replaced by new joining techniques, such as laser welding or friction stir welding [Joo 2004, Taban 2010]. The second method is to replace materials of high specific weight with lower density materials without compromising other attributes such as strength, stiffness, creep resistance or wear resistance. The last one implies the combination of various materials and functional characteristics based on the use of bonding technologies and production processes.

For the last decades, steel and aluminum have been the most important construction materials for the mass production of automotive structures. The combination of these metals leads to significant technological and economic advances by maximizing the advantages inherent in each metal [Springer 2011, Qiu 2009]. Weldments between steel and aluminum allow the creation of new kind of structures which combine the high-temperature resistance, hardness and wear resistance of steels with the low density and high heat conductivity of aluminum alloys [Ryabov 1998, Lin 2009]. However, it is well known that metallurgical bonds between dissimilar materials run into great difficulties because of large differences in physical properties such as, melting point, the coefficient of linear expansion, density and the presence of superficial oxide film in aluminum Al_2O_3 [Rathod 2004]. Furthermore, the chemical interaction of these two metal lead to irreversible formation brittle Fe_xAl_y intermetallic phases which cause the property degradation of the joint [Wang 2012, Schäfer 2011, Chun 2008, Choi 2010].

Currently, the vast majority of the hybrid joining techniques such as, MIG [Thomy 2012], TIG [Lin 2009], resistance welding [Qiu 2009], friction stir welding [Chen 2008], are used to join thin steel-base sheet with aluminum-base sheet with thicknesses ranged between 0.5 and 3mm.

Hence, the need of advanced welding methods to produce functional massive parts for automotive industry which combine multi-material design methodologies and low cost fabrication process. Semisolid forming or thixoforming of aluminum on steel is a promising method to manufacture near net shape components with good mechanical properties in a single process step.

Thixoforming is an alternative fabrication route for forged parts in the automotive sector that combines the advantages of forging and casting processes. It is related to a decrease in manufacturing costs by means of a reduction of the forming steps and forming loads as well as a reduction of material quantity and final machining operations [Hirt 2009]. Conventionally forged components can be geometrically complicated, but the relation between flow length and wall thickness is much smaller than in semisolid forming. Compared to casting, semisolid forming provides reduced part defects and higher mechanical properties [Lozares 2014, Azpilgain 2008]. Thixo transverse forging process is one of forming operations in thixoforming family. In addition, the lowered process temperature of the semisolid metal significantly decreases the final thickness of the interfacial layer.

Nevertheless, this joining technology is done at relatively recent years [Springer 2011, Liu 2006]. Therefore, it is necessary to carry out fundamental investigations for the purpose of obtaining additional information about the general characteristics of the bonding between the base metal and the insert. In the present work a range of processing conditions for improving the bond strength between S355J2H steel inserts and A356-A357 alloys were investigated. In order to improve the interfacial joining properties, different surface treatments, such as zinc plating or aluminization will be applied in the steel tube prior to forming in order to study the effect of each treatment in the formation of intermetallic phases in the reaction zone. On the other hand, the mechanical properties of the component were analyzed to demonstrate the feasibility of such structures comparing with other conventional solutions such as the steel-aluminum welded joints.

1.2 Objectives

The main goal of this dissertation is the development of hybrid structures by semisolid forming of aluminum on steel. This study is specially focused on the left front cradle mount middle (LCM) of the car, to demonstrate the feasibility of such structures with other conventional

solutions such as the steel-aluminum welded joints. In order to achieve this goal the following operational objectives were defined:

- Design, mechanical modeling of the hybrid structure and thermo-mechanical simulations of the thixoforming process.
- Design and implementation of the experimental set up to produce hybrid parts by thixoforging.
- Determine the influence of the forming parameters on mechanical and microstructural properties of the hybrid structure.
- Mechanical and microstructural characterization of the hybrid component and the joint interface.

1.3 Outline of the present dissertation

This dissertation covers both theoretical and experimental work. The research exposed in this dissertation is divided into seven chapters. The first one is this introduction.

Chapter 2 describes the state of the art of existing hybrid joining processes. The review is divided into three main subsections: Technologies to join dissimilar materials, thixoforming process and formation of Al-Fe intermetallic compounds to settle the theoretical bases of this work.

In chapter 3, it is fully described the design of an automotive front cradle mount middle and the procedures followed for the obtention of prototypes and its characterization.

In chapter 4 the structural modeling of the part and the thermomechanical simulation of the thixoforming process is carried out. Some components will be produced in order to define the optimized working parameters and to find out possible shortcomings that must be taken under control to obtain successful components. The microstructure and mechanical properties of the components are analyzed in chapter 5.

Chapter 6, attempts to elicit the influence of the forming parameters and the microstructural parameters which govern the formation and growth of the intermetallic reaction layer during interdiffusion between aluminum and steel under different superficial conditions. Finally, chapter 7 describes the conclusions of this dissertation and the future work.

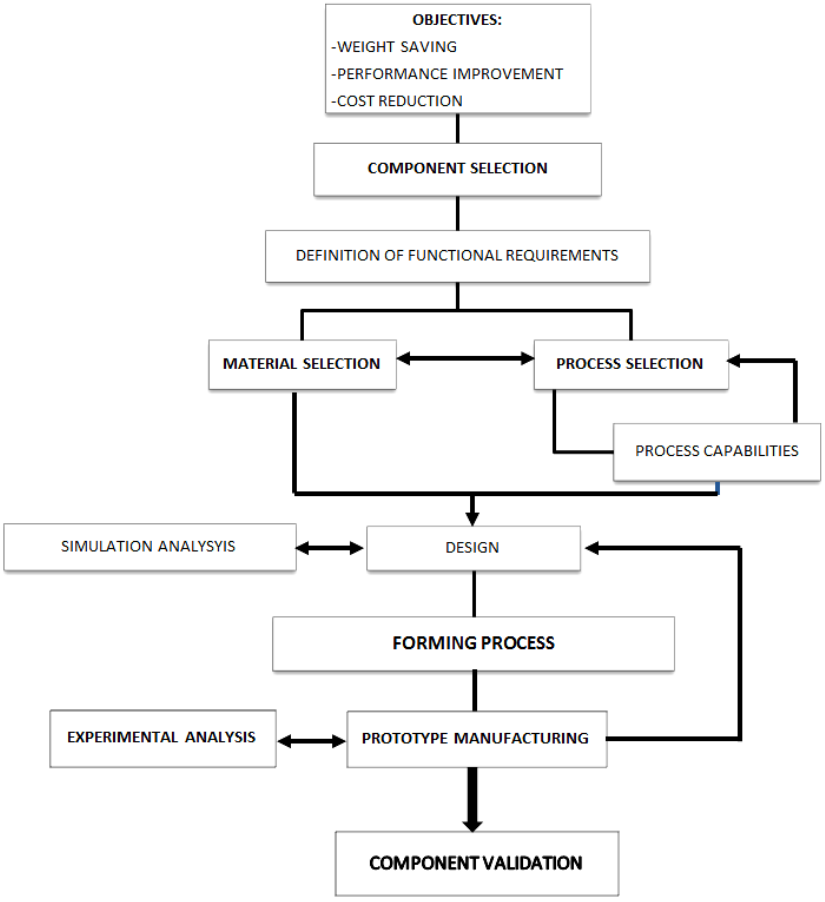

Figure 2. Diagram of the work carried out.

CHAPTER 2

LITERATURE REVIEW

Chapter 2 is an introduction to the state of the art of hybrid joining processes. The review is divided into three main subsections. In the first section technologies to join dissimilar materials are briefly explained. In the second sections of the review is specially focused in the main aspects of the thixoforming process. Finally the formation and growth of Al-Fe intermetallic layer is explained.

2.1 Introduction

With the increasing trend toward lightweight vehicles, the body materials for automobiles are changing from mostly low carbon steels to a mix of materials that includes both low carbon steels and high strength steels, light non-ferrous alloys, such as aluminum and magnesium alloys, and fiber reinforced polymers [Jeswiet 2008]. The acceptance of these materials will depend not only on their structural performance and manufacturability, but also on the joining methods that can be used to assemble them in a rapid, robust and reliable manner [Kleiner 2003]. The structural performance of a joint depends on the joining method, joint geometry and joint quality and the joining method often also depends on the materials being joined. Additionally, under mass production conditions it must also be quick, less dependent on fit and dimensional variations of the parts being joined and as defect free as possible.

Joining is an important consideration in the design of an automobile, since joints are usually the weakest areas in the structure and they are often the failure initiation locations in service. Joining becomes more important as the body material changes from a single material to a mix of materials, since the compatibility between different materials in terms of their mutual joinability, surface characteristics, corrosion, assembly stresses, etc. may pose many technical challenges and need to be considered in the design process and selection of materials.

The joining method can be divided into four categories: Liquid phase welding or fusion welding, solid phase welding, mechanical joining or adhesive bonding.

Liquid phase welding

Liquid phase welding is performed by locally heating the materials to be joined to their liquid phases, applying pressure to create fusion bonding between them and allowing the fusion bonded liquid phase to cool under pressure to form the joint. Spot welding [Gean 1999], arc welding [Lu 2009, Vranakova 2005], TIG welding [Lin 2009, Sanbao 2010] or resistance welding [Choi 2010, Sun 2004a, Sun 2004b], are widely adopted in the automotive industry. However high temperatures and long times associated to this kind of processes, generally result in defects such as, porosity, embrittlement of the heat affected zone and the formation of thick intermetallic compound layers at the joint interface [Qiu 2009a, Qiu 2009b, Qiu 2010].

Solid phase welding

In solid phase welding, two sheer of the same material or different material are joined by creating metallurgical bond without melting the material. The weld quality is usually excellent, since porosity [Sun 2004a, Sun 2004b], grain boundary cracking and other problems associated with liquid phase welding do not occur in solid phase welding. The mechanical properties, in general are equal or better than those obtained by liquid phase welding. Another advantage is that by not creating molten pool of material which shrinks significantly on solidification [Choi 2010, Agudo 2008], distortion of the part and residual stresses after welding are relatively low [Rathod 2004, Springer 2011, Chengand Chaur-Jeng 2010].

In contrast, solid state joining processes required large amount of deformation [Rathod 2004, Shi 2011]. The absence of macroscopic deformation and relative motion of the parts makes difficult the good contact of the joining surfaces requiring higher deformations to promote bonds [Kumai 2010]. Furthermore, the joint occurs at relatively low temperature compared with fusion welding, resulting in a lack of wettability and reduced diffusion rates hindering the formation of a phase seam, which is essential to create a firmly bonded joint.

Mechanical joining

Conventional mechanical joining methods using bolts and nuts are not very common in automotive body applications since its shape is limited and require a complex preparation of the joint [Lu 2009, Sun 2004b, Barreiro 2008]. Although bolted joints have the advantage that they

can be disassembled easily if replacement or repair of parts is needed, they require drilling of matching holes in the parts to be joined and the drilled holes must align accurately during the assembly process. Although they are used in assembling many chassis and suspension components, they are considered too slow for assembling body components compared to the available welding processes. In recent years, two relatively new mechanical joining methods are finding greater use in assembling sheet metals for body applications. These two methods are the self-piercing riveting [Chrysanthou 2014] and clinching [Lee 2014].

Adhesive bonding

Adhesive bonding offers improved joint stiffness compared to spot welding and mechanical joining, since it produces continuous joining instead of localized, discrete joining [Hayat 2011]. This also results in more uniform stress distribution over a larger surface area. A properly designed adhesive join produces high joint strength and is capable of high energy absorption. It also provides good noise and vibration damping. Another advantage of adhesive joints in automotive applications is that they prevent ingress of water and debris into the joint area, thus acting like a seal. However adhesive bonding may require surface preparation, which may include surface cleaning and surface pretreatment. Furthermore, the adhesive may need heat curing, which is not only time consuming, but also may affect the properties of the base material [Ebnesajjad 2013].

Long-term durability of adhesive joints and the possibility of adverse effects of humidity, temperature, salt water and other environmental conditions on the properties of the adhesive need to be considered before using adhesive bonding in automotive applications [Zhang 2013]. Adhesive joints also have low peel strength, which can pose problems in certain bonding situations and must be taken into consideration at the design stages, particularly with respect to crashworthiness.

The vast majority of these hybrid joining techniques are limited to join simple geometries such as metal sheets with thicknesses ranged between 0.3 mm and 2 mm. Hence the need of advanced welding methods able to produce complex massive components for automotive industry which combine multi-material design methodologies and low cost fabrication process.

2.2 Joining aluminum to steel

Iron and aluminum alloys are among the most important materials in automotive industry because of their good properties. Combination of steel and aluminum in a hybrid structure will implement the integrated load-supporting of steel with the advantages of aluminum in weight reduction, and result in the whole body structural optimization.

However, it is well known that metallurgical bonds between aluminum and steel run into great difficulties because of large differences in physical and chemical properties of two metals [Joo 2004, Taban 2010, Rathod 2004, Schäfer 2011, Bach 2005]:

- Large difference between the melting points of Al (660ºC) and Fe (1536ºC).
- Presence, of high melting point Al_2O_3 oxide films in the aluminum surface.
- Nearly zero solid solubility of iron in aluminum (0.053% at the eutectic temperature of 654ºC).
- Bad wetting of molten aluminum with solid steel.
- Great difference in the coefficient of linear expansion, thermal conductivities, and specific heat. Here, the thermal conductivity of the aluminum is roughly three times that of steel suggesting 3/4 of the developed heat is conducted away through that side of the joint which lead to the development of high thermal stresses.

These properties are summarized in the Table 1:

Table 1. Physical and thermal properties of aluminum and iron [Vranakova 2005].

PROPERTIES	Al	Fe
Melting point (ºC)	660	1536
Density (kg/dm3)	2.7	7.8
Coefficient of elasticity (GPa)	71	210
Coefficient of thermal expansion (10-6 K-1)	23.9	11.5
Thermal conductivity at 20ºC (W/mK)	220	74
Electric conductivity (MS/m)	37.66	10.29

Besides, the chemical interaction of these two metal at high temperature lead to irreversible formation of aluminum-rich intermetallic phases which result in mechanical degradation of the joint [Wang 2012, Schäfer 2011, Chun 2008, Choi 2010, Gean 1999, Sun 2004b]. Thus,

understanding the interfacial characteristics of the steel/aluminum alloy joint is essential to optimize processing-property relationship so as to obtain a strong joint. Effect of these intermetallic is further explained in section 2.6 of the current chapter.

2.3 Thixoforming

Semisolid metal (SSM) processing is a technology halfway between foundry and forge with a great scientific and technological potential.

The technology was born at MIT (Massachusetts Institute of Technology) in the early 70s following the work of Fleming *et al.* [Spencer 1972].The key to the process resides in the peculiar behavior of alloys containing solid particles in a non-dendritic shape. Fleming *et al.* found that uniform agitation of certain alloys during the solidification process produces the globularization of primary particles due to the breakage of dendrites. In semisolid state, these materials exhibit thixotropic properties, that means its viscosity decreases with increasing shear forces acting on them, whereas in the absence of such forces practically behave as solids, which can be easily manipulated. At the beginning, the process was limited to low melting point alloys, among them we can find the AlSiMg alloys. This kind of alloys, specifically A356 (AlSi7Mg0.3) and A357 (AlSi7Mg0.5) alloys, have been employed in a wide variety of industrial applications of semisolid forming which has demonstrated the potential of the process [Kirkwood 1994, Fan 2002].

A couple of decades later, in the mid 1990s steel thixoforming become the focus of various research activities [Spencer 1972, Kirkwood 1994, Flemings 1991, Püttgen 2007, Rassili 2010]. These investigations demonstrated the feasibility of semisolid forming of high melting point alloys. However, the surface to interior temperature differentials in steel thixoforming dies are much larger than with aluminum and magnesium, and the cyclic thermal stresses produced require very specific features of tool materials. At the same time, because of the high temperature difference between the billet and surroundings, severe heat loss due to radiation and, also, surface degradation caused by scale formation must be taken into account [Lozares 2014]. Depending on the liquid fraction and the process used to shape the material it is closer to casting or forging.

In comparison with conventional casting, the high viscosity of semisolid metal avoids the turbulent filling of the dies and consequently reduces part defects coming from air entrapment. Due to the high solid fraction during filling the loss of volume during solidification is reduced, leading to less shrinkage porosity. Furthermore, the low gas content lead to microstructures that are suitable for welding and heat treatment, which among others is an essential condition for the thixocasting serial production of aluminum alloys for the automotive industry [Ghassemieh 2011]. In addition, the lowered process temperature of the semisolid metal lead to significantly increase in tool life compared with conventional die casting [Lozares 2014].

Moreover in the thixoforming process the blank metal is caused to flow due to the pressure causing the break up of the surface and top layers of the aluminum oxide film allows a better contact of the base materials thus promoting the formation of a stable joining zone [Behrens 2011]. In addition, thixoforging is able to produce more complex geometries with slight spline and long flow lengths. Compared to conventional forging, the process is shortened right at the beginning because pre-forming of the precursor material is not necessary. There are significant differences in the forging operation itself. Whereas conventional forging requires few forming steps until the end geometry is reached, semisolid forming is carried out in just a single step. Draft angles can be designed very flat and core pullers enable near-net-shaped geometries to be produced without piercing the component after forming, reducing the final machining to a minimum.

Also, deburring of the component can be minimized or even avoided. In addition, the resulting mechanical properties are similar to those of forging parts whereas geometries adapted to requirements of lightweight component can be achieved more easily because of existing component potentials. In particular, this lead to advantages regarding process costs mainly based on material savings. However, it is also important to bear in mind that production cycles are shorter in forging than in thixoforming, which requires time for solidification.

2.3.1 Semisolid material

For thixoforming, the alloy has to fulfill at least these specific requirements:

- The material needs to have a freezing range where liquid and solid phases coexist. Low temperature sensitivity is really important for the correct adjustment of the solid-liquid fraction, this way; a little change in temperature will not suppose a big change on the solid-liquid fraction.

- Particular micro-structural formation is needed in the semisolid state, globular solid particles should be embedded inside a liquid matrix.

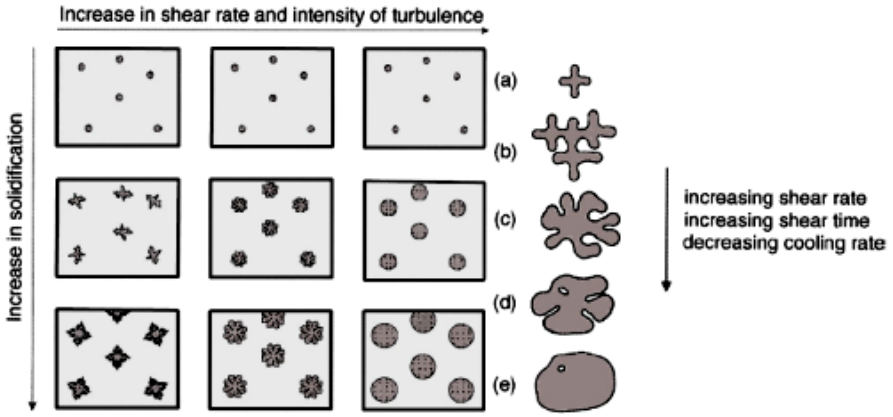

Figure 3. Structural changes during the solidification and shearing of metallic suspensions [Hirt 2009].

During processing, semisolid material in contrast to Newtonian fluids, which increase the viscosity increasing the shear stress, exhibit thixotropic behavior. They become fluid when shear stress increases and return to being solid when allowed to stand (Figure 4). In fact, they can be handled like solids due to the development of a rigid network in the quiescent state between solid particles. Of course, this is possible whenever shearing forces do not exceed the network resistance. If sufficient shear stress is applied, the framework breaks and the agglomerates are dissolved. A suspension of solid particles within a liquid matrix develops, resulting in a reduction in viscosity which makes the semisolid alloy fluid and capable to fill the die.

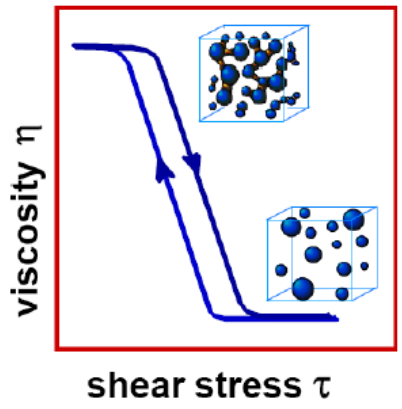

Figure 4. Semisolid material behaviors [Uggowitzer 2001].

The most relevant parameters for thixoforming materials are: first, the temperature sensitivity, and second, from a microstructural point of view, the solid fraction, the grain size and shape and the steric arrangements of the solid phase [Hirt 2009].

Solid fraction

The solid fraction is one of the most important parameters in semisolid metals because it has a crucial influence on the viscosity and therefore on the flow and filling behavior of the material. It is directly related with the temperature of the aluminum, the higher the temperature the lower the solid fraction. At high solid fraction values, the high viscosity of semisolid metal avoids the turbulent filling of the dies and consequently reduces part defects coming from air entrapment, however, the fluidity of the alloy may not be sufficient and may cause filling problems. In contrast, at low solid fraction values, the fluidity of the material is increased and thus decrease the forming load needed to form the component, although, the low viscosity of the semisolid metal can cause a turbulent filling of the die and material losses in addition, handling of the billet can be complicated [Azpilgain 2006]. Depending on the forming process it varies steeply, typically showing a steep increase when the solid fraction becomes higher than 35-50%.

On the other hand regarding to a joining process, high joining temperatures, as it happens in solid-liquid interaction, promotes formation of intermetallic compounds by diffusion, which quickly deteriorates the mechanical properties of the join with the normal growth of the layer. However, this mechanism supports the formation of a phase seam, which is essential for creating a firmly bonded joining. Working in the semisolid state the diffusion rate is considerably faster than in the solid state, but to a lesser degree than in a liquid state decreasing the final thickness of the interfacial layer in order to obtain sound joints.

In this case, thixo transverse forming, the material is expected to be able to fill up the die completely avoiding turbulent flow and to form a phase seam with a solid fraction between 50-70 %.

Temperature sensitivity

The impact of the temperature variation on the solid fraction can have devastating consequences in the forming step. Because of that, it is important for semisolid alloys to have a low temperature sensitivity, thereby a little change in temperature will not suppose a big change in the solid fraction. The impact of temperature variations on the solid fraction can be expressed by the negative slope of the equilibrium solid fraction curve.

$$S = -\frac{df_s}{dT} \qquad \text{(Eq. 2.1)}$$

Grain size and shape

The spherical morphology of the particles is essential for the flow behavior of semisolid metals. When solid particles exist in a globular form within a liquid matrix and a shear stress is applied over them, they are able to translate, rotate or slide past each other.

Furthermore, the grain size must be large enough to build a tree dimensional network and withstand the manipulation of the billet. At the same time, it has to be small enough to flow across the thinnest sections of the part. It also plays a crucial role on the mechanical properties of the final component and because of that, reheating has to be tightly controlled in order to avoid an excessive growth of solid particles.

2.3.2 Micro and macrosegregation

Segregation terms the demixing of elements as a result of non-equilibrium states during solidification. It occurs as a consequence of the different solubility of these elements in the solid and the liquid phase, respectively. These segregations remain for the most part present even after complete solidification. Furthermore, segregation is highly influenced by mass transport phenomena (e.g. diffusion) in the solid phase and in the liquid phase. Segregation can be seen as short range micro-segregation and long range macro-segregation. Concentration differences of the latter are in the order of the component and remain unchanged even after long-term heat treatment. Short range segregations are in the order of the grains and can mostly be eliminated by a homogenization heat treatment.

2.3.3 Forming operations

Semisolid forming process consists basically of three stages: (1) manufacture of material with globular structure, (2) achievement of the semisolid state, and (3) forming the material by pressure die casting or forging.

Depending on the type of the semisolid process it can be classified in two major categories.

- Rheocasting processes, in which the semisolid slurries produced from the liquid phase are directly used in shaping operations.

- Thixoforming processes, where a particular type of solid feedstock is reheated into the semisolid range to form globular, non-dendritic slurry that is then used in subsequent forming operations. Figure 5 shows both alternatives in a schematic way.

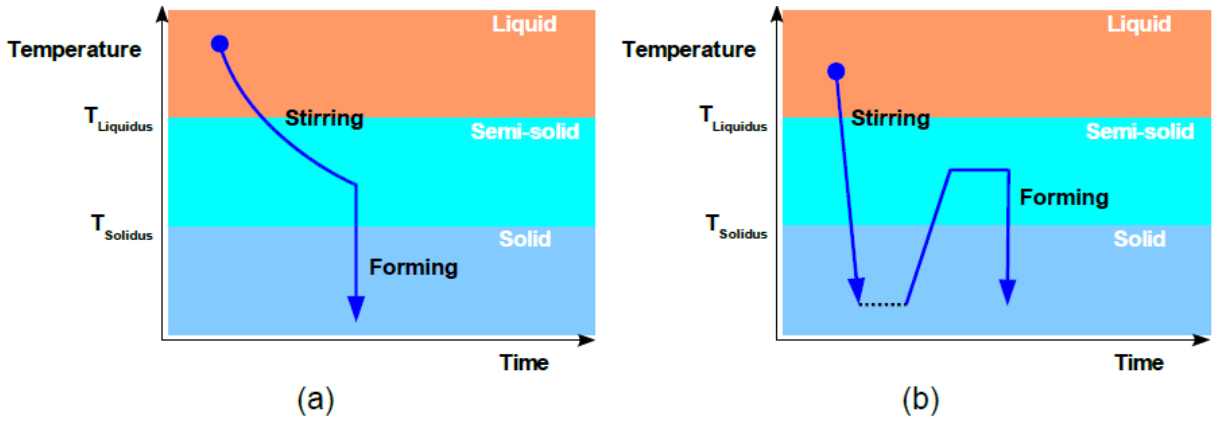

Figure 5. (a) Rheoforming (b) Thixoforming [de Figueredo 2001].

The further processing of the billet or slurry is performed using modifications of conventional processes (Figure 5) such as high-pressure die casting, forging, transverse extrusion, bar extrusion and rolling. Of these, only semisolid casting and to a lesser extent, modifications of semisolid forging have so far been applied to industrial production. Next figure summarizes the main semisolid forming routes:

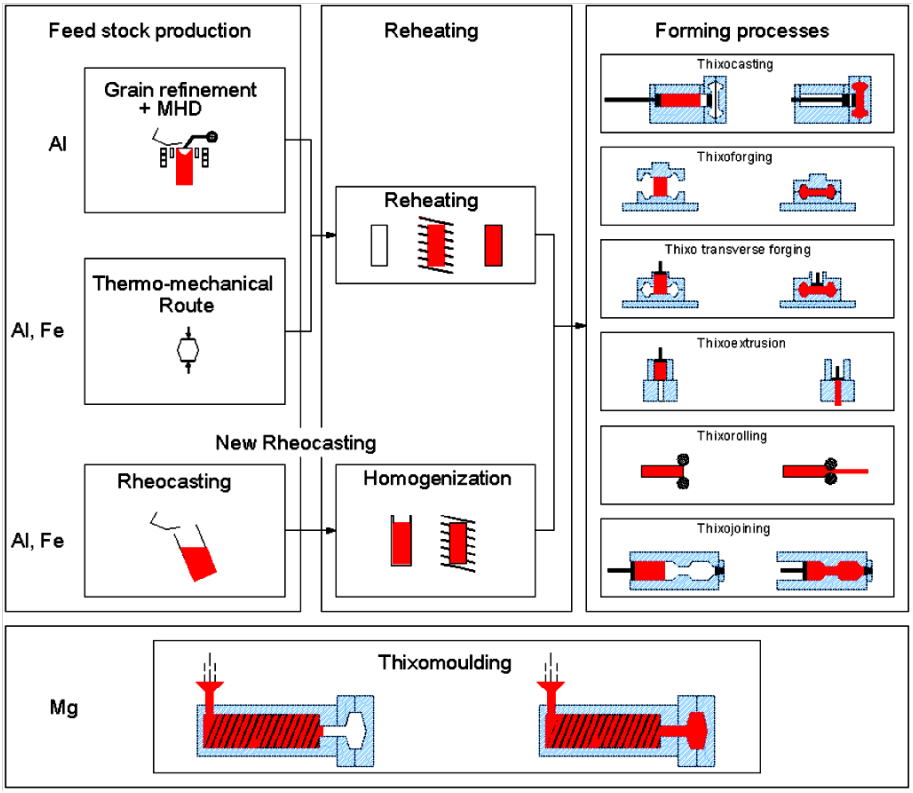

Figure 6. Semisolid metal process routes [Hirt 2009].

The term thixoforming includes all forming processes of semisolid alloys into a metallic die. If the forming process is carried out in a nearly conventional die casting machine, is called thixocasting; otherwise, if it is performed using a forming press, it is known as thixoforging.

In thixocasting a billet, with solid fraction in the range of 20-40 %, is placed in an adapted shot chamber, modified to accept semisolid billets instead of liquid metal, and squeezed into a closed die by a shot piston. The flow during die filling is laminar and the velocity is significantly higher than in thixoforging but lower than in conventional high-pressure die casting. One of its strengths is the possibility to use the highly advanced high-pressure die casting technology that makes possible to manufacture very complex components.

In thixoforging, a semisolid billet of a higher solid fraction, 50-80 %, is inserted directly in the lower half of a horizontally sectioned tool, analogous to the conventional drop forging process. The forming operation is performed by closing either one or both die halves. In contrast to thixocasting, the force transmission for the forming and densification step is applied over the whole tool surface, not only on the shot piston area, so that hydrostatic pressure is affected

evenly during solidification. However the geometric complexity is limited to geometries which allow forging without flash.

The thixo transverse forging, using servo-mechanical or servo-hydraulic presses, is an alternative forming process with some important advantages over the conventional thixoforging. Although the forming velocity is of the same order of magnitude, thixo transverse forging is characterized by squeezing the semisolid material into an already closed die, thus eliminating possible material ejection. The thixo transverse forging process has some industrial advantages, such as the successful fabrication of high quality components with fewer inner defects, suitable for less machining, high productivity comparable to high pressure die casting, and being an energy-saving system without the conventional melting process. The semisolid metal is able to fill the die with a laminar flow, preventing any gas entrapment (porosity) in the final component. Therefore, besides the high quality reachable in the as cast part, it is possible to improve the mechanical properties by heat treatments, not possible for some castings made of high pressure die casting.

Other big advantages are achievable by thixoforming, due also to the fact that the material is heated and formed at a temperature of about 100 °C below the melting point: energy saving, tighter part tolerances (less shrinkage in the die, less residual stress, less component distortion), less machining operations (near net shape process), no dangerous molten metal handling etc. Besides, in terms of diversity of parts, it allows an increased degree of geometric freedom.

Concerning the mechanical loads of the tools, the low forces that are required for the forming operation reduce the mechanical wear and permit a longer tool life in comparison with the drop forging process. However, there also disadvantages regarding higher cycle times, higher thermal load of the tools and limited suitability of alloys for the forming operation.

For lightweight steel/aluminum joining technology, key processes includes laser welding, MIG welding, TIG welding or fiction welding. However, there are yet significant barriers in large scale use of these structures mainly due to the great difficulties that arise when joining dissimilar materials. Hence the need for further development of suitable manufacturing processes and high performance lightweight structures at low cost. In these fields, Thixo transverse forging of aluminum on steel is a promising method to manufacture near net shape hybrid structures for the automotive sector.

2.3.4 Semisolid joining

In recent years, the semi-solid technology is widely applied. But as a method of different metal joining it is relatively rare [Liu 2006]. In contrast to welding using semisolids, the most commonly used welding methods include a local heating of the substrate above the liquidus temperature (arc welding in all forms, laser and electron beam welding) [Lu 2009, Bach 2005].

The liquid metal generally solidifies with a dendritic microstructure. This effect is not desirable from a metallurgical point of view because of the lack of control of the microstructure, which can possess porosity, inclusions and uncontrolled grain orientations. Also, the high temperatures necessary to completely melt parts of the substrate induce a heat affected zone. In this zone the material undergoes a thermal history that makes its properties different and generally worse than those of the rest of the bulk material in the substrate, often lowering fracture toughness, corrosion resistance and yield strength. The decrease of fracture toughness facilitates the appearance of cracks along the weld due to thermal and residual stress.

Welding with semisolid slurries offers the potential to avoid the problems mentioned above because the solidification and heat transfer processes are radically different than those of welding using a purely liquid phase. In welding with semisolids the solidified microstructure is globular because in semisolid slurry solidification starts at all solid particles simultaneously. The heat affected zone is greatly decreased in welding with semisolid slurries because it is not necessary to completely melt the material and the material is at a relatively low temperature. Semisolid welding also dramatically decreases welding distortions [Mendez 1995, Mendez 2002]. The temperature difference between the weld pool and the bulk substrate is much smaller than in common welding since the slurry temperature is below the liquidus temperature.

The specific advantages of semisolid joining include:

- Dissimilar material welds are possible.
- Properties and microstructures remain similar to those of base metals.
- Multiple welds can be made in one setup at the same time.
- Produces a product finished to size and causes minimal deformation.
- Presents less shrinkage and stresses compared to other welding processes.
- Highly automated process does not need skillful workforce.

On the other hand, the main limitations of the process are:

- Costly equipment especially for large weldments.
- Costly preparation with smooth surface finish and exceptional cleanliness.
- Protective atmosphere or vacuum may be required.
- Difference in thermal expansion of members may need special attention.
- Limited nondestructive inspection methods available.

Semisolid state joining processes, including diffusion welding, involve two characteristic steps. The first is to achieve mechanical intimacy of contact; the second is to induce complete mechanical bonding across the area of contact. The necessity of these two steps to form a bond in a semisolid state weld is given by the nature of a real metal surface. A schematic cross sectional view of Figure 7 illustrates several characteristics of a real surface.

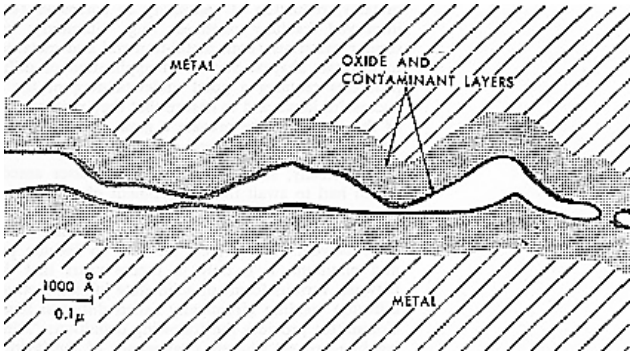

Figure 7. Schematic illustration of the real metal surface.

These steps must occur in a proper sequence in each welded area but need not proceed at uniform rates in the entire part. Therefore, the final bonding must be completed in certain places in a joint before contact is established elsewhere. Successful application of diffusion welding to engineering problems requires a good understanding of the fundamentals both to make sound joints and to ensure that they perform in service as expected.

In thixo transverse forging, the semisolid material is deposited in a single stroke, and not by droplet deposition as in arc welding. Since the semisolid slurry is fully dense, so will be the weld bead, dramatically reducing the porosity that can form in other kinds of welding. Semisolid slurries allow for the control of the apparent viscosity of the deposition material in such a way that the material remains where it was applied and does not flow along the weld groove, even for large cross sections. This viscosity control is not possible with liquids.

Since semisolid welding does not involve electric currents for deposition (as in arc or resistance welding), the substrate can be a non-conductive material such as ceramics. The present limitation is in the production of a high temperature semisolid slurry, not in the concept of joining materials with semisolid slurries [Mendez 2002].

2.3.5 Establishment of contact

A typical surface, even if perfectly clean, is rough in a microscopic sense. Surface roughness prevents full contact when parts are pressed together. The individual asperities which make up the roughness are deformed by application of increasing pressure.

When pressure is applied, deformation begins at the highest asperities and gradually spreads until plastic flow is general. This initial contact does not occur between metal surfaces, but rather between the barrier films trapped between the surfaces under compression (Figure 7). Very stable and insoluble superficial oxide films restrict metallic interface contact and further limit welding. In case of aluminum, the superficial film consists mainly of Al_2O_3. [Joo 2004, Taban 2010, Rathod 2004, Schäfer 2011, Bach 2005]. At places where the surfaces move together under shear, the films are disrupted and metal to metal contact begins.

Once true metal to metal contact is established, the atoms are within the attractive forces fields of each other and hence a high strength join is generated by diffusion welding. The joint at this time resembles a grain boundary because the metal lattices on each side of the line have different orientation. However, it may differ from an internal grain boundary in that it may contain more impurities, inclusions and voids which remain at a weld interface if full asperity deformation has not occurred.

A planar interfacial boundary is not thermodynamically stable and tends to migrate to a more stable configuration if conditions permit. Its migration will proceed more easily in few voids or inclusions existing at the boundary. The overall process takes place in three steps: 1^{st} deformation forming interfacial boundary, 2^{nd} grain boundary migration and pore elimination and 3^{rd} volume diffusion and pore elimination. Figure 8 is a simplification since the sequences described vary with process conditions and alloys.

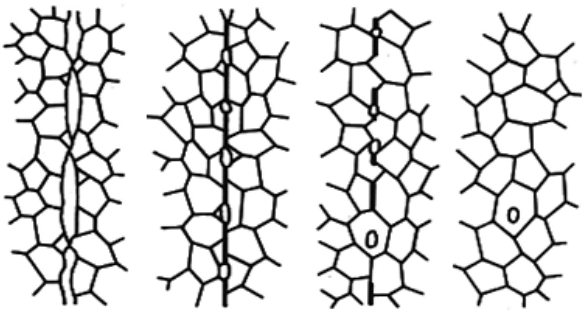

Figure 8. Steps of diffusion welding process.

2.4 Wettability of steel by aluminum

In order to obtain a sound joint between steel and aluminum it is required not only the mechanical bonding but also the chemical interaction as this mechanism supports the formation of a phase seam.

As mentioned before, one of the necessary conditions for joining successfully this couple of dissimilar metals is to obtain good wettability and spreadability of liquid aluminum over steel. According to thermodynamics, a fluid only will spread if the energy resulting from the new interface solid-liquid is less than the corresponding solid-vapor interface. The wettability of a liquid metal on a solid surface is commonly evaluated by measuring the contact angle (θ) as shown in Figure 9 [Aguilar-Martínez 2008]. The shape of the drop is a function of three energy terms, as described by the classical Young equation [Eustathopoulos 1999, Liu 2010, Moraes 2006, Ouyang 2007]:

$$\cos\theta = \frac{\gamma_{sv} - \gamma_{sl}}{\gamma_{lv}} \qquad \text{(Eq. 2.2)}$$

Where, γ_{lv} is the surface tension of the liquid/vapor metal, γ_{sv} is the surface energy of the solid/vapor, and γ_{sl} is the solid/liquid interfacial energy.

Figure 9 shows the edge angle adjustment of a molten droplet on a solid base for different values of the interface energy. At an angle of $> \pi/2$ a non wettable system is described and for an angle limit of $< \pi/2$ a wettable system. With decreasing angle the wettability improves [Eustathopoulos 1999, Laurent 1987, Candan 2011].

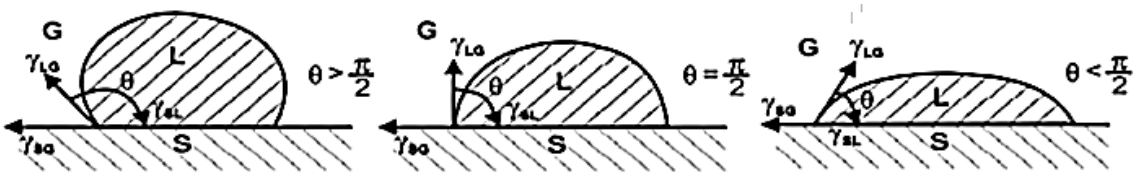

Figure 9. Edge angle adjustment of a melt drop on a solid base.

The contact angle value is related to the bonding quality of the liquid/solid interface [Liu 2010, Moraes 2006, Kainer 2006] but it is also desirable that the reaction products formed at metal/metal interface were thermodynamically stable and mechanically strong.

However, spreading of liquid aluminum on the surface of iron (steel) differs from spreading of other melts, particularly in that aluminum is covered by dense oxide film, which has a high melting temperature (2054 ºC) and is chemically very stable and resistant. This oxide film usually works as a wetting inhibitor [Ryabov 1998]. As a result, there is in practice not a combination of these three phases: gas-melt-solid body, but a system of four phases: gas phase-alumina-molten aluminum-steel.

Thomy *et al.* [Thomy 2012] studied the effect of wettability in the mechanical properties of the steel aluminum hybrid joint. They observed that at low wire rates the tensile strength of the joint decreased drastically because wetting was insufficient or non-existent as shows Figure 10.

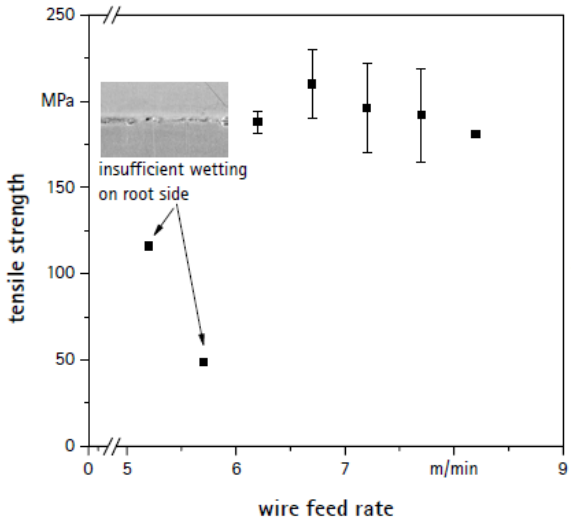

Figure 10. Effect of wire feed rate on tensile strength [Thomy 2012].

Superficial oxide can be avoided by either etching of the surfaces in combination with a protective atmosphere or the application of fluxes [Springer 2011, Bach 2005]. Fluxes are solid chemical powders that spread over the melt metal surface to inhibit the oxidation. Fluxes are generally used in brazing and soldering to remove oxides from the base metal surface by a reduction and/or dissolution reaction, to protect the clean surface from reoxidation, or to modify the surface tension of the molten metal [Rathod 2004, Bach 2005]. In case of the combination between the application of the non-corrosive flux FL20 led to an excellent wetting between steel and aluminum melt, Figure 11 shows the results obained by Lin *et al.* [Lin 2009] of wetting and spreading of aluminum based filler on the stell surface.

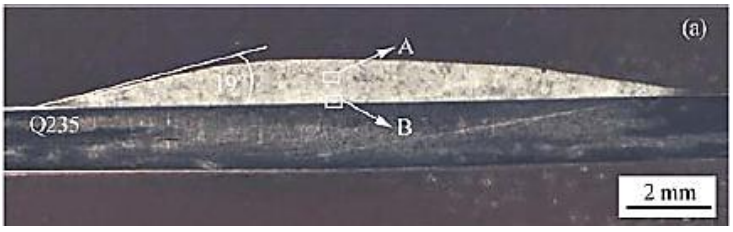

Figure 11. Wetting and spreading of the filler metal on the surface of the Steel [Lin 2009].

2.5 Protective coatings

Solid/liquid joining procedures where little or no mechanical pressure is applied to form the bond generally require clean, oxide free surfaces so that the molten Al can successfully wet the solid Fe or steel. Another approach to prevent the reoxidation of the clean surface is the pre-coating of the Fe/steel substrate with a very thin layer (few µm) of Al or Zinc [Bach 2005, Murakami 2004, Harada 2012].

2.5.1 Zinc coating

When left unprotected, steel will corrode in almost any environment. Zinc coatings protect steel by providing a physical barrier. Another outstanding protection mechanism is zinc's remarkable ability to galvanically protect steel. When base steel is exposed, such as at a cut edge or scratch, the steel is cathodically protected by the sacrificial corrosion of the zinc coating adjacent to the steel. In practice, this means that a zinc coating is not undercut because the steel cannot corrode adjacent to a zinc coating. The extent of this cathodic protection is determined by the type of coating, its thickness and that of the underlying steel, as well as by the area of damage.

Zinc plating involves the electrolytic application of zinc by immersing clean steel parts in a zinc salt solution and applying an electric current. This process creates a thin layer of pure zinc (99.9 %) that covers the steel homogeneously. The electroplated zinc coating has an ultra-smooth surface finish which is desirable for surface critical parts such as automotive exterior body panels [Choi 2010]. In general, pure zinc is used for electrogalvanized coatings although alloy coatings such as, Zn-Fe and Zn-Ni are also commercialized.

Regarding to a joining process, the Zn layer covers the steel substrate quickly dissolves during contact with liquid Al due to its lower melting temperature (T_S of Zn= 419 ºC) and thus enables the contact of the metal without the interference of oxygen [Lin 2009, Vranakova 2005]. However, it is important to consider the joinning process temperature in order to avoid the volatilization of the zinc at temperatures above 900 ºC which reduces the wetabilitty of the system as in case of electric ARC welding process [Lu 2009] or TIG welding process [Lin 2009]. The effectiveness of zinc coatings in any given environment is directly proportional to coating thickness. Coating life is determined by the coating corrosion rate, itself a function of many factors such as time, composition of the atmosphere and the type of coating.

The castings fabricated with Zn coated inserts by Aguado *et al.* [Aguado 2013] showed metallurgical bonding with reaction layers of approximately 100 and 30 μm mean thickness. They detected small amounts of Zn the reaction layers that suggested that Zn has been partially dissolved in the Al melt or has evaporated by the heat of the aluminum melt due to its high vapor pressure. In the reaction an intermetallic compound (IMC) layer rich in Fe and Al (identified as Fe_2Al_5) could be observed close to the steel interface (Figure 12):

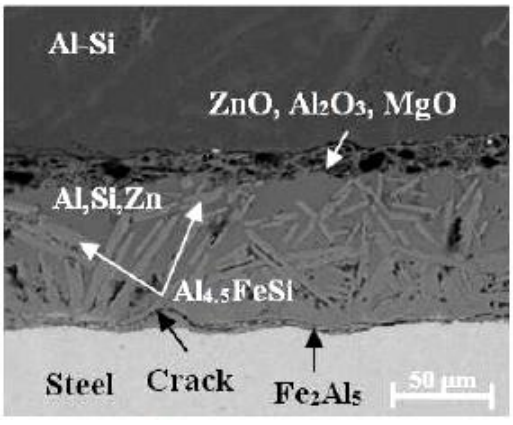

Figure 12. SEM micrographs of the interface of zinc coated insert with aluminum [Aguado 2013].

The Fe-Zn IMC layer was followed by another reaction layer consisting of an aluminum matrix with eutectic Si and small amounts of Zn. Additionally, plenty of blocky and needle-shaped intermetallic compounds, identified as Al4.5FeSi, are detected.

2.5.2 Aluminum coating

Aluminide treatment is an alternative method to produce an aluminum containing layer over the steel surface to improve the oxidation resistance of steel by generating a fine and dense aluminum layer on the surface of the steel.

Aluminized steel was developed for providing more structural durability and a high yield strength in highly corrosive environments. It is comparable to the strength of some high-alloyed steels, but at a fraction of the cost. The coating can withstand 550 °C with almost no change in the base material. Possible end uses are mufflers, furnaces, ovens, ranges, heaters, water heaters, and baking pans. However, despite the good corrosion resistance of aluminized steel, if the aluminum layer is disrupted and the steel is exposed, then the steel may oxidize and corrosion may occur.

An aluminide coating can be achieved by several methods such as physical vapor deposition, chemical vapor deposition, pack cementation, thermal spray and hot dipping [Chengand Chaur-Jeng 2010]. Among these coating, methods hot dipping has been widely adopted in industry because of its characteristics of high efficiency and low cost [Cheng 2011]. The process of hot dipping starts by cleaning the steel generally with HCl, then placing the tubes in an aluminum bath and finally tubes are pulled out and air dried. During this immersion Fe-Al interdiffusion reaction occurs in which permanent bonds between steel and aluminum are formed. The product of hot dip aluminized steel is a continuously coated surface on both sides with an interfacial Fe-Al intermetallic layer that provides a tight metallurgical bond between the steel and the coating [Cheng 2011].

Commercial hot-dipping coatings are generally made with pure aluminum although is silicon is added to the aluminum bath to create a thinner layer of aluminum on the steel. Moreover, a silicon content of 5% to 11% promotes the adherence between substrate and coating.

As the coating layer is formed by interdiffusion, the thickness of the intermetallic layer is a function of temperature and dipping time. The longer the immersion time the thicker the coating. This was asserted by different authors [Chengand Chaur-Jeng 2010, Aguado 2013, Cheng 2011]. To prepare the coating Cheng *et al.* immersed specimens in pure molten

aluminum at 700 ºC for 3 minutes then specimens were exposed in a furnace with static air at 750 ºC for 5 minutes to 480 h [Cheng 2011]. They found that the as coated layer consisted of an outer aluminum topcoat, minor $FeAl_3$ and major Fe_2Al_5 with further exposure at 750 ºC the top coat was consumed, $FeAl_3$ disappeared and left an aluminide layer of Fe_2Al_5 phase.

Later, Aguado *et al.* observed that the minimum immersion time to create a protective layer at 750 ºC for AlSi7Mg alloys was 5 minute, however, a fine oxide film was found in the joining process even after using an aluminum protective layer in the insert.

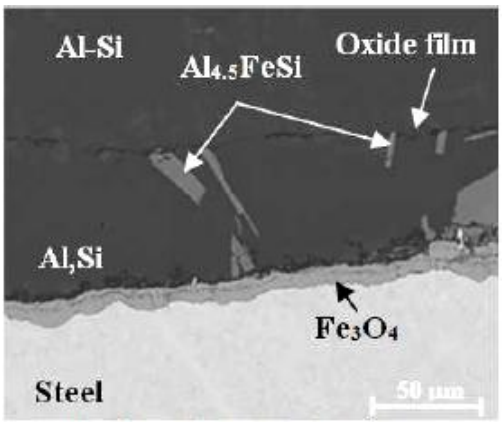

Figure 13. SEM micrographs of the interface of hot dip aluminized insert with aluminum [Aguado 2013].

The layer analyzed by Aguado *et al.* Fe-Al IMC layer consisted mainly by the IMC phases Fe_2Al_5 followed by another reaction layer consisting of an aluminum matrix with eutectic Si. The reaction of Fe, Al and Si additionally formed plenty of blocky and needle-shaped intermetallic compounds, identified as Al4.5FeSi [Aguado 2013].

Regarding to a joining process, the Al layer covers the steel substrate to protect the clean surface from reoxidation. During the forming process liquid aluminum will be in contact with the Al coating, the same chemical composition of the coating, promotes the wetting and diffusion to form a phase seam.

2.6 Intermetallic compounds

When two or more dissimilar materials come into contact at elevated temperatures, the formation of several complex intermetallic compounds (IMC) occurs. Intermetallic phases can be defined as phases with crystal structures deviating from those of the constituting elements. The formation of the IMC is mainly driven by diffusion which is mathematically described by Fick's law:

$$J = -D\frac{\partial \phi}{\partial x} \qquad \text{(Eq. 2.3)}$$

Where, J is the diffusion flux, D is the interdiffusion coefficient, ϕ is the concentration (for ideal mixtures) and x is the position. The interdiffusion coefficient is expressed as a function of the temperature T by the following equation [Lu 2009]:

$$D = D_0 \exp\left(-\frac{H_A}{RT}\right) \qquad \text{(Eq. 2.4)}$$

Here, D is the interdiffusion coefficient, D_0 is Arrhenius' equation pre-exponential constant, R is the Universal gas constant and H_A is the activation enthalpy.

These interactions can occur in many alloy systems. Their existence, stability and solubility, however, depend on the relative position of their respective free energy curves in the alloy system. In general, intermetallic phases possess a more complex crystal structure than their constituting elements. This result in a strong increase in hardness and a limited formability, despite the retaining prevalence of metallic bonding for intermetallic phases formed in metal-metal alloy systems [Springer 2011].

2.6.1 Formation of intermetallic compounds in binary Al-Fe system

In the binary system iron-aluminum, low solubility of iron in aluminum leads to a formation several brittle and complex intermetallic compounds of the type Fe_xAl_y. The formation of these phases starts above the recrystallization temperature of aluminum at approximately 350-400 °C [Bach 2005, Behrens 2011]. The system is characterized with an iron-based solid solution and four non-stoichiometric intermetallic compounds of Fe_3Al, FeAl, Fe_2Al_5 and $FeAl_3$ [Ryabov 1998, Lin 2009, Agudo 2008, Harada 2012, Shahverdi 2002] as it is displayed in the Fe-Al equilibrium phase diagram in Figure 14:

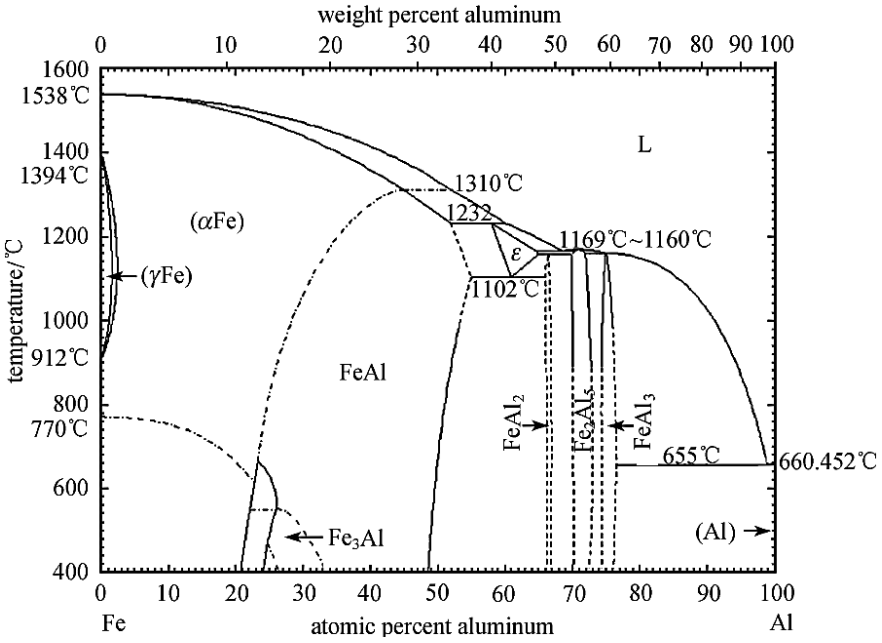

Figure 14. Fe-Al phase diagram.

Physically, four stages involve solid steel-aluminum interaction [Lin 2009, Lu 2009, Temizel 2007]:

- Spreading and wetting of molten aluminum over the surface of solid steel.
- Dissolution of iron into liquid aluminum.
- Diffusion of iron in liquid aluminum and formation of intermetallic phases at the interface.
- Diffusion of Al in the intermetallic compound layer.

Diffusion of iron into aluminum is much faster than vice versa [Tanaka 2010, Kobayashi 2002], this condition is favorable for forming brittle intermetallic compounds in the interface layer [Lee 2006]. With the arrival of iron atoms at an aluminum edge, a solid solution will be formed at first. With longer period of constant arrival of iron at a given temperature the iron content in the solid solution is increased and the Fe_xAl_y phases in the Al-Fe system precipitate from it. $FeAl_3$, Fe_2Al_5, FeAl, Fe_3Al, $FeAl_3$ and $FeAl_2$ phases will successively formed according to the following reactions [Ryabov 1998, Lu 2009, Lee 2006]:

$$5/3\,Fe_3Al + 1/3Fe \rightarrow Fe_2Al_5 \qquad \text{(Eq. 2.5)}$$

$$2/3\,Fe_3Al + 1/3Fe \rightarrow FeAl_2 \qquad \text{(Eq. 2.6)}$$

$$1/3\,Fe_3Al + 2/3Fe \rightarrow FeAl \quad \text{(Eq. 2.7)}$$

$$1/3\,Fe_3Al + 8/3Fe \rightarrow Fe_3Al \quad \text{(Eq. 2.8)}$$

$$Fe_2Al_5 + Al \rightarrow 2FeAl_3 \quad \text{(Eq. 2.9)}$$

The $FeAl_2$ compound is metastable as show in Table 3 and consequently the probability of its formation is minimal at the temperatures of welding, as at increased temperatures is decomposed by the following reaction to stable compounds Fe_2Al_5 and FeAl [Ryabov 1998]:

$$3FeAl_2 \rightarrow Fe_2Al_5 + FeAl \quad \text{(Eq. 2.10)}$$

Table 2 summarizes the composition, hardness, temperature of formation and crystal structures of the intermetallic compounds. The intermetallic compounds present on it are grouped as Fe-rich compounds (Fe_3Al and FeAl) and Al-rich compounds ($FeAl_3$ and Fe_2Al_5). $FeAl_2$, Fe_2Al_5 and $FeAl_3$ compounds, which have a high aluminum composition, is problematic due to their brittleness [Rathod 2004]. Conversely, Fe_3Al and FeAl, which have a high iron composition, may be used as structural materials because of their good wear resistance, oxidation resistance, corrosion resistance and specific strength properties [Chengand Chaur-Jeng 2010]. Therefore, the preferential growth of Fe_3Al and FeAl layers can improve the fracture toughness, oxidation resistance and interface strength of aluminized steel [Chengand Chaur-Jeng 2010].

Table 2. Crystal structure and stability range of the phases formed in Fe-Al binary system at room temperature [Ryabov 1998, Rathod 2004, Bach 2005, Shahverdi 2002].

Type of IMC	Wt% of Al	T (ºC)	Crystal structure	Vickers hardness 9.8(N)
$FeAl_3$ (θ)	59.18	1160	BC monoclinic	772-1017
Fe_2Al_5 (η)	54.71	1160	Orthorhombic	1000-1158
$FeAl_2$ metastable (ζ)	49.13	1165	Triclinic-anorthic	1058-1070
FeAl (β_2)	32.69	1310	BCC	491-667
Fe_3Al (β_1)	13.94	552	FCC	344-368

Additionally, Table 3 shows thermodynamic data for this IMC.

Table 3. Thermodynamic constant for the intermetallic phases form in Fe-Al binary system [Shahverdi 2002].

Type of IMC	ΔH_{298} (J/mol)	ΔS_{298} ($K^{-1}mol^{-1}$)	ΔG_{973} (J/mol)
$FeAl_3$ (θ)	-112560	95.6	-22869
Fe_2Al_5 (η)	-194040	166.7	-19636
$FeAl_2$ metastable (ζ)	-81900	73.3	-16999
FeAl (β_2)	-51240	51	-11090
Fe_3Al (β_1)	-57372	28	-4827

2.6.2 Intermetallic reaction layer

Reaction diffusion is a physicochemical process resulting in the occurrence of a continuous solid compound layer at the interface between initial substances. The term reaction diffusion reflects the most important feature of the layer-formation mechanism, namely, that the layer growth is due to a continuous alternation of the three consecutive steps [Dybkov 2010] that will overrule on the structure and properties of the welded joints:

- Transition of the atoms (ions) of a given kind through the interface from one phase into the other.
- Redistribution of the electronic density of atomic orbitals resulting in the formation of molecules, ions, radicals or other stable groupings of atoms included in a growing compound layer.
- Rearrangement of the crystal lattice of an initial phase into the crystal lattice of a chemical compound formed.

2.6.3 Intermetallic compound layer morphology

According to bibliography, the interfacial layer theorically is comprised of three different regions which goes from rich in aluminum IMC to Fe rich IMC [Lin 2009]: a reaction layer in the welded seam side (I layer) with α-Al and $FeAl_3$ phases [Rathod 2004], a diffusion layer in the center of the layer (II layer) comprised of a Fe_2Al_5 phase and a little of the $FeAl_2$ phase [Temizel 2007], and a diffusion layer in the steel side (III layer) with $FeAl_2$ and FeAl phases [Taban 2010, Tanaka 2010]. The three layers are shown in Figure 15.

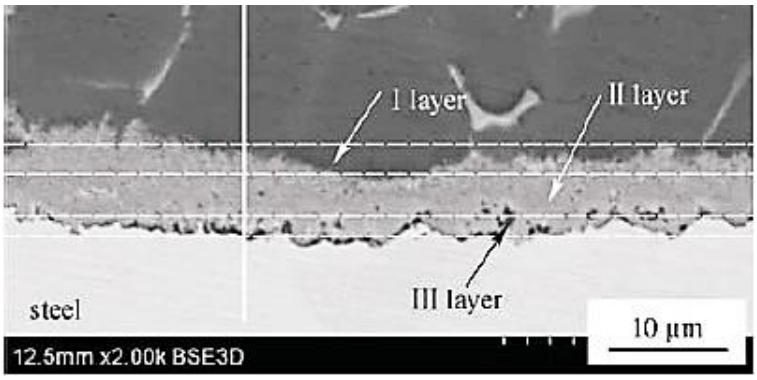

Figure 15. SEM micrograph of the interfacial layer [Lin 2009].

Although there are different possibilities to combine the iron with the aluminum, it is known that above 500 ºC the intermetallic layer consisted of two major phases, Fe_2Al_5 phase the side of the iron material and $FeAl_3$ phase in the side of aluminum material [Lin 2009, Schäfer 2011, Vranakova 2005, Agudo 2008, Tanaka 2010]. The $FeAl_3$ phase firstly forms in the interface of the welded seam/steel due to the highly stable crystal structure, whereas the formation of other phases like FeAl and Fe_3Al is difficult because the lowest contents of Fe atom and its higher formation free energy [Qiu 2010]. Then, the initial layer can inhibit the diffusion of Fe atom into the external liquid metal, while the Al atom can diffuse through the layer and react with the Fe atom in the interface in the steel side, where the contents of the Fe atom are high and the Fe_2Al_5 phase is formed. The large number of aluminum vacancies (30 %) along the c-axis of the orthorhombic structure of Fe_2Al_5 shown in Figure 16, offered rapid diffusion path in [0 0 1] direction to increase growth rate of Fe_2Al_5 which makes a significant contribution to the overall reaction layer thickness [Springer 2011, Tanaka 2010]. Hence, the growth of the intermetallic layer is predominantly governed by this phase.

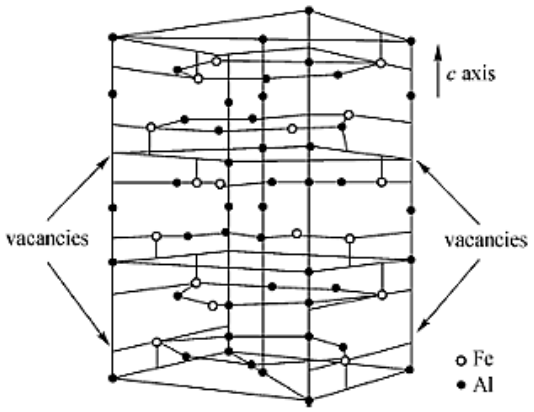

Figure 16. Crystal structure of Fe_2Al_5 [Lin 2009].

Finally, Qiu *et al.* [Qiu 2009a, Qiu 2009b, Qiu 2010] studied the interfacial microstructure of steel/aluminum alloy joints welded by resistance spot welding and observed fine needle-like reaction products in the boundary between the reaction layer and the aluminum alloy and the formation of tongue morphology elements due to the anisotropic growth of Fe_2Al_5 and, showed in the Figure 17 and Figure 18. Other researchers such as Lee *et al.* [Lee 2006], Agudo *et al.* [Agudo 2008], Cheng *et al.* [Chengand Chaur-Jeng 2010] and Wang *et al.* [Wang 2013] saw the same morphology.

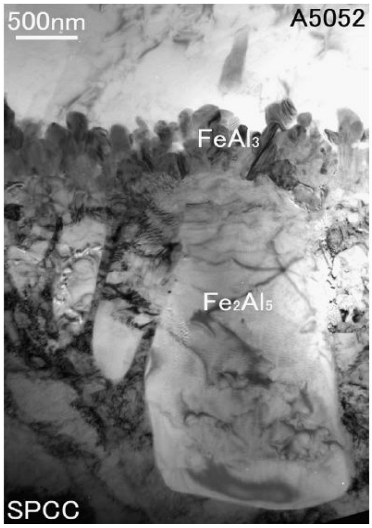

Figure 17. Bright field image taken from the central region of the weld [Qiu 2009a].

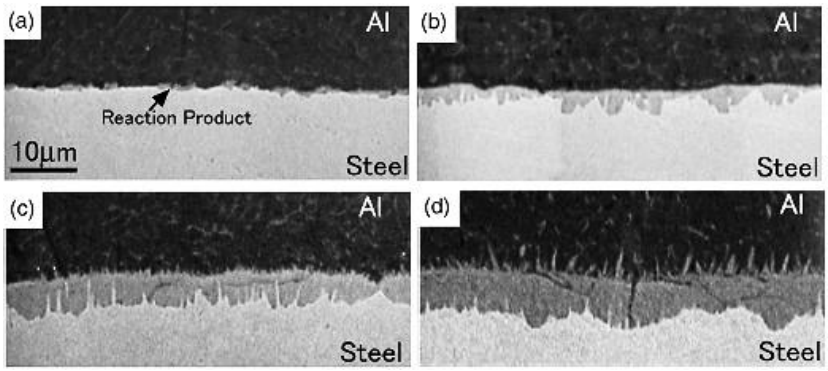

Figure 18. SEM images of the weld cross section at the Al/Fe interface [Qiu 2010].

2.6.4 Growth kinetics of the intermetallic compound layer

In order to determine the growth kinetics of the intermetallic layer Bouayad *et al.* [Bouayad 2003] and Murakami *et al.* [Murakami 2004] investigated the interaction between molten

aluminum and solid iron using immersion tests, and reported that interfacial reaction layer thickness X is a parabolic function of interaction time t and temperature T under constant temperature. Tanaka *et al.* [Tanaka 2010] investigated Fe/liquid Al interdiffusion couples between 780 and 820 ºC for reaction times of up to 600 s using scanning electron microscopy (SEM). Their results clearly show that the phase Fe_2Al_5 layer exhibits parabolic growth behavior, which meant that in the initial stages at least the rate of growth was too high. Finally, Springer *et al.* [Springer 2011] studied the interaction between low-carbon steel/pure aluminum in solid/solid, solid/semisolid and solid/liquid diffusion couples at both 600 and 675 ºC using electron backscatter diffraction (EBSD) using SEM and analytical transmission electron microscopy (TEM) characterization techniques and determined that the total width of the reaction layer is governed mainly by the parabolic growth of the Fe_2Al_5 phase according to equation 2.11:

$$X = K\sqrt{t} \qquad \text{(Eq. 2.11)}$$

and

$$K = K_0 \exp\left(-\frac{E_A}{RT}\right) \qquad \text{(Eq. 2.12)}$$

Here, K is the rate constant of a chemical reaction, K_0 Arrhenius' equation pre-exponential constant, R is the Universal gas constant and E_A is the activation energy for growth of reaction layer.

As intermetallic phases have been found to be detrimental to the properties of joints it is of general interest to limit their thickness at the joint interface [Achar 1981]. According to Achar *et al.* [Achar 1981] and many other researchers, the thickness of the interfacial layer should be controlled to less than 10 μm in order to obtain a sound joint[Qiu 2009, Wang 2012, Springer 2011, Shi 2011, Bach 2005], and therefore the joint strength is more influenced by the properties of the base material than the brittle intermetallic compound layer [Lin 2009, Shi 2011, Behrens 2011]. Nevertheless, when the thickness of the IMC layer remain below 3-4 μm, the embrittlement of these joints is attributed to the formation of Kirkendall porosity rather than the intermetallic compound layer [Rathod 2004, Chengand Chaur-Jeng 2010, Behrens 2011]. The Kirkendall effect is the motion of the boundary layer between two metals that occurs as a consequence of the difference in diffusion rates of the metal atoms leading to a formation of voids at the boundary interface. The material with the higher diffusion coefficient will have a larger associated vacancy flux into it, so the net movement of vacancies will be from the

material with the lower diffusion coefficient into the material with the higher diffusion coefficient. Hence, it is important to clarify the main parameters that influence the growth kinetics of this intermetallic layer for the design and control of high fracture resistant interface.

Effect of temperature

Equations 2.3, 2.4, 2.11 and 2.12 show that temperature has a strong effect in the formation and growth of the intermetallic compound layer. Increase in temperature means an increase in molecules' speed (kinetic energy). So the atoms move faster and there will be more spontaneous spreading of the metals resulting in a quicker diffusion.

The influence of welding temperatures in tensile shear strength of the joint between steel aluminum metal couple was analyzed by Kuroda *et al.* [Kuroda 1999] and later by Shi *et al.* [Shi 2011]. They reported that once the IMC is formed by increasing the temperature in few degrees the thickness of the IMC layer increases exponentially. Regarding to a mechanical properties interfacial increases at the initial stages of the process (T<475 ºC) and remain on a satisfactory level between 500-540 ºC. Maximum strength in the joint is obtained at 525 ºC and with further formation of a continuous layer of this phase, although the mechanical properties quickly deteriorate with further growth of the layer (T>540 ºC). Figure 19 displays the growth of the IMC layer as a function of temperature and the influence of the reaction layer thickness on the tensile strength of the joint.

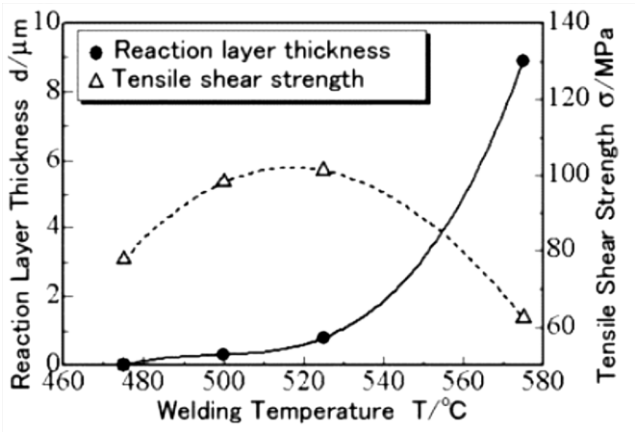

Figure 19. Relationship between the reaction layer thickness, fracture shear strength of the joint and welding temperature [Shi 2011].

Similar results were obtained by Thomy *et al.* [Thomy 2012] in a recent work, when studied the effect of the MIG arc power to join aluminum to zinc-coated steel. They observed that increasing peak temperature (by means of increasing the laser power input) between 700 ºC and 900 ºC the thickness of the layer increased from 7 to 17 µm. These results are in a good agreement with the result obtained by Fan *et al.* [Fan 2011] when joined pure aluminum with steel by laser welding using power inputs in the same range. The dependency of the IMC thickness with temperature is shown in Figure 20.

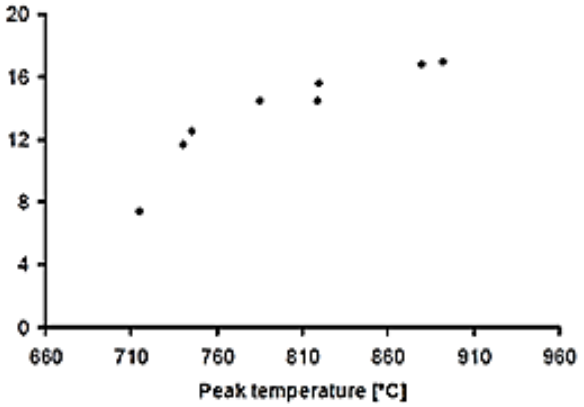

Figure 20. Dependency of the thickness of the IMC on peak temperature of MIG laser [Fan2011].

Regarding to welding speed, Chen *et al.* [Chen 2008] noted that decreasing welding speeds from 120 mm/min to 60 mm/min the thickness of the IMC significantly increased from 7.7 to 58.1 µm. that means that, lower welding speed means higher welding heat input and longer holding time.

Effect of holding time

In addition to temperature, the interfacial reaction layer thickness is also highly dependent on interaction time between the two metals (Eq. 2.11). Zhang *et al.* [Zhang 2009] observed that when diffusion time is short, the concentration of Al atoms at the interface is very small. However, increasing the diffusion time the reaction of Al atoms to Fe happened and therefore, the Fe-Al intermetallic compounds grew further and began to form a continuous layer at the whole interface.

Kumai *et al.* investigated joint strength and interface morphology of steel/aluminum by several advanced high-speed solid-state joining methods, such as magnetic pulse welding and friction

spot welding and noted that long holding times increased the welded area as well as the thickness of the interfacial reaction layer. The main reason lies on the increment of the in time of interaction between the two metals [Kumai 2010].

Rathod *et al.* [Rathod 2004] quantified the growth of IMC layer when welded aluminum AA5052 and low carbon steel for different time conditions. They observed that increasing time from 100 s to 3600 s at a constant diffusion temperature (550 ºC) and pressure (31.5 MPa) the total thickness of the intermetallic layer increased substantially.

Effect of Pressure

Besides temperature and holding time, the pressure plays an important role in interface layer formation. When high pressures are applied, deformation of the superficial asperities takes place which lead to an increased contact area facilitating the heat transfer and thus the atomic mobility [Taban 2010, Rathod 2004, Fan 2011]. In addition to the improved diffusion, the plastic deformation causes the break up of the aluminum oxide film, which generates new and clean surfaces suitable and necessary for joining [Harada 2012]. Rathod *et al.* joined low carbon steel with aluminum using laser roll welding and found that, with constant diffusion temperature (600 ºC) and time (100 s), an increase in pressure form 15.75 MPa to 47.25 MPa caused the growth of the IMC layer thickness from 37 µm to 59 µm [Rathod 2004]. Same tendency was observed by Sahin [Sahin 2009] when joined aluminum to stainless steel by friction welding.

When diffusion temperature was constant and pressure was increased, incubation time for formation of the interface layer was reduced. With constant diffusion time, an increase in pressure caused formation of the interface layer at lower temperatures. Finally, when the diffusion temperature and pressure were constant increasing the interaction time thickness of the intermetallic layer increased. Thus, there is the combined effect of interaction time, increased contact area due to pressure and increased atomic mobility due to high temperature.

CHAPTER 3

GENERAL METHODOLOGY

In this chapter, working methodologies followed to accomplish the objectives of this work are fully described, including materials, equipment, process parameters, experimental procedures and methods of analysis.

3.1 Introduction

With the aim of developing thixo transverse forging process for the production of steel aluminum hybrid structures, a serial of forming experiments will be performed in next chapters. The objective of the experiments is first to select the optimum forming parameters and second to understand the fundamental reactions that govern the phase formation and evolution at the interface between steel and aluminum alloys; especially in temperatures of the semisolid range of Al.

Regarding to its applicability in the automotive sector, mechanical properties of the component will be analyzed from a much closer perspective to the industrial reality, where, besides the mechanical properties, it is of high relevance to determine the internal and external quality of the components. In this sense, besides the mechanical characterization, it will be conducted a thorough metallographic analysis of the parts and joint by diverse techniques such as, optical microscopy, visual inspection, X-Rays and scanning electron microscopy.

The chemical analysis of those interfacial layers will provide the information needed to understand the role that different coatings applied in the steel tube and alloying elements in the aluminum play in the formation and evolution of intermetallic phases. As a result, more scientific and technical knowledge of the relationship between processing parameters the mechanical properties (strength, fatigue, etc.) and interface formed between dissimilar materials.

3.2 The forming part

3.2.1 Weight reduction in the vehicle

Nowadays, the focus of lightweighting has shifted towards vehicle components such as, chassis, body, suspensions or power train parts (engines, gear boxes and transmissions). These parts are traditionally distributed between: steel forged parts for high mechanical property requirements, cast iron or stamped parts for lower cost parts and aluminum alloy parts for lightweighting.

The current dissertation is focused on the weight reduction in the front axle of segment C vehicles (medium compact size) by the integration of a thixoformed aluminum part over the steel frame. Segment C vehicles will remain similar to the current architecture for the next 15 years with front-wheel drive, where wheels will be powered by an internal combustion engine (gasoline or diesel), and depending on the car model combined with an hybrid electric motor. Thus, the combustion engine configurations supported on the front axle are maintained, along with a nondriver rear axle.

Axles are an integral component of most practical wheeled vehicles. In a live-axle suspension system, the axles serve to transmit driving torque to the wheel, as well as to maintain the position of the wheels relative to each other and to the vehicle body. Figure 21 shows an example of segment C vehicle front axle of a top range BMW car:

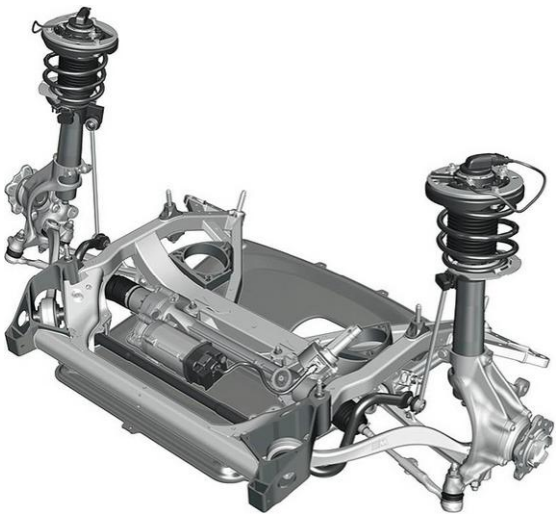

Figure 21 . Example of front axle in top range BMW [European Aluminium Association 2013].

Front axles that currently exist in the C segment are mainly steel (over 85%), so the development of a hybrid structures combining steel with aluminum (used in top range vehicles), maintaining economic criteria in its design and performance requirements (durability, corrosion resistance, crash, etc.), could be very well received by European manufacturers. With developments that arise, the potential weight reduction of these axles could be up to 40% compared to a similar axle made of steel that will minimize the unsprung mass of the vehicle.

The application of aluminum with steel delivers immediate results in the responsiveness of the suspension and steering systems. The lower the weight that has to be moved, the easier it is to control. At the same time, light structures are so stable that the front wheels always have optimum traction on the road surface, thanks to the highly rigid diagonal front axle sub-frame which also carries the steering gears, track control arms and push bars, as well as the anti-roll bar.

Compared to other traditional solutions the fabrication cost of hybrid sub-frames can be reduced by the application of properly designed high quality aluminum components (reduction of assembly cost by part integration). Furthermore, the elimination/reduction of assembly joints improves the overall performance of the sub-frame. The possibility to assemble the hybrid sub-frame separately from the rest of the vehicle facilitates its integration into a steel or mixed material car body.

3.2.2 Part design

The engine cradle is an important structural element from the front axle of the vehicle which is manufactured in steel and, thus, an interesting candidate for lightweighting. The purpose of the front cradle is to provide structural support for various subsystems of the car such as, engine, drivetrain or suspension. The structural functionalities of axle sub-frames, such as the front cradle ask for fairly complex geometrical shapes and the need to integrate different attachment points. Consequently, the potential of the aluminum extrusion technologies and the various high quality aluminum casting methods for the integration of additional functions into a structural part must be fully exploited. An interesting variant of design which also meets its performance requirements is a bimetallic steel aluminum structure shown in Figure 22.

Figure 22. Bimetallic engine cradle.

In this bimetallic engine cradle steel tubes are applied instead of the aluminum extrusions [European Aluminium Association 2013]. During the casting process for the bimetallic cradle, aluminum is injected into a die which already contains the steel cross members. The process produces a mould over the tube ends. The differential in coefficient of thermal expansion between steel and aluminum creates a shrink fit at the joint. In addition, an anti-rotation feature ensures that no separation can occur between the steel and aluminum components. The achieved weight reduction compared to steel is about 10 kg or 30 % (combined with a drastically reduced number of parts).

The geometry selected as a demonstrator for this work is a component of the front cradle called left front cradle mount middle (LCM). The purpose of the mount middle is to join this sub-frame to the main structure of the car, (Body in White), by means of bolted joints. Special attention should be devoted to the component's critical cross section (in terms of external loads of stresses), proper die design and process parameters optimization. Looking at the functional requirements, the component is subjected to fatigue loads, impulsive and crash loads; therefore it is important to guarantee minimum mechanical properties of the material with high reliability.

In order to produce sound, high quality components, optimization of the filling ratio is necessary. Low filling ratio might cause pre-solidification of the semisolid metal in the die resulting in defects such as porosity, cold shuts, etc. Thin machining allowance is also required in order to exploit completely the near net shape capability of process transformation at semisolid state. This aspect is important for minimizing the cost for obtaining the finished component, ready for assembling. Figure 23 shows the reference geometry proposed by the car manufacturer:

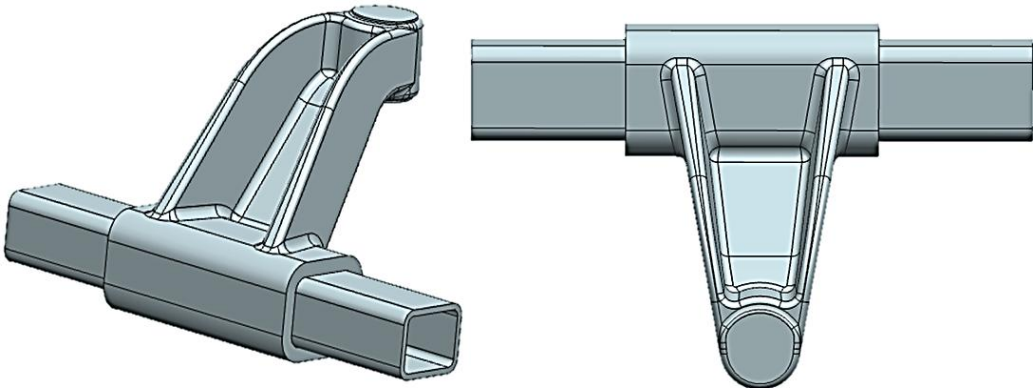

Figure 23. CAD drawing of the original hybrid left front cradle mount middle.

However, the transfer from one technology to another is never straightforward, it is necessary to: 1) resize of the existing component in order to make it suitable for the thixoforming process and 2) a geometry redesign. It is of course necessary for the redesign to keep connecting and functional dimensions unchanged. In the case of the LCM represented in Figure 24, the aluminum body is modified by increasing the total section width which simplifies significantly the mold design (section 3.3) by changing the partition line of the part. In order to obtain a laminar flow of the semisolid material and prevent tool deterioration the number of sharp edges has been reduced to a minimum. Part redesign can take advantage of the enhanced freedom in part design that is offered by thixoforming.

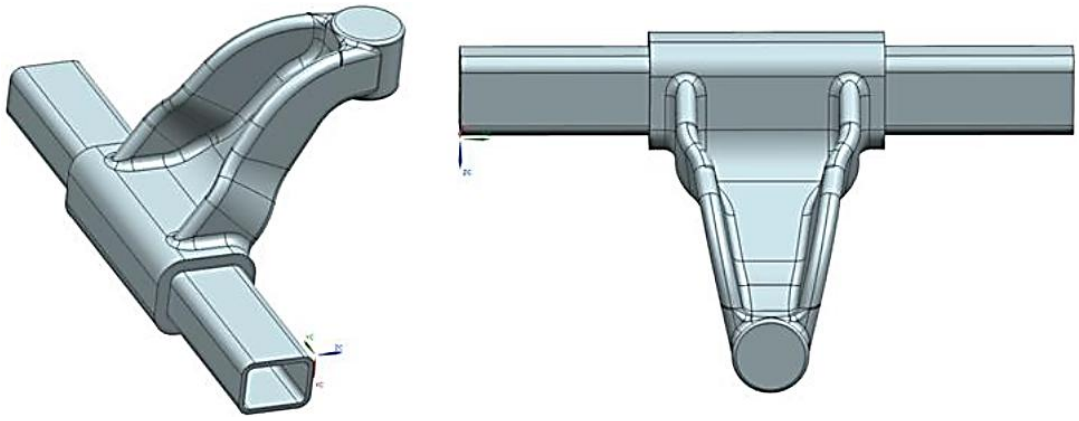

Figure 24. CAD drawing of the redesigned hybrid left front cradle mount middle.

The resulting redesign does not modify heavily the reference geometry and will allow exploiting at maximum the process capabilities. Furthermore, the proposed design allows reducing the assembly cost as the part forming and structure joining occurs in a single punch stroke.

Conversely, the performed modifications increased the total weight of the reference LCM in only 20 grams.

The estimated **weight reduction** of the new design compared to the existing commercial steel solution, which includes several stamped parts joined by several welded joints, **is approximately 35-40 %**. The choice of the mixing a thixoforged aluminum part over the steel frame is guided by the intention to limit the number of joints.

Currently this component is not produced industrially neither used in any commercial car; nevertheless this geometry allow testing the mechanical properties of the hybrid structure (chapter 5) as well as to study the intermetallic compounds formed from the interaction between steel and aluminum (chapter 6).

3.3 Mold design

The design of forming dies involve careful consideration of some guidelines or rules such as, dimensional tolerances between the punch and die, avoiding of sharp corners and rapid change in cross sections, undercuts, contraction of aluminum, etc. Furthermore, the punch must be designed to maximize the pressure exerted in the joining zone in order to avoid the apparition of pores or discontinuities along the joint. Figure 25 shows the CAD drawing of the molds for the left front cradle mount middle:

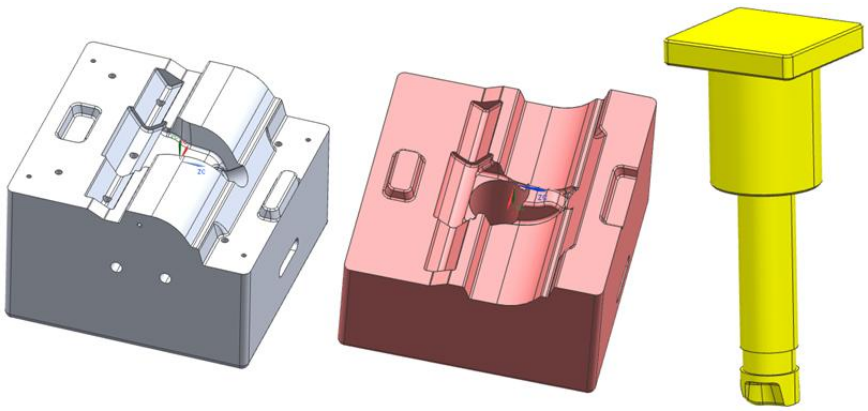

Figure 25. CAD drawing of the mold and punch

The constructions of the molds have been performed by MUVELASA S.L.:

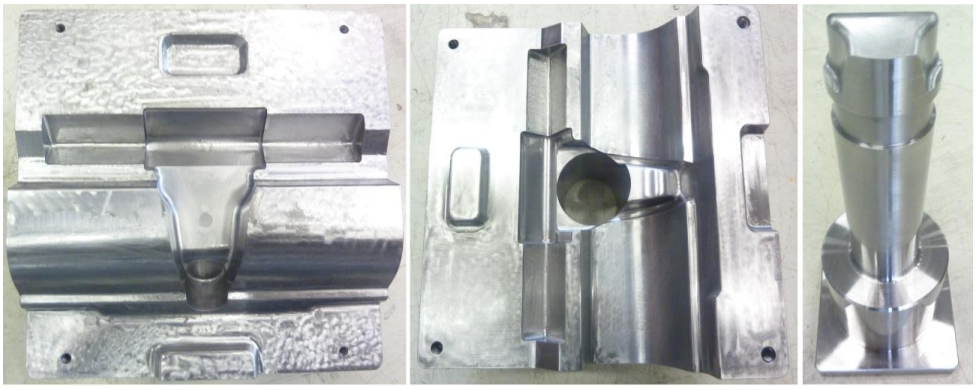

a) b) c)

Figure 26. a) Lower die, b) Upper die, c) Punch.

The dies and punch were made of Orvar Supreme® supplied by Uddeholm; a Cr-Mo-V alloyed H13 hot work die steel, as the tools will be subjected to high mechanical and thermal fatigue stresses, e.g. die casting dies, forging tools and extrusion tooling. For the rest of the components such as, ejector pins lower grade steels as the F-1140 have been used.

3.4 Forming process and thixoforming cell

Due to the demands involved in semisolid forming and the narrow thixoforming windows of some aluminum alloys, the use of a semi-automated thixoforming cell is strongly recommendable, since little variations in the process, material reheating, handling of the billet, etc. can have a huge influence on the final result.

In order to meet the required reproducibility of the forging process an integrated automation of the production cycle has been introduced in the thixoforging cell available at MGEP, which consists of an induction unit, a forming tool and a servo-mechanical forging press as shown in Figure 27.

Figure 27. Overall view of thixoforming cell for hybrid structures.

3.4.1 Induction heating

Heating of the billets to the semisolid state is a critical stage, mainly because it defines the microstructure and flow behavior of the material. The temperature distribution inside the slug must be as homogeneous as possible to enable a uniform distribution of the liquid fraction through the billet volume. In the case where the solid fraction is very large, the fluidity of the alloy may not be sufficient and may cause filling problems. In contrast, if the solid fraction is too small, in addition to cause a turbulent filling, material losses can occur and handling of the billet can be complicated [Azpilgain 2006]. In addition, the heating schedule must be such that, whilst achieving the above requirements, the time-temperature curve should be as short as possible since the heating operation regulates the process productivity.

In forging industry, the most used heating devices to reheat thixoforming feedstock are induction furnaces due to the shorter heating time and flexible process control. For thixoforming it is mandatory to reach the process temperature as quickly as possible in order to avoid unwanted grain coarsening and to keep the risk of scaling.

3.4.1.1 Induction heating for thixoforming

To obtain an adequate globular structure as well as the correct filling of the dies, the following requirement must be fulfilled [Hirt 2009, Behrens 2011]:

- The heating must be as fast as possible to avoid an excessive growth of globules but ensuring that the material surface does not start melting too early promoting liquid pooling and the so called "run off" [Kirkwood 1994]. Furthermore, since it has to be as economic as possible, a fast heating is crucial.
- Be precise in order to be able to reproduce the desired liquid fraction. It has to be a very accurate process due to the narrow thixoforming window of some alloys.
- Be homogeneous throughout the billet. The temperature distribution throughout the material has to be as homogeneous as possible to obtain an acceptable liquid phase in every section of the billet. It can be monitored with direct measurements obtained from thermocouples during trials, but it is not possible to monitor under production. This means that the heating has to be made in an unsupervised way by application of previously proven heating cycles [Behrens 2011].

Induction reheating starts with a quick heating while the material remains solid, followed by a power decrease when it starts melting. The objective of this power decrease is to achieve a homogeneous temperature throughout the billet reducing the skin effect generated by Eddy currents. During this stage, radiation losses must be compensated while the heat is transferred into the billet by conduction.

If enough power is not supplied to compensate radiation losses, the surface can start to solidify. When this happens, a solid skin of various millimeters is created on the surface. In any case, the control of the process and the heating parameters depend on the means at our disposal.

3.4.1.2 Induction unit

The system used in this work is a low frequency vertical heating equipment (<200 Hz) that allows deeper penetration of the current and therefore faster and more homogenous heating up of the billet to the semisolid range (Figure 28). The system is equipped with an electrolytic copper coil; $Ø_i$=100mm and h=100mm.

a) b)

Figure 28. a) Equipment used for the induction heating of the billets b) Induction coils.

3.4.1.3 Control of the heating process

The thixoforging process is carried out within a small temperature range between the solidus and the liquidus temperature. Therefore, an exact controlling of the heating process is necessary which can be realized by different methods. All of these methods use the part's temperature as an indicator for the proportion of the liquid phase to the solid phase in the microstructure.

One the most common method is measuring the inductivity changes of the heated part. The method is based on the changes of the magnetic and electric properties that occur during the heating process. The changes can be used to determine the state of the material during heating. This variation occurs both in solid state as in liquid state, and is distinguished by abrupt drop in the inductance at the beginning of the melting phase. However this method has the main disadvantage in the difficulty to measure the losses of heat energy through radiation and convection [Gräf 2000].

Other researchers such as Behrens *et al.* [Behrens 2011] introduced an approach to conduct an unsupervised heating process by application of heating curves that were optimized with a fuzzy-logic controller. The main advantages of the fuzzy logic based approach are that no specific material data is required, system specific properties such as the efficiency have not be explicitly determined, and that the practical implementation can be done with a minimum of experimental work. This can be a good way to control the heating cycle in an industrial environment, where

due to technical restrictions, temperature measurements, especially inside the billet, are difficult to conduct.

Another way to at least measure the billet´s surface temperature is the one proposed by Schönbohn *et al.* [Schonbohm 2006] based on a radiation pyrometer. The accuracy of the pyrometer mainly depends on the exact knowledge of the radiation coefficient. Usually, it is roughly known and changes from billet to billet and during the course of heating owing to scale formation, for example, leads to wrong measured values. As the measured temperature is not necessarily close to the real value, the control scheme cannot rely on the pyrometer directly.

Finally, the simplest method to measure the temperature is the direct measure of the temperature using thermocouples. It also lets you control the temperature uniformity of the billet arranging multiple thermocouples at different areas of the workpiece (Figure 29). Placing thermocouples to each piece is the main drawback, especially in the case of an industrial process.

In this work, since the tests presented in this dissertation are laboratory scale experiments, it was decided to control the heating step using four K type thermocouples as Azpilgain *et al.* [Azpilgain 2006] made before.

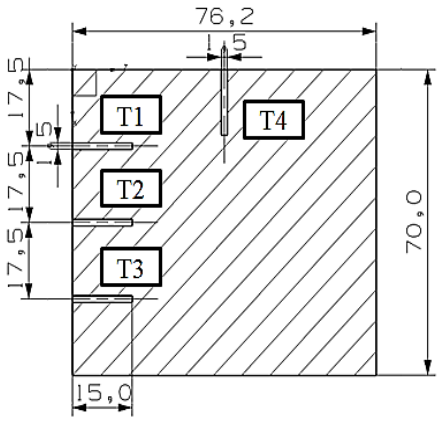

Figure 29. Thermocouple´s location into the billet during heating.

3.4.2 Transfer of the billet

The transport of the billet from the induction furnace to the forming tool is another critical step. The approximation to the billet must be as fast as possible in order to avoid premature cooling and to minimize the cycle time. During this transfer heat losses in the material are unavoidable and have to be minimized because they increase the solid fraction, especially on the billet

surface, and consequently the forming loads. To compensate these heat losses, which can be big enough depending on the billet size, temperature in the reheating step can be raised a little bit more [Rassili 2010].

As in the heating stage, the minimization of oxides is also important, since the increase of the friction coefficient affects the material flow during forming, spoiling the properties of the final product. Due to this, in order to achieve the required reproducibility of transfer and handling operations, robots are necessary [Lozares 2014]. Depending on the cell´s automation degree, more than one robot could be required. In any case, in hot forging industries billet cutting and introduction into the continuous heating device is made by different handling systems. Once the billet has reached the forging temperature, a robot is used to make the transfer to the forming zone. A second robot located in the forging area could transfer the part from one step to the other and, finally, to the evacuation or heat treatments zones. However, this is usually made by a person because the forged part is not always ejected in the same place and the robot is not able to pick the part and put it in the next step.

3.4.3 The servo-mechanical press

The press available at MGEP is a Fagor SDM2-400-2400-1200 4000 kN servo-mechanical press. The mechanical servo-drive press offers the flexibility of a hydraulic press (infinite ram speed and position control, availability of press force at any ram position) with the speed, accuracy and reliability of a mechanical press [Osakada 2011].

Because all the press motions such as starting, velocity change and stopping are done only by the servo-motor, the mechanical servo-press has a simple driving chain without any flywheel, clutch and brake which are essential for a conventional mechanical press, and thus, the maintenance of the servo-press is simplified.

However, servo-motor driven mechanical press employed in this research work has a disadvantage compared with a hydraulic press. It has a reduction by means of a gear and transmits the movement from the motor to the crank. Due to this, the nominal press capacity is not available at any ram position (it depends on the crank angle). Nevertheless, this can be easily compensated by the stroke adjustment which allows locating the upper ram in the right position to work with the nominal press force.

The most important feature of the servo-press is the flexible ram movement. In fact, the flexibility to perform a wide range of working cycles is what makes it suitable for semisolid

forging. The main characteristics of the press used in this dissertation were summarized in Table 4.

Table 4. Characteristics of Fagor SDM2-400-2400-1200 4000 kN servo-mechanical press.

SERVO-MOTOR DRIVEN MECHANICAL PRESS	
Press capacity (kN)	4000 at 20 mm from the BDC
Number of points	2
Working torque Max / Nominal (N.m)	5500 / 3000
Max stroke (mm)	400
Max ram speed (mm/s)	800
Die height (mm)	1000 to 1200 (str 400mm)
Stroke adjustment (mm)	200
Table size (mm x mm)	2400 x 1200
Max cadence (spm)	100
Die cushion capacity (kN)	400
Die cushion stroke (mm)	100
Motor power Maximum / Nominal (kW)	450 / 250

Taking into account the geometry of the forming parts as well as the press limitations, it has been decided to carry out the forming stage by thixo lateral (or transverse) forging Figure 6. The forming velocity is of the same order of magnitude and it is characterized by squeezing the semisolid material into an already closed die, thus eliminating any possible material ejection. To make this possible and in order to use all the force capacity of the press during forming, Lozares [Lozares 2014] designed a special tool that has been used in this dissertation (Figure 30).

3.4.4 The forming tool

Four hydraulic cylinders, located at the upper die holder give the closing force by clamping the wedges of their rods in the holes of the columns opposite them. Thus, the columns will be tensioned with the desired force, which is in turn the die´s closing force. This system is able to provide a maximum die closing force of 1200 tons. Once the component is formed and the ram is up, two lateral cylinders open the die and the expulsion system ejects the part.

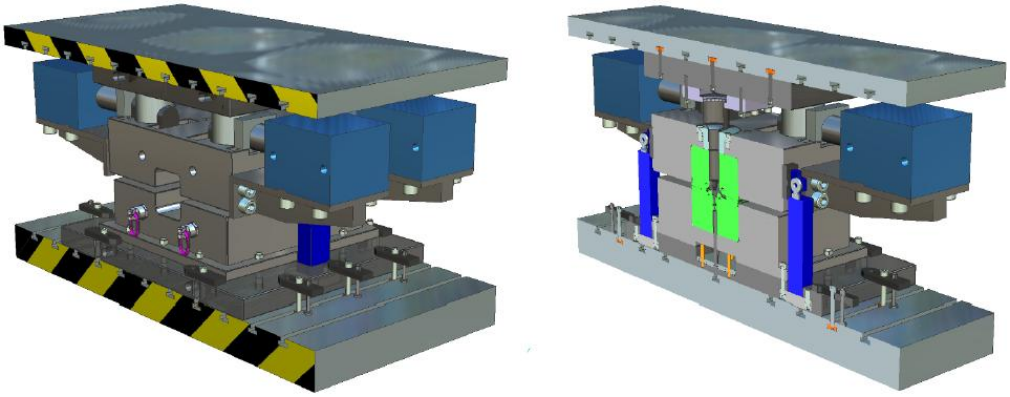

Figure 30. CAD design of the forming tool.

3.4.5 Forming step

The semisolid forming stage, which requires a special movement of the ram, is made by high-speed presses that can be hydraulic or mechanical [Azpilgain 2008]. The approximation to the billet must be as fast as possible in order to avoid premature cooling and to minimize the cycle time. Once the forming tool gets in contact with the semisolid material, the speed should decrease significantly to prevent liquid ejections. An arrangement between high and low speed has to be always maintained since a high speed entails high shear rates and low forming loads, but also, possible liquid ejections and turbulent die filling that can generate defects on the finished component. On the other hand, low ram speed avoids those defects and makes a better flow of the material during die filling possible; but it promotes unexpected cooling during forming with its subsequent problems and larger cycle times.

Finally, when the die is filled, the solidification of the liquid phase starts, and pressure should be increased and maintained until it finishes completely in order to prevent shrinkage problems.

3.4.6 Overall coordination of the forming cell

The heating and forming processes are performed independently on dedicated hardware, so that changes conducted at these components do not affect the sequence control of the production cycle. The production cell is sealed with railings and equipped with a door which must be locked to keep the cell working. Once it is opened everything stops, and for security reasons, clearance has to be given manually to all working devices. A person is needed to place the steel tube on the lower die (Figure 31) and the aluminum slug on the furnace pedestal (Figure 28). Once reached the forming temperature the billet is transported to the forming tool. Finally the

final part is removed from the die (Figure 31). The operator thus opens the door in every cycle, making manual clearance compulsory before each forming cycle.

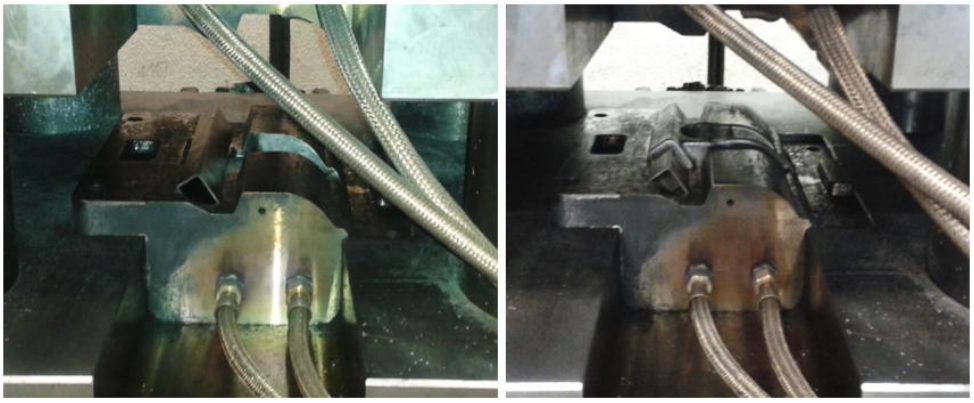

Figure 31. View of the die before and after forming process.

3.5 Analysis methods

To determine the effect of the most influencing parameters in the final properties of the component, a complete metallographic characterization has been conducted by techniques such as, optical microscopy, visual inspection, X-Rays and scanning electron microscopy. The methods of analysis used will provide information on the external and internal characteristics of the components.

3.5.1 Visual inspection

Visual inspection is a common method of quality control. Visual examination should be performed prior to any required non-destructive test (other than specific in-process tests) and shall provide examination of the surface for compliance with the applicable requirements of specified nondestructive tests, which will subsequently be performed. The inspection was performed all of raw human senses such as vision, hearing, touch and/or any non-specialized inspection equipment. Other non-destructive inspections requiring ultrasonic, X-ray equipment, infrared, etc. are not typically regarded as visual inspection as these inspection methodologies require specialized equipment, training and certification.

3.5.2 Metallographic analysis

The properties of the hybrid structure are highly dependent on their microstructural characteristics: grain size, phase distribution, phase composition, etc. Microscopic examination is an extremely useful tool in the research and characterization of these parts. Once the external inspection is done, to get further information on the quality of the body and the joint some samples were taken. The metallographic cuts were performed as displayed in Figure 32 and Figure 33:

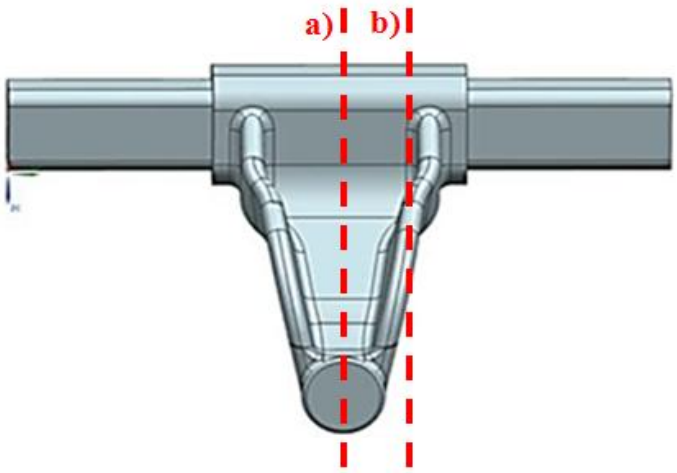

Figure 32. Position of the sections cut.

The joining zone was cut in different sections as indicate the dashed lines a) or b). Moreover, when the structure is cut in two halves (line a)) the inner part of the joining zone is accessible for its visual inspection. On the other hand, to analyze the body of the LCM samples were taken from the joint (A), the center (B) and the head (C) as indicated in Figure 33.

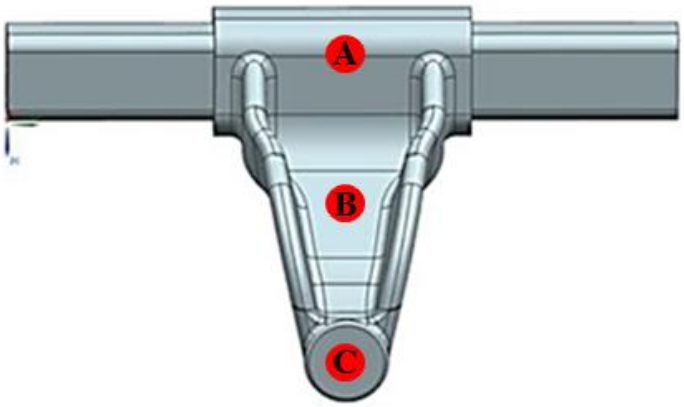

Figure 33. Schematic view of the analyzed sections.

The cross sectional area of the samples intended for microstructural analysis were prepared by grinding and polishing with standard metallographic techniques.

Obtained cross sections were investigated using a Leica DM IRM optical microscope (OM) and an EOL JSM-5600LV electron scanning microscope (SEM). Average values of reaction layer thicknesses were determined following same procedures as Springer in his dissertation [Springer 2011]: The cross sectional area of the reaction layer was measured over a reference distance; dividing this area by the length of the base line yielded the average thickness. The SEM is equipped with an energy dispersive X-ray spectrometer (EDS) that was used in the characterization. Element mapping and line scanning profiles of the interfacial cross samples were analyzed by SEM/EDS, to observe the preferential location of different elements in the reaction layers.

In line scanning, the electron probe is written in a line across an area of interest on the sample obtaining a graph that represents the number of X-ray quanta being counted (roughly the amount of element present) Vs the spatial location along a line. In this way, for example the diffusion profile of elements at an interface can be plotted as shown in Figure 34.

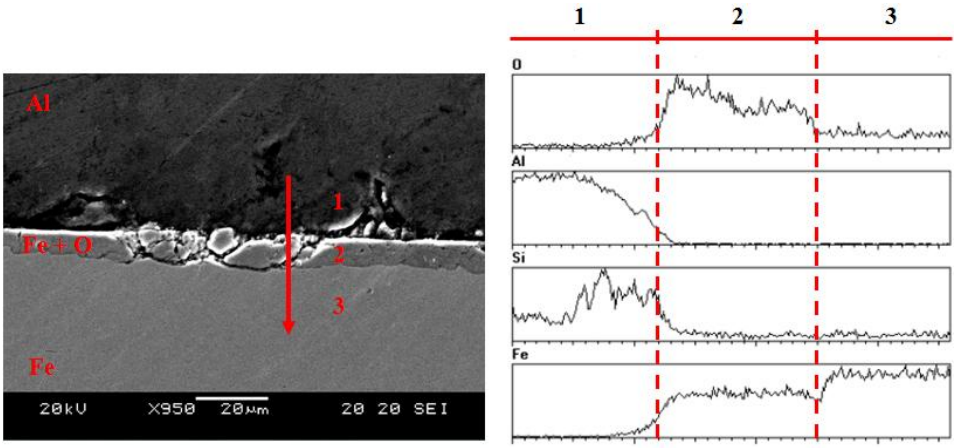

a) b)

Figure 34. a) SEM micrograph of the cross section and b) EDS line-scan analysis.

3.5.3 Mechanical characterization tests

The mechanical validation of the structure involves the fulfillment of two conditions:

- The vertical stiffness for a static load must be at least 5.5 kN/mm.
- Permanent deformation of the ensemble must be less than 1 mm for a static load.

To determine the strength of the joint and the component 3 tests defined by CIE Automotive were carried out. First one is a tensile test, where load is applied in Z axis with a rate of 2 kN/s up to the failure of the component or till reach the maximum load of the bench (25 kN). If the component experiments any plastic deformation during the tensile test a recovering test is performed. In the recovering test, the part is submitted to a load of 4.7 kN that is maintained during a specific time (40 seconds in this case) and then force is removed. Finally, to estimate the lifetime of the component all parts were tested under fatigue with a senoidal curve up to 4.7 kN and a frequency of 5 Hz. 1.2·106 cycles have been considered as infinite live. All tests were performed on MTS servo-hydraulic testing machine from CIE Automotive. The components were gripped to the bank by 3 points. Both ends of the steel tube 2 were tied by means of clamps and the head of LCM was fastened to the hydraulic actuator through a bolted joint. This clamping system ensured a rigid assembly and good transmission of loads from the actuator to the component. Figure 35 and Figure 36 show the experimental set up used for the mechanical characterization of the component:

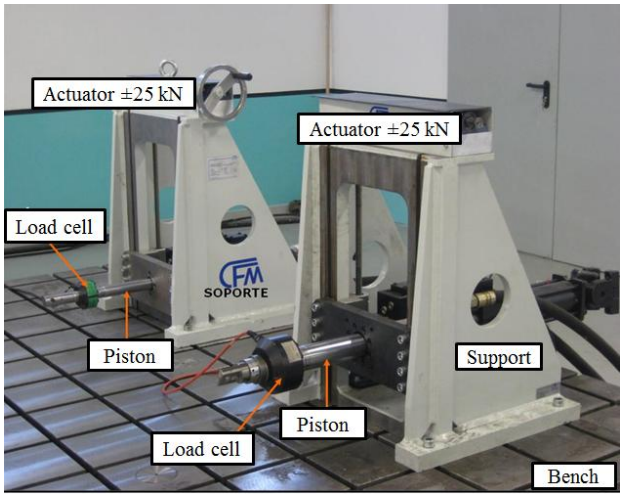

Figure 35. MTS servo-hydraulic testing machine from CIE Automotive

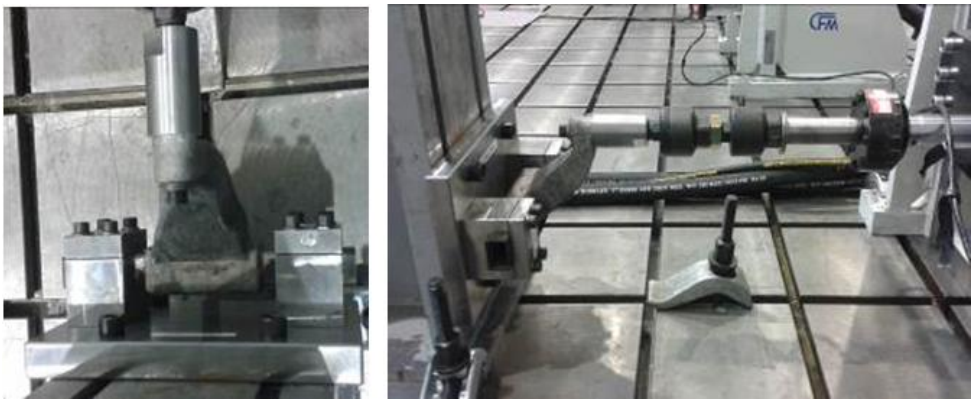

Figure 36. Experimental set up for the mechanical characterization of the component.

3.6 Material selection

Among commercial aluminum casting alloys those with silicon as the major alloying element are the most important, mainly because of their excellent casting characteristics. Aluminum-silicon alloys that do not contain copper additions are used when good castability and good corrosion resistance are needed. Mg_2Si precipitates after a heat treatment and therefore the strength levels are increased; these alloys are known as precipitation hardening alloys or high strength heat treatable alloys [Sajjadi 2011, Sajjadi 2012]. Due to their excellent castability and good strength-ductility ratio, AlSi7Mg (0.3-0.4) A356, and AlSi7Mg (0.45-0.7) A357 are both standard alloys for light metal cast components. These alloys solidify in a broad temperature interval (≈555 ºC-615 ºC) and thus, are also suitable to process in the semisolid state.

The aluminum thixoforming process requires billets with an excellent geometry: flat and perpendicular extremities along with a very good cylindrical surface. The diameter tolerances must be the minimum possible within the batch with the minimum variation among batches. These parameters are essential to ensure precise and reliable induction heating. The aluminum feedstock billets used in this work were supplied by the company SAG (Austria) in cylindrical bars of Ø=76.2 mm and 3000 mm length already presenting globular structure that is obtained by electromagnetic agitation during the solidification process. The overall composition of these alloys is shown in Table 5:

Table 5. Chemical composition of the aluminum alloys.

	Chemical composition (wt %)							
	Si	**Fe**	**Cu**	**Mn**	**Mg**	**Zn**	**Ti**	**Al**
A356	6.5-7.5	0.15 Max.	0.05 Max.	0.10 Max.	0.25-0.40	0.05 Max.	0.2 Max	Balance
A357	6.5-7.5	0.15 Max.	0.05 Max.	0.10 Max.	0.40-0.70	0.05 Max.	0.2 Max	Balance

However, in rough-cast state the α-Al particles of this kind of thixotropic materials provided by SAG are not entirely globular (Figure 37 (a) and Figure 37 (f)). Heating up to semisolid temperature and subsequent homogenization produces the optimum globularization of particles. Figure 37 shows the evolution of α-Al particles during isothermal treatment at 580 °C, corresponding to 50 % of solid fraction. Figure 37 also shows that excessive heating time results in an undesirable growth of grains, which can affect the rheological behavior of the material [Azpilgain 2006].

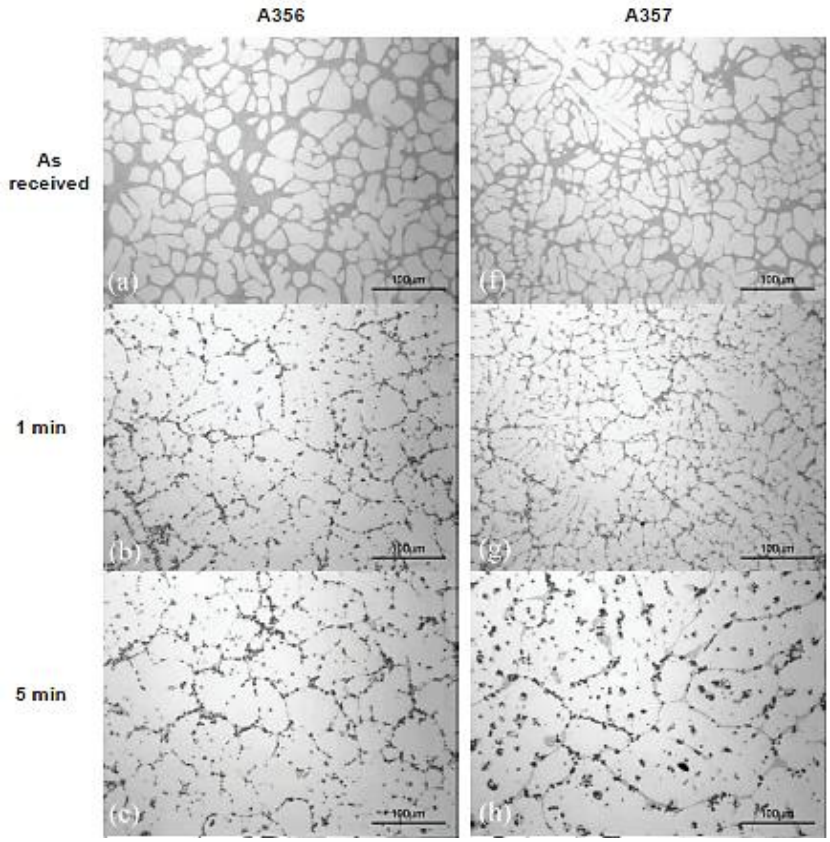

Figure 37. Microstructural evolution of semisolid alloys A356 and A357 according to the temperature; (a) and (f) wrought material. All other figures are for specimens that remained in semisolid state (580ºC) for 1min (b) and (g), 5min (c) and (h), [Azpilgain 2006].

On the other hand, the insert selected was a S355J2H quality structural steel tube with yield strength 355 MPa. This steel is widely used in general metal, civil engineering and bridge engineering as well as for water engineering, vehicle construction and mechanical engineering. The tubes were manufactured by Grupo Condesa according to the standards EN 10219 and EN 10210 with rectangular section of 40 x 30 x 295 mm and 3 mm thickness. Table 6 shows the chemical composition of this material:

Table 6. Chemical composition of the steel tube.

Chemical composition (wt %)											
C	**Mn**	**Si**	**P**	**S**	**Nb**	**Ti**	**V**	**Mo**	**B**	**Al**	**Fe**
0.06	0.49	0.01	0.015	0.009	0.0043	≤0.005	≤0.01	≤0.01	≤0.001	≥0.026	Balance

Two different temperatures have been used for steel inserts: ambient temperature and 300 °C. The tubes were preheated in order to minimize the thermal shock between the steel insert and aluminum, thus the cooling of aluminum is slower and the contact time between the two metals at high temperatures is extended. This improves the adhesion between steel and aluminum since the higher the interface temperatures interface the higher the diffusion rate is.

During the compaction of the material a severe plastic deformation of the tube was expected as the punch that was designed to maximize the pressure in the joining zone between aluminum and steel insert. They were introduced steel bumpers with different section thicknesses as shown in Figure 38 (1: 15 x 30 mm; 2: 20 x 30 mm and 3: 25 x 30 mm) over the whole length of the steel tube to control the plastic deformation generated in the tube and therefore the aluminum necessary to fill the die will be always the same.

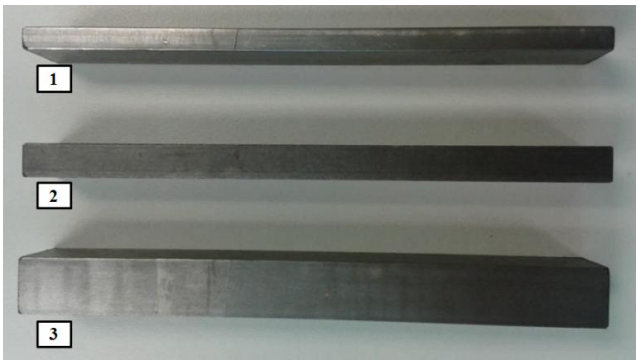

Figure 38. Steel bumpers.

3.7 Surface treatments

When left unprotected, steel will corrode in almost any environment. Different surface treatments such as zinc and aluminum are applied in the steel tube prior to forming in order to keep the surface clean as mentioned in section 2.5. In addition, the effect of each treatment in the formation of intermetallic phases in the reaction zone is studied in chapter 6.

3.7.1 Raw steel tubes

This surface corresponds to the steel tube as received from the manufacturer (Figure 39):

Figure 39. Steel tubes as received.

The surface was characterized by means of SEM/EDS as shown in Figure 40 and Figure 41:

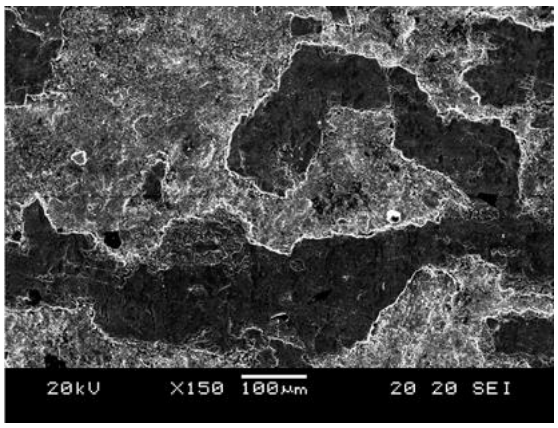

Figure 40. SEM Micrograph of the insert surface.

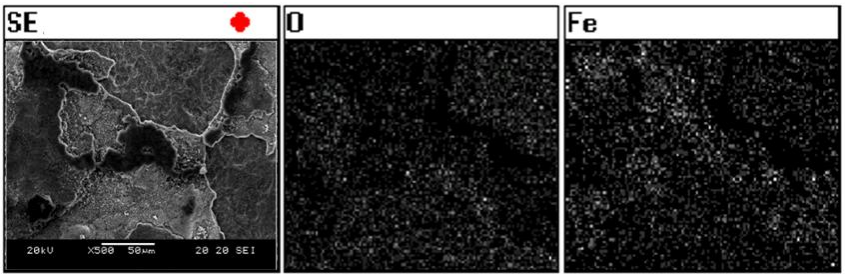

Figure 41. SEM/EDS results of insert surface.

In the SEM/EDS micrographs, it is clear that most of the surface is covered with iron oxides. Elemental mapping performed on the sample reveals that the interface layer is composed mostly of iron and oxygen. Both seem to be evenly distributed along the surface. In order to determine the phases formed on the surface, higher magnification micrographs of the sample were taken:

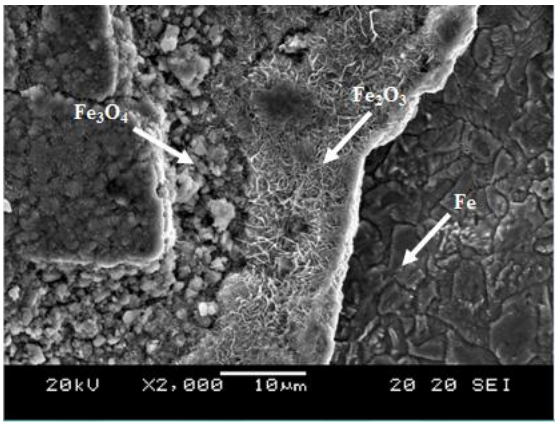

Figure 42. High magnification SEM image of the steel tube surface.

High magnification SEM images obtained in Figure 42 revealed that the surface of the steel insert is comprised mainly by three phases. According to Bigham *et al.* and Maeciuš *et al.* these phases are probably Fe_3O_4 identified by its characteristic granular structure, Fe_2O_3 associated with the acicular structure of the central region, and finally, on the right oxide free iron identified by the intergranular structure [Marciuš 2012, Bigham 2002].

3.7.2 Zinc plated steel tubes

Zinc coatings protect steel by providing a physical barrier. This process creates a thin layer of pure zinc (99.9 %) that covers the steel homogeneously as shown in Figure 43. In addition, as stated previously in section 2.5, zinc influences the wetting between both metals positively [Chen 2008, Bach 2005].

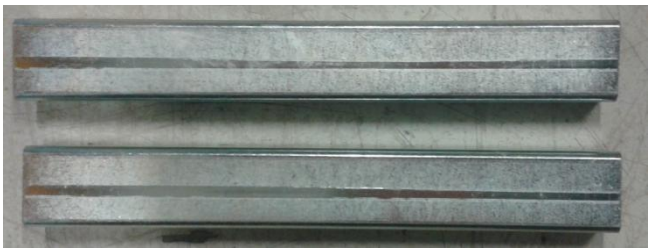

Figure 43. Zinc coated steel tubes.

The surface was characterized by means of SEM/EDS as shown in Figure 44 and Figure 45:

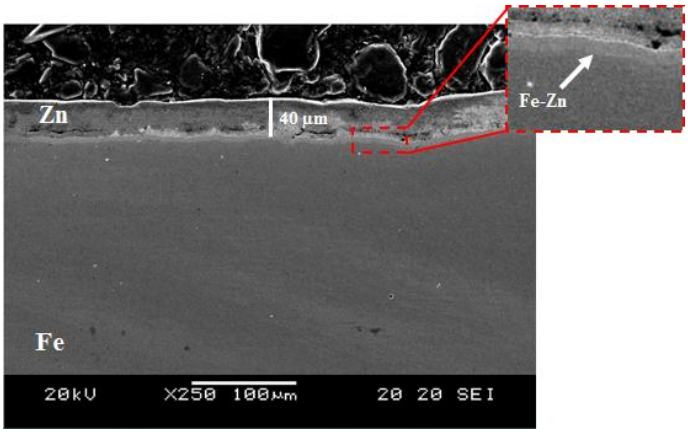

Figure 44. SEM micrograph of zinc coated steel.

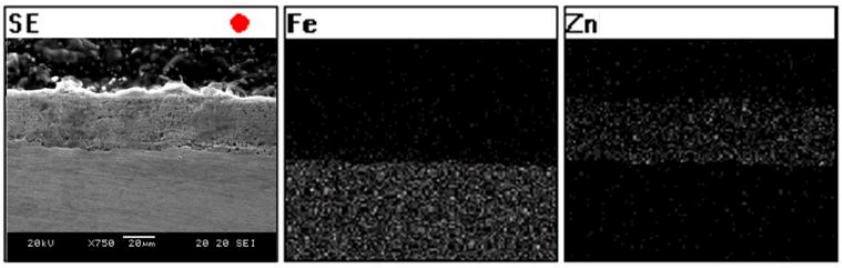

Figure 45. SEM/EDS results of zinc coated steel.

Figure 44 and Figure 45 show SEM/EDS images taken. In one hand, it can be observed that the average total thickness of the interface layer is 40 µm and is practically constant along the section. Fe-Zn plated insert presented a 10 µm intermetallic layer near the steel interface followed by a 30 µm Zn layer. On the other hand, EDS analysis performed on sample cross section reveals that the galvannealed steel interface mainly consists of Fe-Zn intermetallic compounds. According to literature, the most probable intermetallic phases are $FeZn_7$ and $FeZn_{13}$ [Taniyama 2004].

3.7.3 Aluminized steel tubes

Aluminide treatment is an alternative method to produce an aluminum containing layer over the steel surface, to improve the oxidation resistance of steel by generating a fine and dense aluminum layer on the surface of the steel.

As mentioned in the literature (section 2.5) the thickness of the intermetallic layer is a function of temperature and dipping time. The longer the immersion time the thicker the coating. Aguado

et al. observed that the minimum immersion time to create a protective layer at 750 ºC for AlSi7Mg alloys was 5 minutes. Furthermore they found the optimum immersion time between 7 and 9 minutes [Aguado 2013], other way the layer will grow in excess. Steel inserts were coated following the procedure described before and were allowed to react for 8 minutes. After the reaction time had passed, the specimens were pulled out of the bath and cooled in air. Figure 46 shows an image of the steel tubes with the aluminum coating:

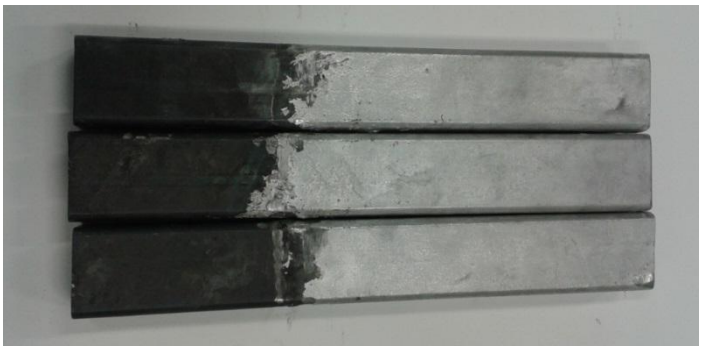

Figure 46. Hot dip aluminized steel tubes.

The obtained coatings were characterized by means of SEM/EDS as shown in Figure 47, Figure 48 and Figure 49:

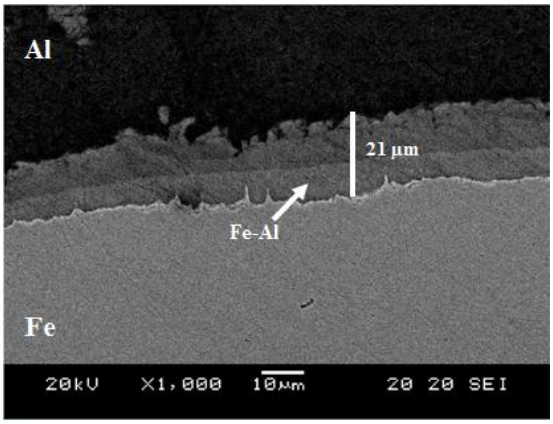

Figure 47. SEM Micrograph of hot dip aluminized steel.

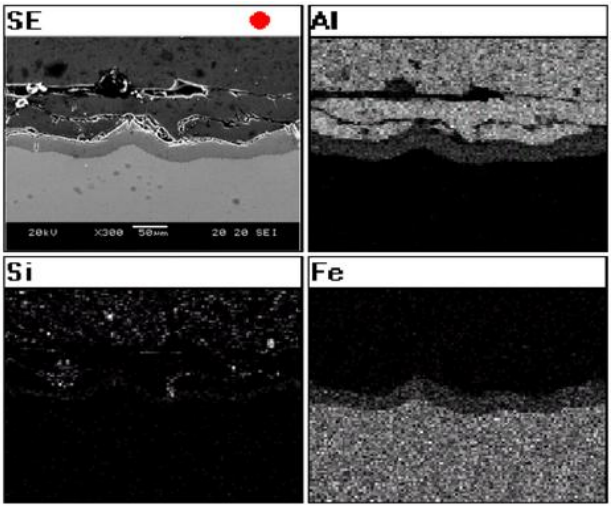

Figure 48. SEM/EDS results of hot dip aluminized steel.

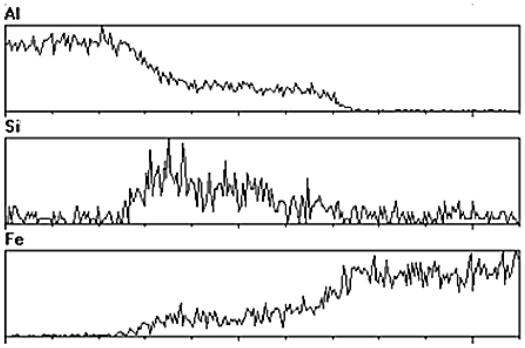

Figure 49. Linescan of the Al-Fe interface.

A continuous intermetallic reaction layer was formed at the interface with an average thickness of 21 μm. The interfacial morphology towards Fe was serrated on a fine scale and the transition towards Al was smooth and wave-like. EDS analysis performed on sample cross section reveals that the interface mainly consists of Fe-Al intermetallic compounds. The tongue-like morphology found in the iron side (Figure 47) suggests that the most probable intermetallic phases are $FeAl_3$ and Fe_2Al_5 [Qiu 2009a, Agudo 2008, Lee 2006]. The linescan confirms widespread areas with a mass distribution of the three elements on the interface.

3.8 Parameter Selection

In semisolid forging the main parameters are: solid fraction, mold temperature, punch speed, forming load and compaction time. The solid fraction is directly related with the temperature of the aluminum, the higher the temperature the lower the solid fraction. At low solid fraction values the fluidity of the material is increased and thus decrease the forming load needed to form the component. Moreover, filling the mold and component quality are influenced forming speed. Once the mold has been filled it is necessary to keep the pressure during the solidification of the material (compaction time) to ensure pore free internal microstructure. In order to attain to the aforementioned objectives, a set of experiments with the most representative surface-punch velocity-temperature combinations has been conducted. The experimental conditions used are listed in Table 7.

Table 7. Summary of the experimental conditions for interdiffusion experiments.

Surface	Temperature (ºC)	Forming velocity (mm/s)
None	580	320, 360, 400, 420
	570	320, 360, 400, 420
	565	320, 360, 400, 420
Zn Coated	580	320, 360, 400, 420
	570	320, 360, 400, 420
	565	320, 360, 400, 420
Hot dip aluminized	580	320, 360, 400, 420
	570	320, 360, 400, 420
	565	320, 360, 400, 420

Two different temperatures have been used for steel inserts: ambient temperature and 300 ºC. The dies are heated by circulating oil, the mold temperature is given by the maximum working temperature of the oil heater which is set at 300 ºC. The compaction time is established in 5 seconds according to the results obtained from the simulations as it is explained in section 4.2.

3.9 Conclusions

With the aim of developing thixo transverse forging process for the production of steel aluminum hybrid structure, a serial of forming experiments will be performed in next chapters.

The objective of the experiments is first to select the optimum forming parameters and second to understand the fundamental reactions that govern the phase formation and evolution at the interface between steel and aluminum alloys in temperatures of the semisolid range of Al.

The geometry selected as a demonstrator for this work is the left front cradle mount middle (LCM). The LCM is a component of the front cradle of a class C vehicle. In order to make it suitable for the thixoforming process the aluminum body of the reference geometry was modified by increasing the total section width which simplifies significantly the mold design by changing the partition line of the part. The resulting redesign does not modify heavily the reference geometry and will allow exploiting at maximum the semisolid process capabilities.

The estimated **weight reduction** of the new design compared to the existing commercial steel solution, which includes several stamped parts joined by several welded joints, **is approximately 35-40 %**. With the component defined it was designed a specific mold for the thixoforming process.

Regarding to materials, A356 and A357 aluminum alloys were chosen to perform the experiments. On the other hand, the insert selected was a S355J2H quality structural steel tube with rectangular section of 40 x 30 x 295 mm and 3 mm thickness.

Tubes were characterized by means of SEM/EDS and the results showed that most of the surface of raw steel is covered with iron oxides. In order to protect the clean surface from reoxidation two coatings (zinc and aluminum) were applied. The metallographic analysis performed on the cross sections revealed that an intermetallic layer was developed at the interface between the substrate and the coating layer. The compounds formed are related with the chemical nature of the coating and the thickness with the coating method.

Regarding to its applicability in the automotive sector, mechanical properties of the component will be analyzed from a much closer perspective to the industrial reality, where, besides the mechanical properties, it is of high relevance to determine the internal and external quality of the components. In this sense, besides the mechanical characterization, it will be conducted a thorough metallographic analysis of the parts and joint by diverse techniques such as, optical microscopy, visual inspection, X-Rays and scanning electron microscopy.

CHAPTER 4

PROCESS MODELLING AND FORMING TRIALS

The present chapter will focus on the of thixo lateral forging process for the production of nearly 2 kg automotive front cradle mount middle. For that purpose, in this chapter it is fully described the structural modeling of the component as well as the thermomechanical simulation of the thixoforming process in order to establish the optimum process parameters. With the process defined a semi-industrialized thixoforming cell has been implemented in the forming laboratory. After setting-up the installation the first trials to produce an aluminum-steel hybrid thixoformed component have been carried out.

4.1 Mechanical simulation of the component

Mechanical validation of the component involves the fulfillment of two conditions imposed by the manufacturer of automotive components CIE Automotive:

- The vertical stiffness for a static load must be at least 5.5 kN/mm
- Permanent deformation of the ensemble must be less than 1 mm for a static load

To simulate the structural behavior of the component the commercial software ABAQUS® was selected. ABAQUS® is suitable for this kind of structural calculus due to its great ability to simulate and analyse many different complex problems, its capacity to be customized and its wide material modelling capability.

In order to simplify the subsequent simulation and the computation time, some assumptions have been made:

- Bond between steel and aluminum is perfect and therefore the interfacial contact is continuous along the whole section

- The steel tube is considered as a rigid element
- The aluminum part is fixed to prevent displacement of the component in axis of the tube
- The loads are homogeneously distributed in the head of the left front cradle mount middle

Taking into account the previous considerations, it can be assumed another simplification. As the steel tube is a rigid element and the load transmission between both materials it is considered perfect, it is possible to eliminate the steel tube from the model. Therefore the mooring boundary was applied directly on the aluminum part. Modeled geometry, as well as the loads application point is displayed in the following figure:

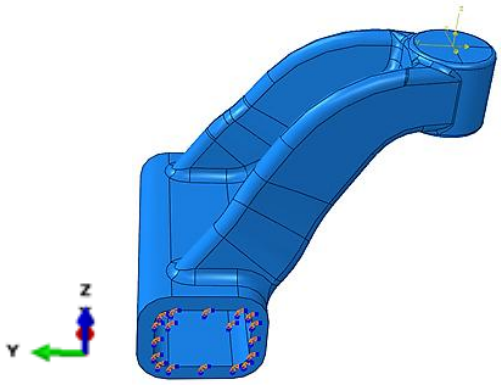

Figure 50. Model geometry.

To model the load applied in the head of the LCM a beam element was used this simplifies the calculation without losing accuracy. This assembly attached to beam will go through a series of spiders turn formed by beams of smaller diameter, thus ensuring transmission of movement between the screw and the other substances constituting the assembly.

Once the model is established the geometry is meshed. C3D10 element type was used for the model discretization. C3D10 is a general purpose second order tetrahedral element (10 node and 4 integration points). Material input data are shown in Table 8; they are based on the bibliography and the supplier specifications [Azpilgain 2006].

Table 8. Material input data.

Density [tonne/mm^3]	**Young's modulus [MPa]**	**Poisson's ratio [-]**
$2.70 \cdot 10^{-9}$	$6{,}9 \cdot 10^{4}$	0.33

4.1.1 Results

As mentioned before in section 3.5, the first criterion to ensure the structural integrity of the component is its vertical stiffness. The structure was modeled after facing to apply previous boundary conditions and assumed external stresses, in order to know the distribution of stresses and see if the above exposed conditions are accomplished or not. To carry out the first simulation, 25 kN load was applied in Z direction in the head of the front cradle mount middle as shown in Figure 51 and then the stresses and vertical displacement were calculated. The results obtained with the simulation are displayed in Figure 52 and Figure 53:

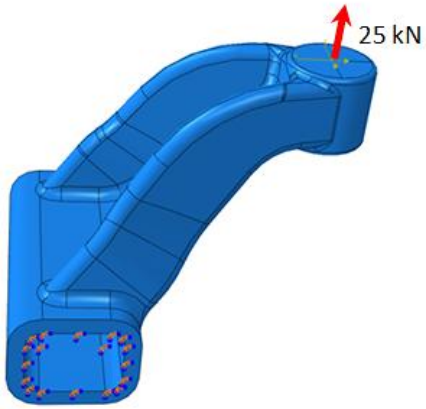

Figure 51. Load application schema for vertical stiffness test.

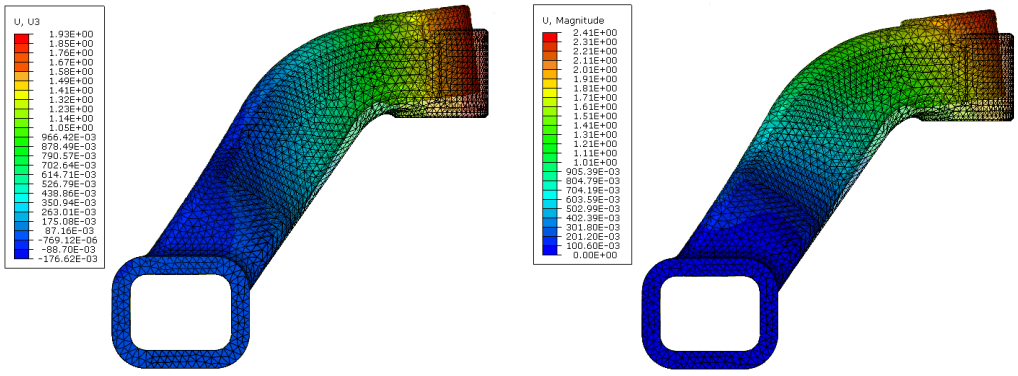

a) b)

Figure 52. Calculated displacement for vertical stiffness test. a) displacement in Z axis, b) total displacement.

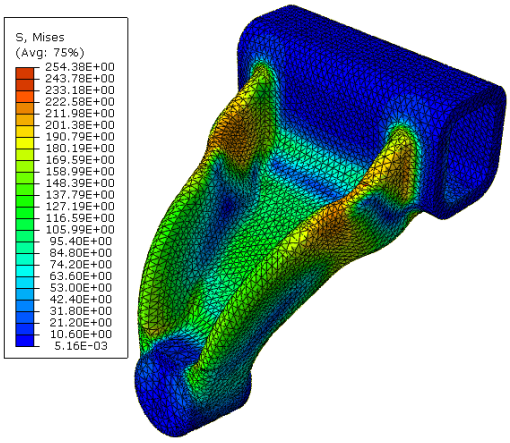

Figure 53. Von Mises stress in vertical stiffness test.

From the simulation results it can be noted that the component meets the requirement described above. Figure 52 and Figure 53 show that the vertical displacement only considering Z axis (Figure 52 a)) reaches the value of 1.93 mm and considering the worst scenario (Figure 52 b)), the total displacement is 2.41 mm that means the rigidity of the structure is at least 10.37 kN/mm (>5.5 kN/mm). Moreover, the resulting distribution of Von Mises stress does not exceed the established yield strength indicating that the assembly formed by the tube and the aluminum will work within the elastic region.

On the other hand, the second criterion to ensure the structural integrity of the component is its permanent deformation. In this case the forces were applied in the same point mentioned before. For the second simulation, the loads were applied in two steps. In the first step the component was loaded with 5.710 kN in X direction, -5.233 kN in Y direction and 4.660 kN in Z direction. Then, in the second step the loads were discharged. Once again, stress distribution and permanent deformation of the component were calculated. The resulting stress and displacement are displayed in the following figures (Figure 54, Figure 55 and Figure 56):

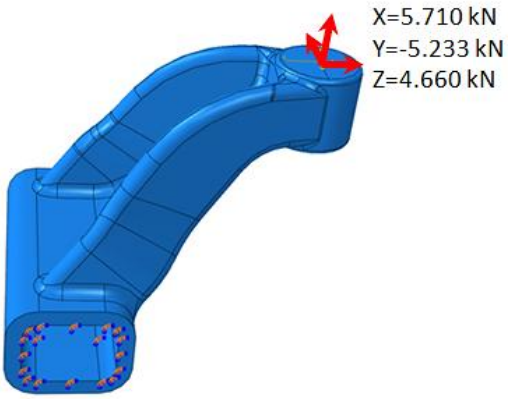

Figure 54. Load application schema for permanent deformation test.

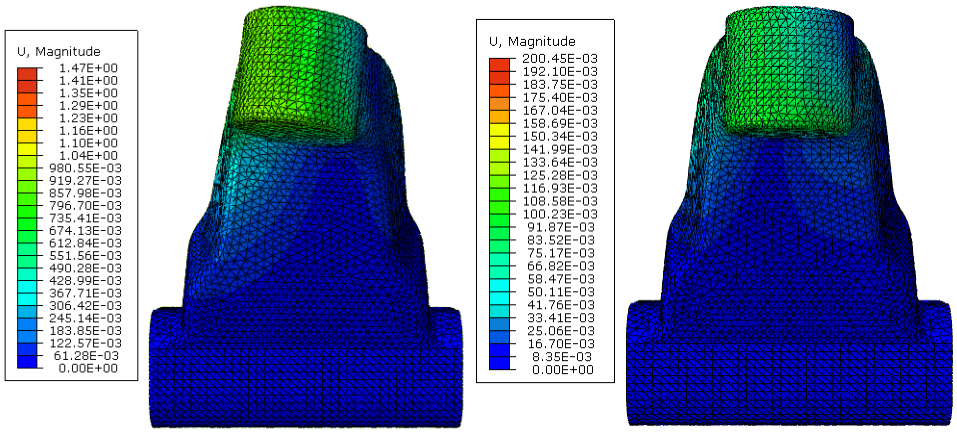

a) b)

Figure 55. Calculated permanent displacement. a) displacement with loads applied, b) permanent displacement.

From the simulation results it can be noted that the component meets the second requirement as well. Figure 55 show that the calculated displacement with the forces applied in the first case that reaches 1.47 mm, Figure 55 a), and the remainder deformation of $200.45 \cdot 10^{-3}$ mm once the loads were discharged in the second case, Figure 55 b).

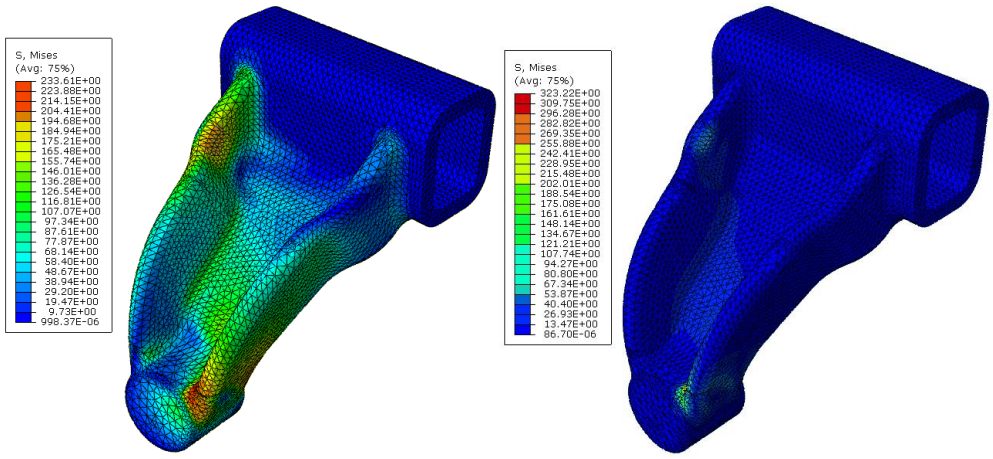

a) b)

Figure 56. Von Mises stress in permanent deformation test. a) with loads applied, b) permanent damage.

On the other hand, Figure 56 show that the resulting distribution of Von Mises stress does not exceed the established yield strength and therefore the permanent deformation caused is almost negligible ($200.45 \cdot 10^{-3}$ mm), that means the component practically will be working within the elastic region.

Although it is not a prerequisite for the structural integrity of the component, it is also required to know the behavior of the part under fatigue as an approach to estimate its service life. To do so a third simulation in dynamic regime was carried out. For this simulation tensile compression cycles were applied with a frequency of 5 Hz and an amplitude of ±4.7 kN. The car manufacturer considered a threshold of $1.2 \cdot 10^{6}$ as an infinite life. The point of the application of loads is considered the same as in the previous two cases. To simplify the calculations only the first full cycle was simulated. This way, the critical areas of stress concentration were determined in order to avoid premature failure of the component during service. Figure 57 shows the stress distribution in the component:

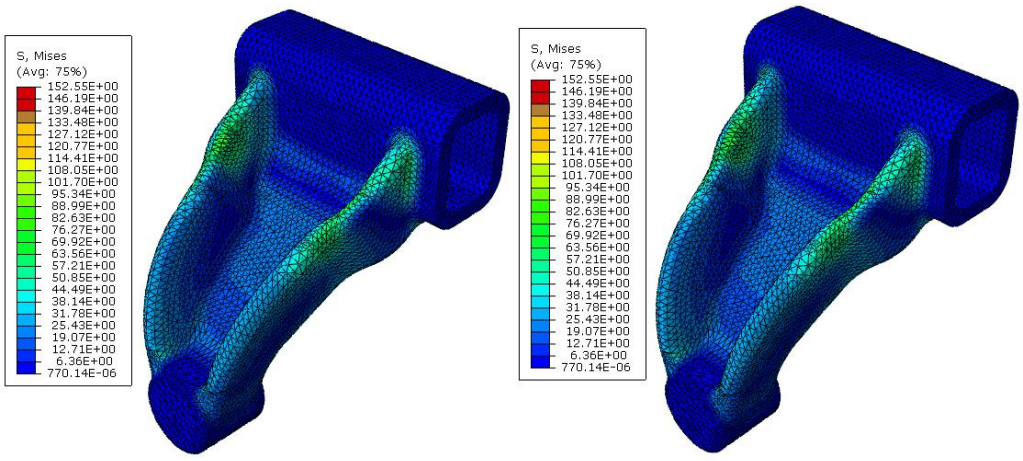

a) b)

Figure 57. Calculated Von Mises stress a) 4.7 kN b) -4.7 kN.

It can be seen that with the current design of the structure withstand properly the applied loads. Although, a stress concentration spots appeared around the mooring and body section where stress concentration peaks of 325 MPa were reached. According to the results obtained from the simulations, the mechanical characteristics of the structure meet the requirements imposed by the car manufacturer CIE Automotive and thus, this geometry design was selected.

4.2 Thermomechanical simulation of the semisolid process

Simulation is a tool to predict the behavior of the material during the forming process, which is applied in the early stages of the design of a new product, can be a huge cost savings and a qualitative leap compared the trial and error. The validity of the simulation results depends on the implemented physico-mathematical models and the data to feed these models. The physico-mathematical models are known as constitutive equations, or rheological state equations, which reflect the stress-strain-time relationship of a material. To fully describe the rheological behavior of such alloys, Christian Jacob Quaak developed its own model combining different aspects of models of Joly and Mada [Quaak 1996].

The simulation tool Flow 3D® was used to improve the mold filling in an early stage of the die design to avoid major mistakes when designing such dies. However, in spite of having thixotropic behavior equations, Flow 3D® not provides values of the parameters of these

equations. In this regard, it was decided to use the Quaak model implemented in Flow 3D® by Azpilgain [Azpilgain 2006] as a part of his doctoral thesis.

4.2.1 Simulation of the die filling

Once the model parameters were established, in order to determine the optimal process conditions and predict the material flows during the forming process, some numerical simulations were performed. Another critical part filling process is to determine where the solidification fronts meet in order to avoid a bad welding at the joint because of early solidification of the aluminum fronts.

The press used for the forming process allowed to work in forming velocities ranged between 0 to 800 mm/s, to validate the model two different forming velocities were simulated 200 mm/s and 400 mm/s. It was chosen a semisolid billet of Ø=76.2 mm x 70 mm of A356 alloy. Table 9 and Table 10 summarize the values for of the aluminum alloy, parameters for the viscosity equations introduced in Flow3D® and mold properties:

Table 9. Values of key variables introduced in Flow3D® related to aluminum A356 alloy for the simulation of the forming process.

VARIABLE	Flow 3D® VARIABLE	VALUE	UNITS
Density	RHOF	2685	Kg/m^3
Specific heat	CV1	963	J/kg·K
Thermal conductivity	THC1	159	W/m·K
Carreau equation coefficient	MU1	11	Pa·s
Carreau equation coefficient	MUC1	1	-
Carreau equation coefficient	MUC2	-0.3	-
Equilibrium viscosity	MUC3	0	Pa·s
Temperature coefficient	MUTMP1	-36.1	-
Temperature coefficient	MUTMP2	659	ºC
Temperature coefficient	MUTMP3	-1	-
Reference temperature	TSTAR	44	ºC
Initial viscosity	MUI	2600	Pa·s
Constant thickening rate	MUTHK	0.1	s^{-1}
Constant thinning rate	MUTHN0	20	s^{-1}
Thinning rate	MUTHN1	0	-

Table 10. Values of key variables introduced in Flow3D® related to the mold alloy for the simulation of the forming process.

VARIABLE	Flow 3D® VARIABLE	VALUE	UNITS
Density x Specific heat	RCOBS	3.81E6	$J/m^3 \cdot K$
Thermal conductivity	KOBS	27.30	W/m·K
Heat transfer coefficient	HOBS1	4500	$W/m^2 \cdot K$
Temperature of the mold	TWOBS	300	ºC

The following figure show the results of the first simulation performed on the left front cradle mount middle, for punch velocity of 200 mm/s, semisolid slug temperature of 580 ºC, and mold temperature 300 °C.

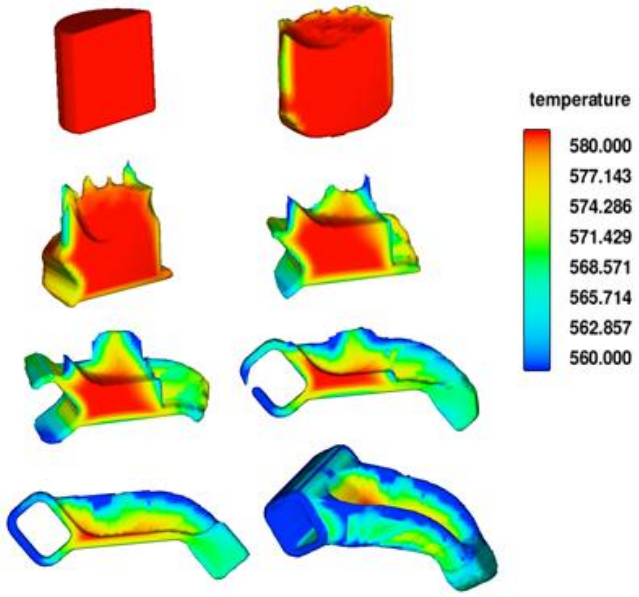

Figure 58 .Mold filling of the left cradle mount middle, alloy A356, slug geometry Ø76.2 x 70 mm, slug temperature 580 ºC, die temperature 300 ºC and punch speed 200 mm/s.

The flow pattern shows that the slug is flattened first. Afterwards, the material approaches near the rear of the component and starts surrounding the steel inset to form a mechanical bond between steel and aluminum. From the results of the simulation, Figure 58, it can be noted the difficulties in the filling process arising from inadequate process parameters, in this case insufficient forming velocity. The blue color represents that most of the material was cooled below the threshold temperature (set at 560 ºC) before the die is filled.

As mentioned before, the joint area is critical for the component. To obtain a sound joint between steel and aluminum it is required first a good mechanical bonding between steel and aluminum that means, the aluminum have to wrap and grip tightly the whole insert. The filling behavior of the aluminum fronts will determine the quality of the bond.

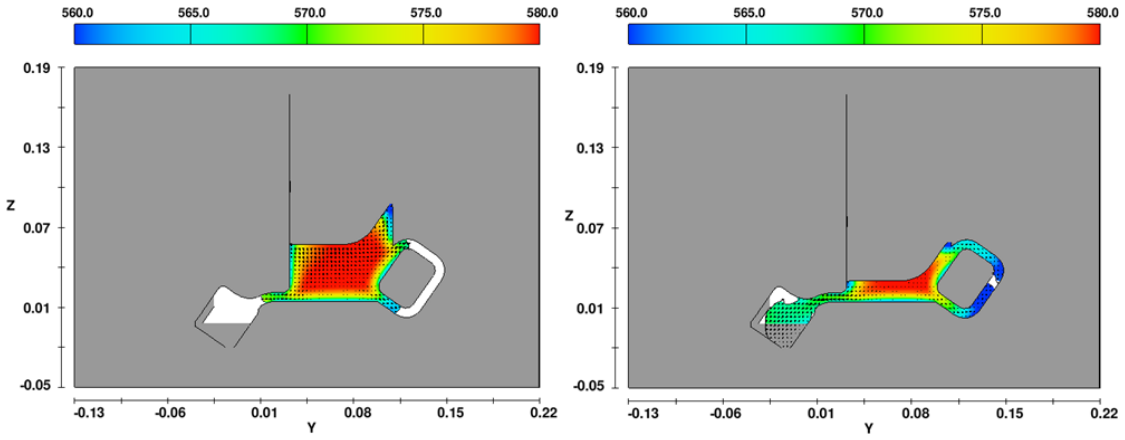

Figure 59. Temperature and flow vectors of the filling process.

Figure 59 show a section view of the Figure 58 during the filling process. The picture on the left show the moment where the solidification started (T_{Sol}=555 ºC and process time 3.8 s), as it can be seen the fronts were still far from the joining point. Besides the picture on the right show the moment where both fronts are solidified (process time 8.4 s) leaving a gap in the joining area. According to these results to achieve a complete filling of the die the process time has to be below 3.8 seconds other way the aluminum solidifies before forming a joint.

In the second simulation, the forming velocity was increased to 400 mm/s in order to achieve a complete die filling before temperature drops below solidification. The semisolid slug temperature was 580 ºC, and mold temperature 300 °C. Results obtained are shown in Figure 60:

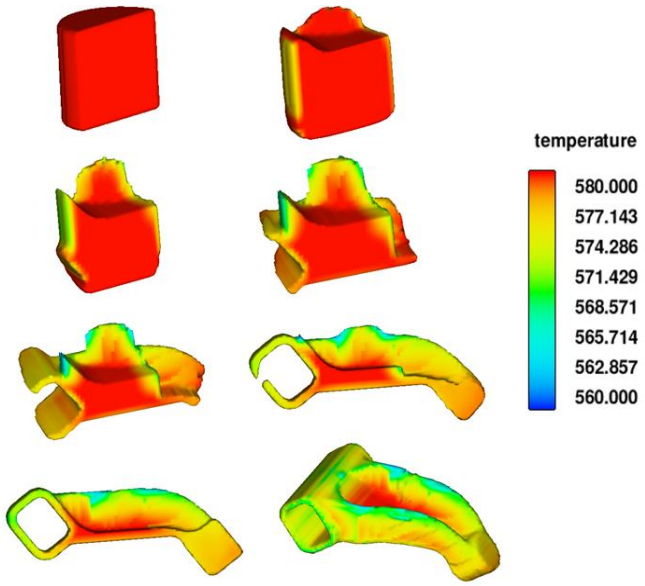

Figure 60. Mold filling of the left cradle mount middle, alloy A356, slug geometry Ø76.2 x 70 mm, slug temperature 580 ºC, die temperature 300 ºC and punch speed 400 mm/s.

Figure 60 confirms that the flow pattern is the same described for Figure 58. In addition, it can be observed that increasing the punch speed the process time is reduced to 2.6 seconds. At 400 mm/s, the filling process occurs above the solidus temperature of the A356 alloy (T_{Sol}=555 ºC) consequently the cavity was completely filled. Figure 61 show a section view of the Figure 60 during the filling process:

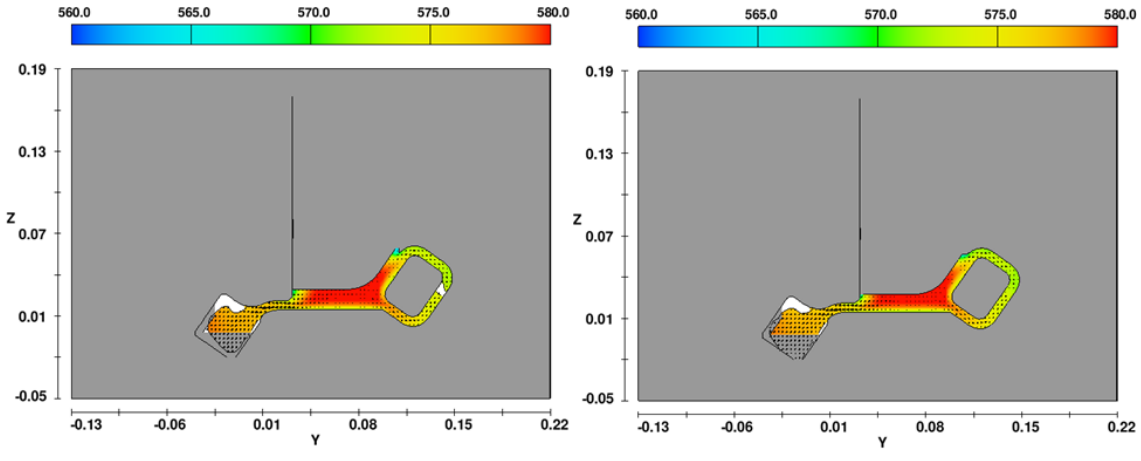

Figure 61. Temperature and flow vectors of the filling process.

With the results obtained in Figure 61 it is evident that the solidification fronts collide while the aluminum fronts were in the semisolid state. Besides, the joint area is located in the rear zone of the component, if necessary will allow adding an overflow to absorb oxide skins and impurities that can be detrimental to the final properties of the junction.

4.3 Prototype manufacturing

4.3.1.1 Heating curves

As mentioned previously in chapter 3, during induction heating most of the power density arrives close to the billet´s surface and then due to the high conductivity of the aluminum, the heat is transferred into the billet by conduction. In order to get a homogeneous temperature throughout the billet, different steps have been programmed for temperature equalizing through heat conduction.

The coil geometry has been designed for a wide range of billet diameters and lengths that means that it has not been optimized for the tested billet dimensions. A set of trial were made in order to define the heating cycle for each alloy (Al A356 and Al A357) and each solid fraction (Fs= 70 %, Fs= 60 % and Fs= 50 %). Down below an example of the typical heart-skin heating curves corresponding to a solid fraction of 60 % (570 ºC) for Aluminum A356 and A357 are presented:

Aluminum A356 Fs= 60 %

Figure 62 shows the heating cycle used for A356 Aluminum with a total duration of 495 seconds, including 95 seconds of homogenization time:

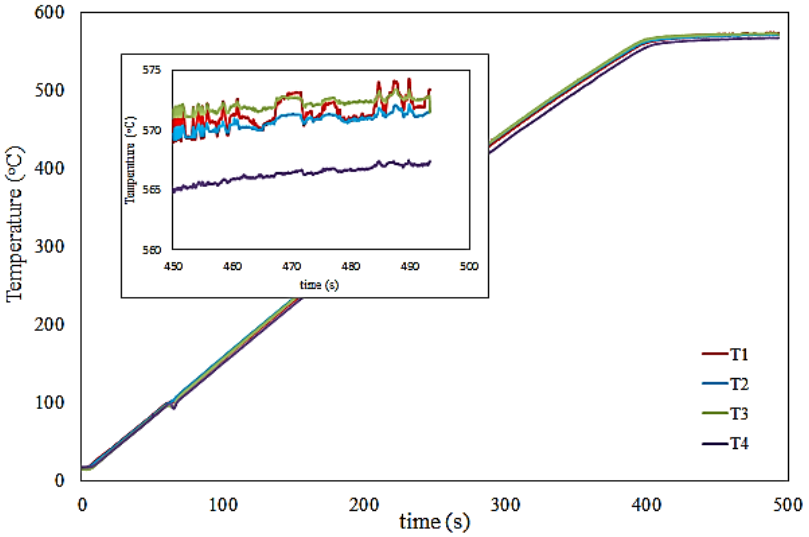

Figure 62. Evolution of temperature for an Al A356 alloy.

The measured temperature gradient at the end of the heating between the surface and the center is of 4 ºC. In this case the center is cooler (T4), with a temperature of 567.5 ºC, due to the skin effect. In contrast, the axial gradient (T1, T2, and T3) is almost negligible ≈1 ºC.

Aluminum A357 Fs= 60 %

Figure 63 shows the heating cycle used for A357 Aluminum with a total duration of 480 seconds including 90 seconds of homogenization time:

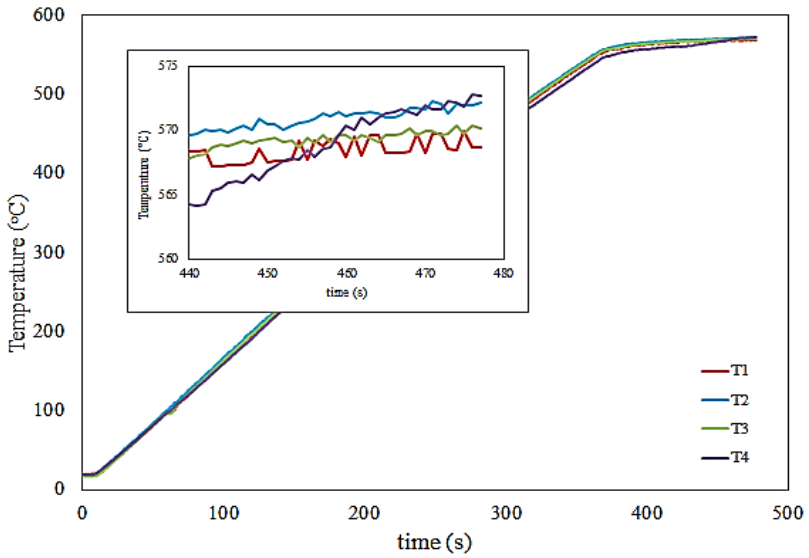

Figure 63. Evolution of temperature for an Al A357 alloy.

The measured temperature gradient at the end of the heating between the surface and the center is of 4.5 ºC. In this case the center is cooler (T4), with a temperature of 567.5 ºC, due to the skin effect. For the Al A357 alloy the axial gradient (T1, T2, and T3) is a bit higher than in previous case ≈2 ºC.

When the outer surface reaches a predetermined temperature, the heating is transferred by conduction to the center of the billet. As mentioned before, due to the skin effect most of the power density arrives close to the billet´s surface leading to higher heating of the surface in comparison with the core. In order to equalize both temperatures, a homogenization time of approximately 90 seconds was left.

Once the experimental data was collected a programmable automata has been implemented in the heating device to avoid deviations in the heating cycle. As the results obtained were very repetitive, to simplify the procedure, the control is taken over time. This obviously introduces some error, but it is not significant. The device lets to control the heating cycle with a panel located outside the cell (see Figure 27).

4.3.1.2 Prototype manufacturing

An operator places the steel insert on the lower die (Figure 31), the aluminum slug on the furnace pedestal (Figure 28). Once reached the forming temperature the billet is transported to the forming tool. After the mold has been filled it is necessary to keep the pressure during the solidification of the material (compaction time) to avoid shrinkage problems. Finally the final part is removed from the die (Figure 31). The operator thus opens the door in every cycle, making manual clearance compulsory before each forming cycle.

The complete die filling was reached with a force of approximately 1200 kN. The Brankamp, a press force control device, was programmed to stop the punch at 1500 kN. In some exceptional cases that limit was exceeded and the press overload system triggered.

To prevent aluminum from sticking to the mold Casting 2150®, lubricant was applied. Is a graphite-water based anti-wear and anti-friction solution that gives high fluidity to the semisolid alloy and aids in the ejection of the part from the die after the part has been forged. The die should not gain excess heat due to continuous contact with hot billets, as this will lead to faster die wear and cracking. This kind of lubricants also works as a barrier to heat transfer by sealing temperature in the workpiece. However, over time tends to form graphite incrustations in the mold causing underfilling of parts so it is useful only for small series/batch productions.

The transportation time was 15 seconds, measured since the coil of the heating furnace is down until the punch gets in contact with the semisolid billet. Once the mold has been filled it is necessary to keep the pressure during the solidification of the material (compaction time) to avoid shrinkage problems. To establish the compaction time they were taken into account the results obtained from the simulations carried out in section 4.2. As stated in Figure 59 the solidification of the critical areas started at 3.8 seconds and the solidification is completed 5 seconds later (8.4 seconds) thus this value of 5 seconds has been used in the forming experiments.

The plunger position against punch load and speed can be seen in Figure 64. Curves show how the approximation to the billet is fast at the beginning and when the ram reaches 125 mm above the BDC (Bottom Dead Centre) the speed is decreased until it stops completely at the established position. While the billet is deformed the press force rises and it is maintained during 5 seconds for the solidification of the liquid phase. After this, the ram returns to the TDC (Top Dead Centre).

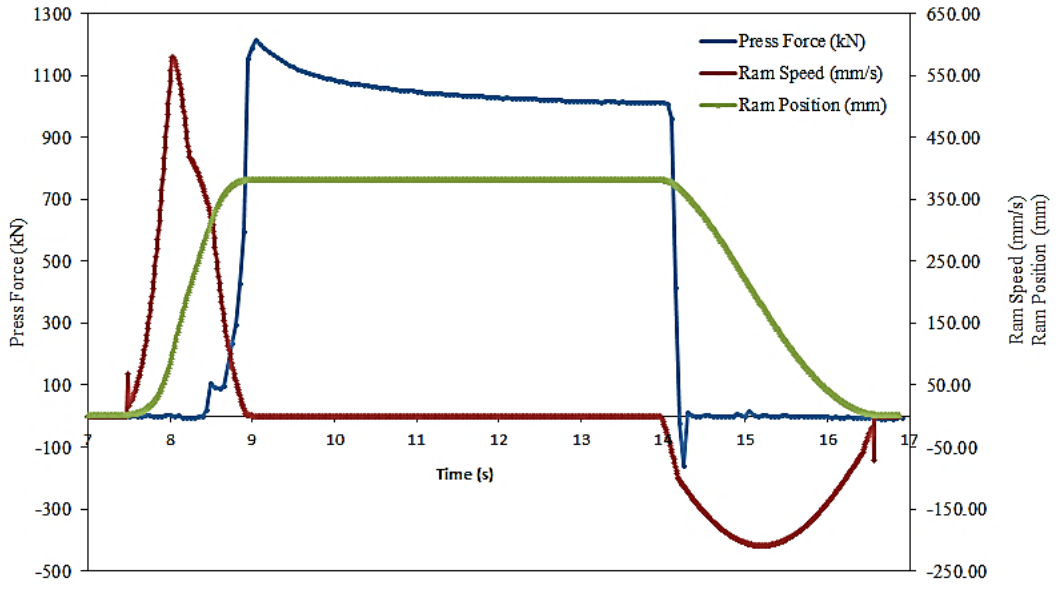

Figure 64. Punch-force punch-stroke diagram.

Table 11 summarizes measured values in the forming trial.

Table 11. Thixo-Lateral forging parameters.

PARAMETER	VALUE
Transportation time (s)	15
Clamping load (kN)	11760
Punch load (kN)	1100-1200
Ram speed (mm/s)	420
Die temperature, thermocouple (ºC)	285

Regarding to Figure 64, the simulations of the die filling carried out in section 4.2 are in a good agreement with the experimental results obtained in the forming process. For a punch velocity of 420 mm/s, the complete forming process occurs in approximately 2 seconds (1.9 seconds calculated with Flow 3D®), which is below the threshold time (3.8 seconds) established in Figure 59 to start the solidification of the aluminum fronts. The manufactured components are shown in Figure 65:

Figure 65. Detailed views of the hybrid structure.

Figure 65 demonstrated that it is possible to manufacture steel-aluminum hybrid structures in one step through the thixo lateral forging process. Once the process was set, some batches of prototypes were manufactured (Figure 66) at different experimental conditions to determine the influence of each parameter in the final properties of the component. The experimental parameters used in forming trial are explained in section 3.8 (Table 7). Figure 66 shows a batch of 12 hybrid structures manufactured with two alloys, Al A356 and A357:

Figure 66. Batch of 12 hybrid components obtained by thixo lateral forging process.

In the view of the results achieved, it is possible to say that geometrically the thixo lateral forging is a geometrically robust process and highly repeatable. Mechanical properties of these alloys can be improved by precipitation of the Mg_2Si phase through the T6 heat treatment [Sajjadi 2011, Sajjadi 2012].The treatment consisted in a solubilization stage at 540 °C for 8 h, followed by quenching in water and further artificial aging at 157 °C for 5.8 h. An example of the microstructures obtained after the heat treatment is displayed in Figure 67:

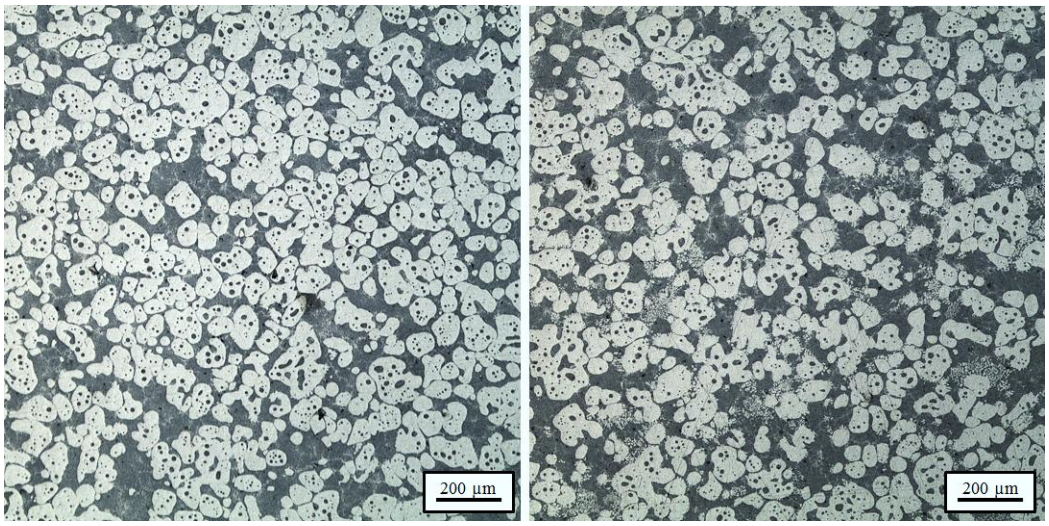

a) b)

Figure 67. Microstructure of the thixoformed material after T6 heat treatment a) Al A356, b) Al A357.

4.3.1.3 Experimental validation of the Flow 3D® model

As stated in the literature in thixoforming process the laminar filling of the cavity is one of the keys to obtain good quality components [Siegert 2000]. In order to validate the results obtained in the simulations with Flow3D® some experimental trials known as step-shootings were carried out. These are forming procedures where the punch is interrupted at several points designated by inserts in the cavity or interrupting the press stroke as in this case. The results obtained from the comparison between simulations and step-shooting pieces are shown in Figure 68:

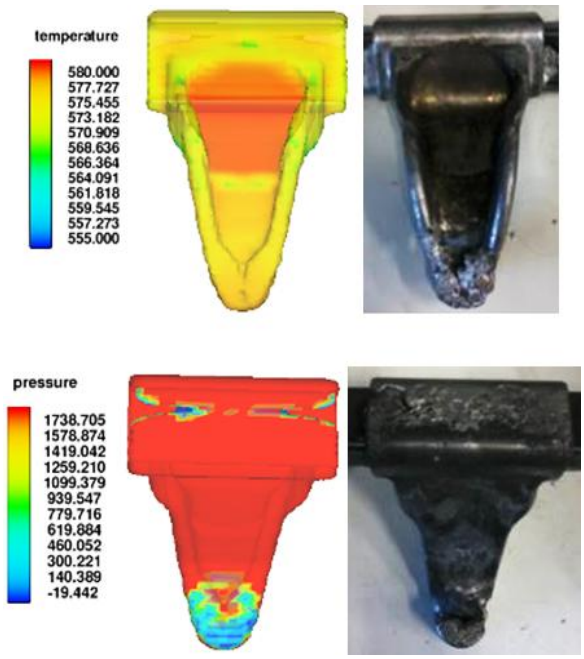

Figure 68. Comparison of experimental and simulated results.

Figure 68 showed the critical areas where there was an incomplete filling of the cavity when there is a lack of compaction of the material caused by the interruption of the stroke. Both front and in rear views show filling defects located in the far removed edges from the punch, the head and the joint of the left front cradle mount middle. Moreover, the detail showed in Figure 69 evidence that the material fronts collide exactly in the middle of the joining zone as stated in section 4.2. The comparison of the simulation with the step-shooting experiments shows a good match in reference to the die filling. These results demonstrated the validity of the implemented numerical.

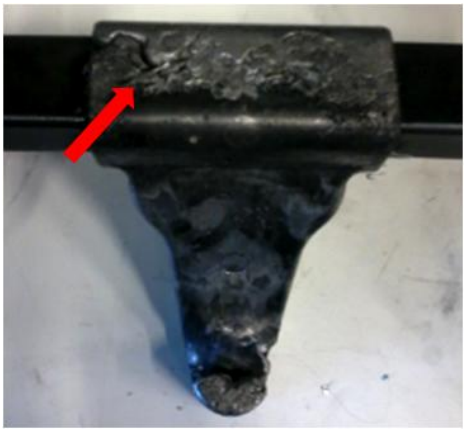

Figure 69. Detail of the rear view of the LFM.

4.4 Conclusions

In this chapter it was fully described the structural modeling of the component as well as the thermomechanical simulation of the thixoforming process in order to establish the optimum process parameters.

After the geometry of the component was designed (chapter 3), some simulations were carried out in order to validate the component. To simulate the structural behavior of the component the commercial software ABAQUS® was used. Results showed that the current design the structure withstand properly the applied loads. Nevertheless, a stress concentration spots appeared around the mooring and body section.

Once the geometry was defined, the simulation tool Flow 3D® was used to determine the optimal process conditions and predict the material flows during the forming process. With the simulations performed they were calculated the time for the beginning (process time 3.8 s) and the complete solidification of the aluminum fronts (process time 8.4 s). To achieve a complete filling of the die the process time has to be below 3.8 seconds other way the aluminum solidifies before forming a joint. When the forming velocity was insufficient, difficulties in the filling process arose; in contrast, increasing the punch speed the process time was reduced and complete filling was achieved.

With the process defined a semi-industrialized thixoforming cell has been implemented in the forming laboratory. After setting-up the installation the first trials to produce an aluminum-steel hybrid thixoformed component have been carried out.

The produced parts depend largely on the heating process and therefore, the temperature distribution inside the slug must be as homogeneous as possible to enable a uniform distribution of the liquid fraction through the billet volume. The direct measure of the temperature by process arranging multiple thermocouples at different points allowed gave an accurate data of the heating process. It has been demonstrated that the heating cycle was highly reproducible for each alloy and is not affected by the environmental conditions, at least at our forming laboratory.

Regarding to forming process, complete die filling was achieved with a force of approximately 1200 kN. Once the mold has been filled the pressure was kept for 5 seconds to avoid shrinkage problems.

Finally, comparing simulated results with step-shooting pieces it was clear that flow patterns predicted with the proposed model are in a good agreement with the experimental results obtained in the forming process. For a punch velocity of 420 mm/s, the complete forming process occurs in approximately 2 seconds (1.9 seconds calculated with Flow 3D®), which is below the threshold time (3.8 seconds) established as the beginning of the solidification of the aluminum fronts.

Keeping all this in mind, the aim of chapter 5 is to show the properties of the thixoforged automotive left front cradle mount middle and demonstrate that semisolid forming of hybrid structures could become an industrially applicable technology.

CHAPTER 5

PROPERTIES OF THE HYBRID STRUCTURES

This chapter is devoted to analyzing the properties of the semisolid forged left front cradle mount middle. The main parameters of the forming process are described and the values of these parameters to obtain repeatable results. Once the process is set, the influence of each parameter in the final properties of the component has been studied. A complete analysis has been conducted mainly focused on the metallographic and mechanical characterization of the part, with the aim of validating the semisolid forging as a possible manufacturing process for the production of hybrid structures.

5.1 Microstructural analysis of the component

Regarding to its applicability in the automotive sector, this part has been analyzed from a much closer perspective to the industrial reality, where, besides the mechanical properties, it is of high relevance to determine the internal and external quality of the components. In this sense, before the mechanical characterization, it has conducted a thorough metallographic analysis of the parts by techniques such as, optical microscopy, visual inspection, X-Rays and scanning electron microscopy.

As mentioned before, the joint of the solidification fronts is critical, the presence of oxides in this place may result in a bad weld weakening mechanical joining of aluminum with steel insert. Figure 70 shows the most representative images obtained during the X-Ray inspection.

5.1.1 X-Ray inspection

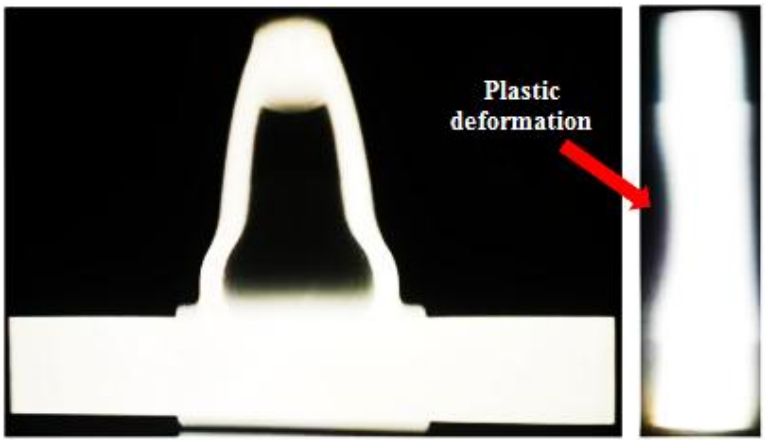

Figure 70. Radiography images of the hybrid structure.

The image shows a good compaction of the material since no discontinuities are appreciated in either the body or the joining zone. Looking at the tube, it is not possible to see traces of the welding line which indicates the good bonding among the two solidification fronts of aluminum. Moreover, a plastic deformation in the insert can be appreciated as explained previously in section 3.6. The plastic deformation of the tube is caused by the punch during the compaction stage as its design maximizes the pressure in the joining zone between the aluminum and the steel insert.

5.1.2 Visual Inspection

A first approach to a metallographic characterization was carried out. Parts made at different forming conditions have been analyzed by visual inspection with a special focus in the joint. In order to get further information on the quality of the component some metallographic cuts were performed as displayed in Figure 32. The results presented in Figure 71 and Figure 72 showed differences in the cross sections obtained in components manufactured with and without bumpers inserted inside the steel tube.

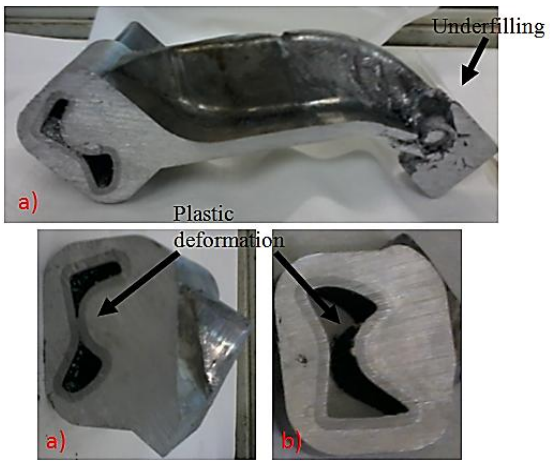

Figure 71. Details of cross sections of the body and the joint without bumpers.

Figure 71 revealed the severe plastic deformation suffered by the steel insert when the aluminum is thixoformed without using a bumper. Taking a closer look in the sections, in Figure 71 a) and Figure 71 b), different degrees of plastic deformation were observed. The deformation increases progressively (Figure 71 b)) approaching to center and reaching a maximum plastic deformation in the plane of symmetry (Figure 71 a)) following the tendency showed in Figure 70. The deformation stopped when both sides of the tube touched (Figure 71 a)). On the other hand, it is noticeable that there is an underfilling of the die due to the lack of material. This happened because a considerable amount of the material was used to fill the gap left by the deformation of the tube. The following results show the corresponding section to the experiments carried out using the bumper.

Figure 72. Details of cross sections of the body and the joint using bumpers.

Sections of Figure 72 confirmed the results discussed previously in Figure 70. In one hand, it is evident that the mold was filled effectively since the aluminum body as well as the joining zone is free of defects. Additionally, it is not possible to distinguish the welding line neither on the joining zone nor in the cross section the component nor on the outside area. According to the results obtained, apparently, the component is sound.

In this case the deformation degree sowed in both sections of Figure 72, a) and b) was the same. Results suggests that the introduced steel bumpers allowed controlling the plastic deformation generated in the tube and therefore the aluminum necessary to fill the gap will always be the same. Inserted bumper does not affect the joint but adds extra weight to the structure. On the other hand, the deformation undergone on the steel tube; generated an aluminum accumulation in the cavity. The accumulated material helps to fix the aluminum body in a specific position, avoiding displacements and rotations in service.

Following with the analysis, parts made at forming conditions, described previously in section 3.4.5, are shown in Figure 73. The most representative results were obtained combining, highest ram speed with lowest forming temperature and lowest ramp speed with highest forming temperature. Component displayed in Figure 73 a) was made of aluminum A356 at 580 ºC and a ram speed 320 mm/s. Part displayed in Figure 73 b) was made of aluminum A356 with a solid fraction of 565 ºC and punch speed 400 mm/s. In the visual inspection post heat treatment revealed significant differences in surface finish of the components.

Figure 73. Hybrid structures after T6 heat treatment. Details of the head and the joining zone.

As it can be observed, after the heat treatment, small blisters appeared in the surface of the part showed in Figure 73 a). The results indicate that ram speed and temperature had a large influence on the blistering, with the amount of blistering becoming larger with decreasing of forming velocity and increasing the temperature. They were taken two actions to solve this problem. The first was to increase the flow speed, as many of these defects are related with the temperature drop during the filling and also because it improves compositional homogeneity due to the turbulent flow. By increasing the ram speed a higher degree of turbulence is obtained resulting in a better mixing of the melt during the filling as well as a more homogenous temperature in the billet. Nevertheless, blistering problems can be associated with air entrapments caused by a turbulent flow during the die filling [Hu 2015]. The second was to reduce the forming temperature. At low temperature only a small amount of liquid is formed, enough to allow the displacement and rotation of the globules and therefore, the aluminum is thixoformed in a quasi-solid state keeping the composition homogeneous as in the solid billet. In order to get more information blistered part was cut in two halves and examined in more detail as shown in Figure 74.

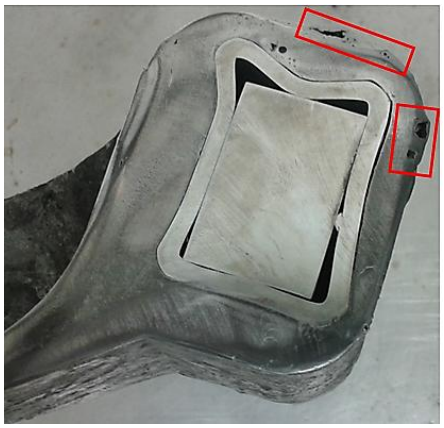

Figure 74. Cross section of the joint.

Figure 74 revealed a superficial skin in the aluminum that in some points it has separated from the bulk of the part body. Probably, the skin is generated due to thermal stress relief imposed during solubilization stage of the heat treatment. In the remaining areas, apparently, the component is sound. Results suggested that are surface irregularities formed by delamination of areas of different composition rather than bubbles formed due to air entrapment. In the view of the results, the following section was dedicated to the study of the segregation phenomena in the component.

5.1.3 Microstructural analysis of the segregation

In order to get further information on segregation phenomena, some samples were taken from the joint (A), the center (B) and the head (C) of the LCM as indicated in Figure 33. Figure 75, Figure 76 and Figure 77 show the typical microstructures of thixoforged and heat treated AlSi7Mg alloys for two forming conditions Fs=50 % and Fs=70%. The globulitic (bright) α-aluminum phase and the (dark) aluminum silicon eutectic can be identified in each micrograph.

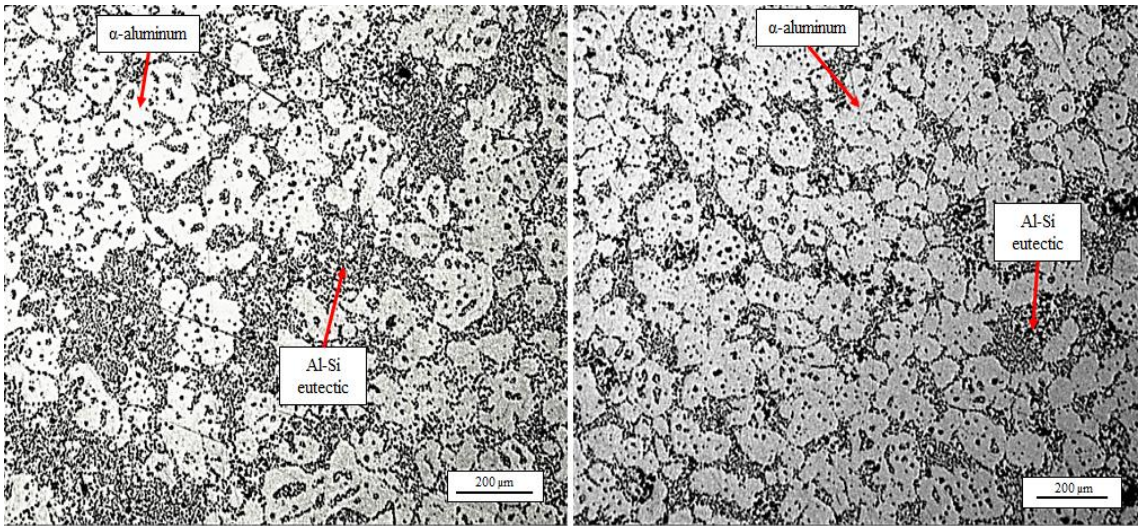

b) b)

Figure 75. Microstructure of the head (C) a) Fs=50 % and b) Fs=70 %.

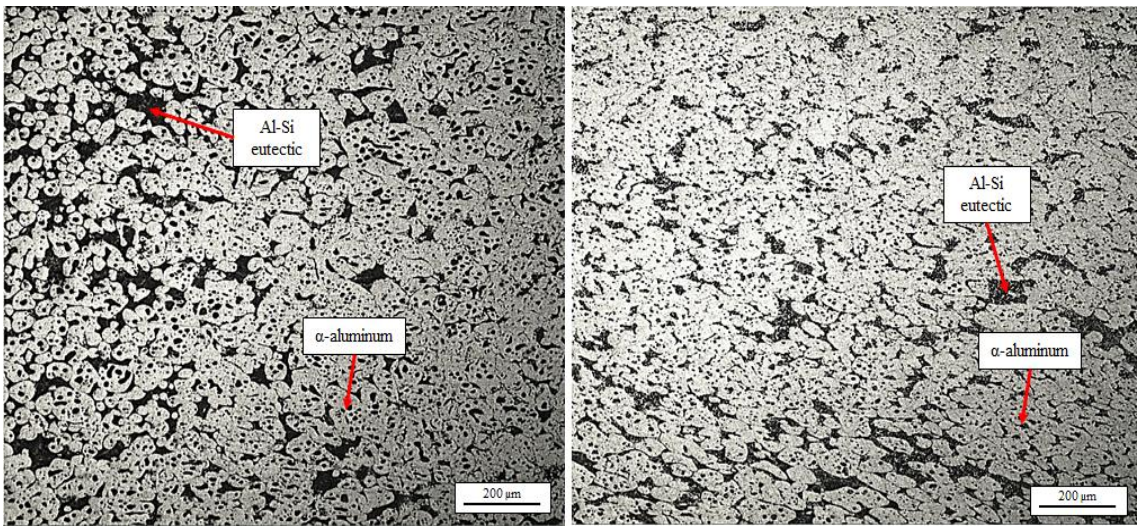

a) b)

Figure 76. Microstructure of the center (B) a) Fs=50 % and b) Fs=70 %.

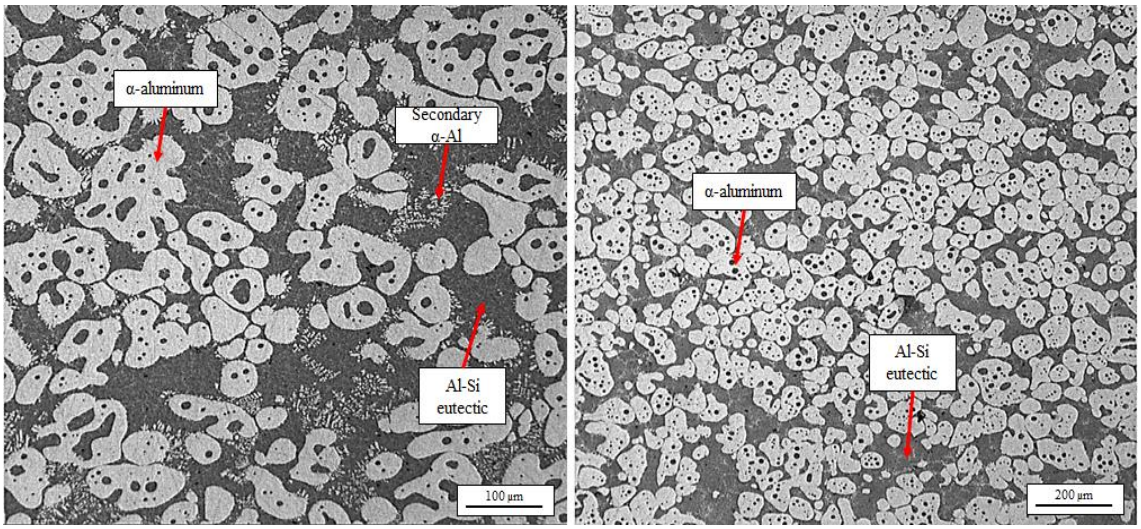

a) b)

Figure 77. Microstructure of the joint area (A) a) Fs=50 % and b) Fs=70 %.

Figure 75 and Figure 77 revealed the typical structure of thixoformed alloys made of α-Al globular grains with some eutectic entrapped into grains in an Al-Si eutectic matrix [Kapranos 2004]. The eutectic entrapment occurred while the precursor slugs are reheated, during ripening of the α-globules.

On the other hand, as shown in Figure 76, the microstructure in transverse section consists mainly of fine equiaxed grains. Some obvious extrusion flows were created along the extrusion direction in the longitudinal section. In the sample formed at low temperature Fs= 70 % the elongated grains can be found in the microstructure. In addition, there are a few incipient islands of eutectic (Figure 76 b)). When the aluminum is formed at Fs= 50 %, elongated grains decrease and the eutectic proportion increase significantly (Figure 76 a)) due to the higher liquid content in the billet.

Depending on the region analyzed, the α-Al to Al-Si eutectic ratio significantly changes between the edges of the component (head in Figure 75 and joint region in Figure 77) and center region (Figure 76). This indicates that a separation of liquid phase and solid phase occurred in the early stage of the filling process (while there is still liquid aluminum in the matrix) due to the hydrostatic pressure exerted by the punch. This is described as a sponge effect because of its similarity to the wringing out of a water filled sponge. When the reheated billet is plastically compressed and no thixotropy occurs, the liquid phase, which is embedded in the spaces

between the solid particles, is extruded from the compacted solid phase. The segregation due to this effect should be avoided because of the resulting poor component properties.

Besides, the section thickness has a notable impact on the microstructure characters of eutectic phase in as thixoformed condition (Figure 78). One notable difference is the higher amount of secondary α-Al particles observed in thin section (joint region, Figure 77 a)) than in thick section (head region, Figure 75). Another notable difference is the different geometric morphology of eutectic phase in the center of the section. In thin section, where the cooling rate is higher, the eutectic silicon and eutectic aluminum are fine and fibrous (Figure 78 b)). In thick section, where the cooling rate is low, the eutectic silicon and eutectic aluminum is bulky and blocky (Figure 78 a)).

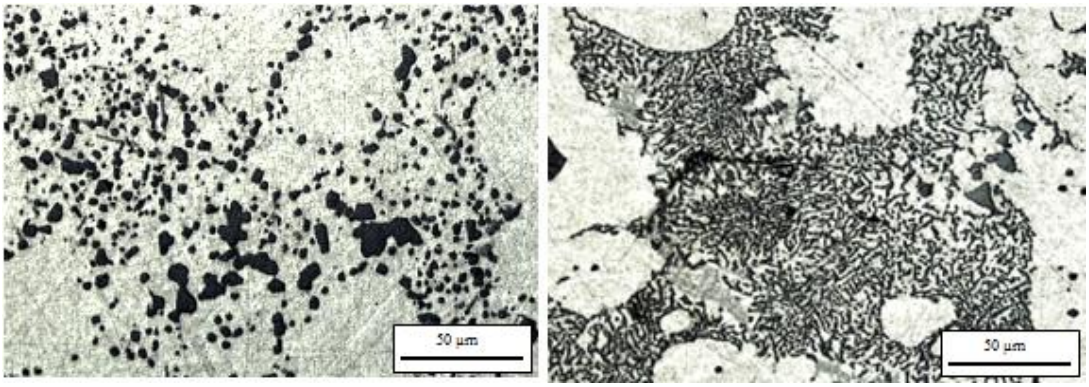

a) b)

Figure 78. Microstructure of the eutectic phase of each section.

5.2 Mechanical analysis of the component

The mechanical validation of the structure involves the fulfillment of two conditions requirements as explained previously in section 3.5.4:

- The vertical stiffness for a static load must be at least to 5.5 kN/mm
- Permanent deformation of the ensemble must be less than 1 mm for a static load.

Figure 35 and Figure 36 of section 3.5.3 show the experimental set up used for the mechanical characterization of the component. The results obtained from the tensile tests are summarized in the graph of Figure 79.

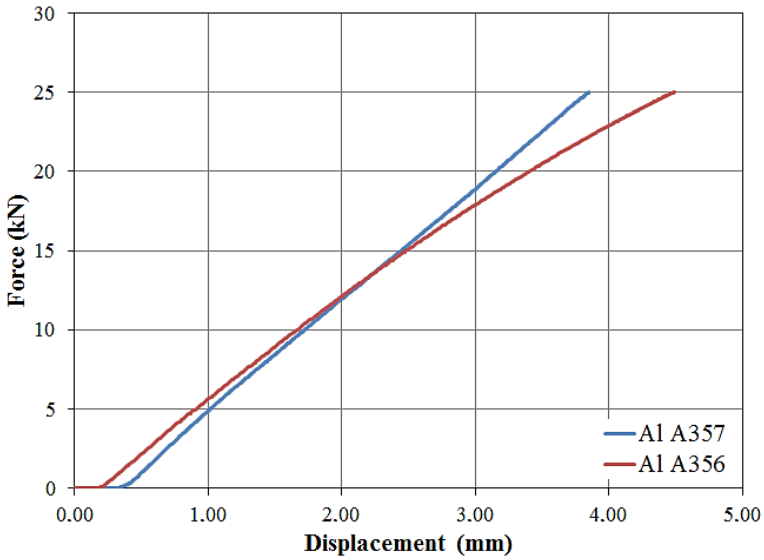

Figure 79. Tensile test results for different alloys.

The result obtained Figure 79 revealed that tests ended up after reaching the maximum force of the actuator. Due to the linearity of the tensile curves and the absence of deformation in the components it is assumed that the parts were working in the linear elastic region of the tensile curve, making unnecessary the subsequent recovering test. However, at the beginning of the curves an off-set of 0.3 and 0.4 mm were observed. These values correspond with the tolerance of the ball-joint of the actuator.

Results obtained from the fatigue test are displayed in Table 12:

Table 12. Number of cycles obtained before failure in the fatigue test.

Part number	Cycle number	Breakage
A356 -7	453,806	Yes
A357-21	492,607	Yes

The data of Table 12 indicate that an early failure of the component occurred before reaching the run-out. In Figure 80 are shown the failure areas:

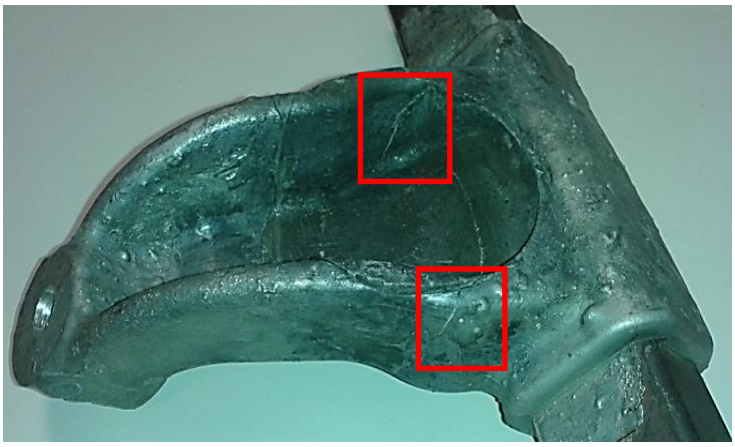

Figure 80. Early breakage of the component under fatige.

Premature failure is attributed to localized stress concentration or combination of bending stress and moment of inertia of the recessed section. The crack proceeds outward toward the surface of the component in a direction perpendicular to the applied stress. Comparison of results obtained in Figure 80 with the finite element method analysis carried out in section 4.1 (Figure 56 and Figure 57) shows a good match in reference to the load concentration spot (Figure 81).

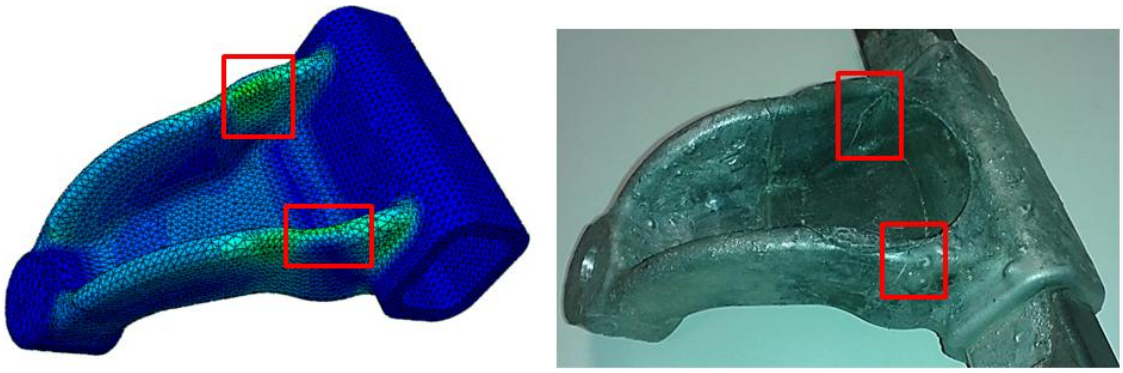

Figure 81. Comparison of experimental and simulated results.

The fracture surface characterizations were carried out on the fatigue fracture samples to determine the type of fracture during the test. A first visual analysis of the broken specimens (Figure 82), showed a mix mode starting from a ductile fracture surface with dull rough textured features followed by more brittle cleavage features with brilliant textured surfaces.

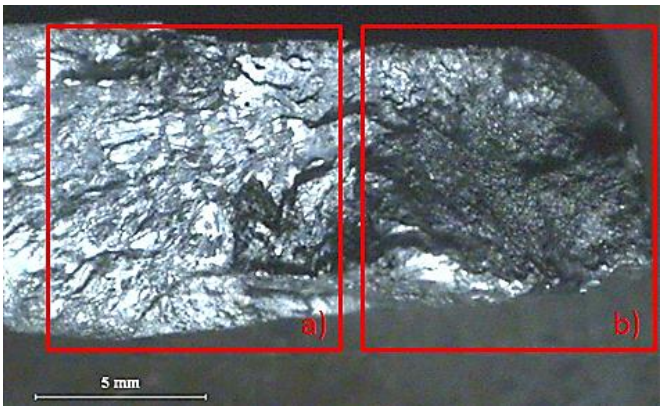

Figure 82. Macroscopic view of the fracture surface.

SEM observations presented in Figure 83 give evidence of two morphologically distinguishable modes of crack propagation.

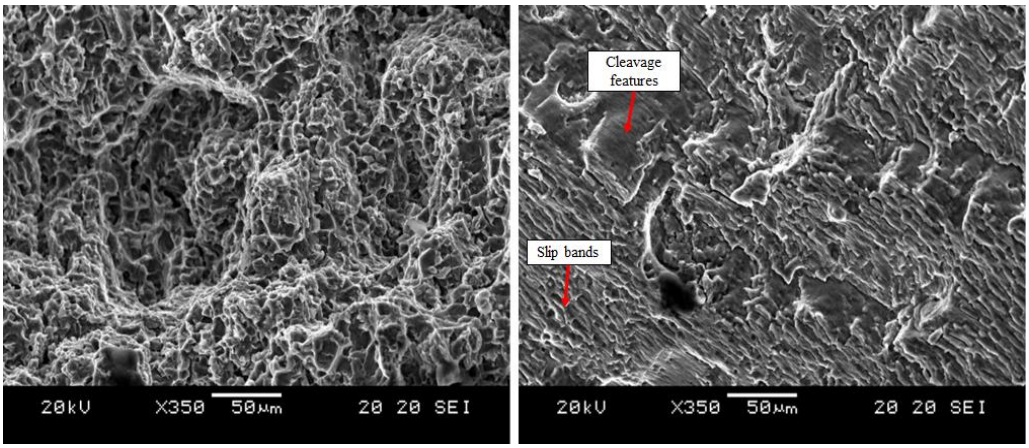

a) b)

Figure 83. SEM micrographs of the failure area.

The fracture surface's at crack initiation shows a brittle fracture, Figure 83 a). A close inspection of intergranular fracture surfaces, Figure 83 a) reveal fine dimples due to microvoid coalescence. Under continued applies stress, the cavities grow and coalesce to form a crack in the center of the component as showed before in Figure 80. Moreover the dimples indicated local deformation in these zones. Figure 83 b) show areas with a strongly curved pattern exhibiting facets of cleavage. Very fine bands, called slip bands, are recognizable among the cleavage features. These results exhibited the typical patterns observed for material fatigue

under cyclic loading (fatigue striations) attributed to a transgranular fragile fracture produced by slip band cracking.

In order to solve the mechanical failure it has been considered reinforcing the weaker sections of the component by increasing the thickness of the wall of the aluminum body at the expense of weight increase. These changes can be implemented either machining the mold cavities, namely increasing the wall thickness of the aluminum body subtracting material from the mold cavity or adding that extra amount of material inside the aluminum body. The second modification is easier to implement and therefore more economical since only the punch should be slightly modified. Figure 84 shows the comparison between the current punch geometry and the new design proposal:

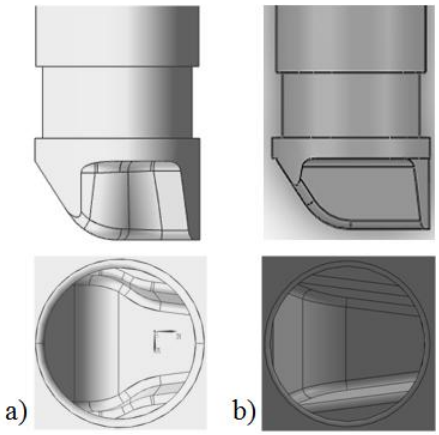

Figure 84. Comparison of a) current punch design and b) new punch design proposal.

This change in the punch means increasing walls thickness in 3 mm which only adds 15 grams to the total weight component. Of course, to validate the new component it will be necessary to conduct additional tests and the subsequent metallographic and mechanical characterization tests. However, due to the lack of time this trial will be carried out as a part of future work.

5.3 Conclusions

Forming conditions have a marked effect on the final properties of the component. After the heat treatment, blisters are generated in the surface of the parts. For the process conditions of highest forming temperature and lowest forming speed the percentage of α-Al decreased in the head and the joint. The transverse macrosegregation in the form of fine equiaxed and coarse microstructure morphology are formed at the surface (skin effect) of the samples. It is clear that

the thickness of skin layer increased by increasing the liquid portion. Therefore, the thickness of this layer is larger for the liquid rich regions. In the case of the lowest forming temperature and highest forming speed decreased the skin thickness making blisters disappear.

In the dark areas in the metallographic cut that identify the material flow, there are no pores or oxide skins; there are, however, areas with a higher eutectic phase amount. These areas with a higher eutectic phase amount indicate where a relative movement of the material takes place. This is attributed to segregation phenomena which cause a dissociation of the liquid phase and the solid phase towards the edges of the part resulting in a heterogeneous composition and component properties.

On the other hand, mechanical properties obtained just after thixoforming are promising, although the current design has not been able to withstand the number of cycles considered for the mechanical validation of the structure. Further work must be carried out to determine the exact causes of the premature failure of the component and optimize the geometry design in order to get the desired mechanical behavior under fatigue.

CHAPTER 6

STEEL-ALUMINUM INTERACTION

This chapter attempts to elicit the influence of the forming parameters and the microstructural parameters which govern the formation and growth of the intermetallic reaction layer. Different interdiffusion experiments between aluminum and steel under different superficial conditions have carried out for that purpose.

6.1 Introduction

In previous chapters the influence of the forming parameters on mechanical and microstructural properties of the hybrid structure were investigated. The objectives of the present chapter are the following:

- Understand the fundamental reactions that govern the phase formation and evolution at the interface between Fe or steel and Al alloys; especially in temperatures of the semisolid range of Al.
- Investigate the role of different coatings in the formation of reaction layers in comparison to raw steel.
- Find the best operating conditions to bridge the gap between scientific studies and technical applications by investigating the mechanisms how intermetallic reaction layers influence the dissimilar joints between steel and Al alloys.

The results obtained from these investigations should represent the basis to settle the thixo transverse forging method as an industrially applicable resource-saving process to manufacture geometrically complex and functional hybrid parts.

6.2 Microstructural characterization of the joints

To characterize the component quality it is necessary to investigate the factors influencing the joining zone. In order to attain to the aforementioned objectives, a set of experiments with the most representative surface-solid fraction combination were conducted. Due to the mechanical requirements of its final application T6 heat treatment was applied. During the solution stage of the treatment the parts are subjected to high temperature (540 ºC) for a long period of time (540 min). As diffusion is mainly driven by temperature the effect of heat treatment the interface has also been considered. Preparation and interface characterization of those coatings was described in section 3.5. On the other hand, the influence of forming parameters in the mechanical properties of the hybrid LCM has been widely discussed in chapter 5. The experimental conditions used are summarized in Table 13.

Table 13. Summary of the experimental conditions for interdiffusion experiments.

Surface	Temperature (ºC)	Forming velocity (mm/s)
Raw	580	320, 360, 400, 420
	570	320, 360, 400, 420
	565	320, 360, 400, 420
Zn Coated	580	320, 360, 400, 420
	570	320, 360, 400, 420
	565	320, 360, 400, 420
Hot dip aluminized	580	320, 360, 400, 420
	570	320, 360, 400, 420
	565	320, 360, 400, 420

Based on the results obtained, it has seen that the experiments carried out at intermediate temperature (570 ºC) do not reveal additional information to the experiments performed at end temperatures. For that reason, only the results obtained with the lowest and highest forming temperatures, 565 ºC and 580 ºC are shown. Corresponding microstructural response of the intermetallic phases have been analyzed by means of SEM and EDS as explained in section 3.5.

6.2.1 Interfacial interaction between aluminum and raw steel tubes

The results from the solid/semisolid interdiffusion experiments between aluminum and raw steel tubes at different forming temperatures are given in Figure 85 and Figure 87. SEM micrographs

compare the reaction zones obtained at different forming temperatures, the first corresponds to a high solid fraction trial, T= 565 ºC or Fs= 70 %, and the second to low solid fraction trial T= 580 ºC or Fs= 50 %.

6.2.1.1 T= 565 ºC or Fs= 70 %

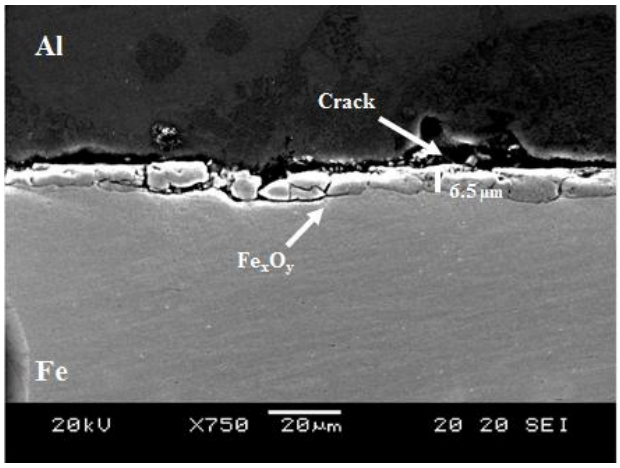

Figure 85. SEM micrographs of the reaction zone between raw steel and Al, Fs = 70 %.

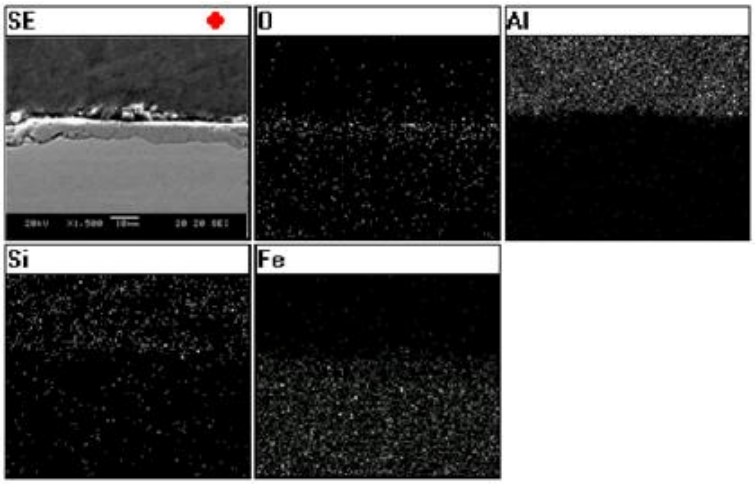

Figure 86. EDS analysis of the reaction zone between raw steel and Al, Fs = 70 %.

In Figure 85, three phases can be differentiated. The brightest region on the lower side corresponds to Fe specimen, and the darkest region on the upper side to Al specimen. As can be seen, a compound layer with an intermediate contrast is observed between the Fe and Al specimens. Besides, the average thickness measured for the interfacial layer is 6.5 µm. The results show no bond connection between the base materials since gaps and breaks appeared in

the phase seam [Behrens 2011]. The formation of cracks in the oxide layer are attributed to the shear stress caused by the plastic flow of the metal when is thixoformed to form the mechanical bonding around the steel insert. The gaps are attributed to the lower spreadability of the aluminum associated to a high liquid fraction.

The results obtained with EDS analysis (Figure 86) confirmed that the existing interface consists of three clearly differentiated phases, two base materials, aluminum and iron, and an interfacial iron oxide layer comprised by two phases as seen in Figure 42, according to Bigham *et al.* and Maeciuš *et al.* these phases are Fe_3O_4 and Fe_2O_3 [Marciuš 2012, Bigham 2002].

At the same time, the elemental mapping performed in Figure 86 revealed no evidence of intermetallic phases. The stable and insoluble nature of the interfacial oxide film restricted metallic contact and further inhibits the diffusion of elements preventing the formation of intermetallic compounds at the interface and thus the chemical bonding.

6.2.1.2 T= 580 ºC or Fs= 50 %

Figure 87 shows microstructures and respective EDS analysis of low solid fraction thixoformed specimens. Regarding to Figure 87 same phase distribution of Figure 85 was found.

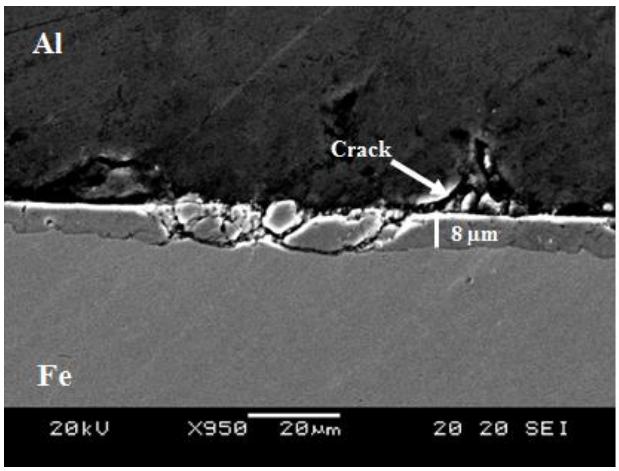

Figure 87. SEM micrographs of the reaction zone between raw steel and Al, Fs = 50 %.

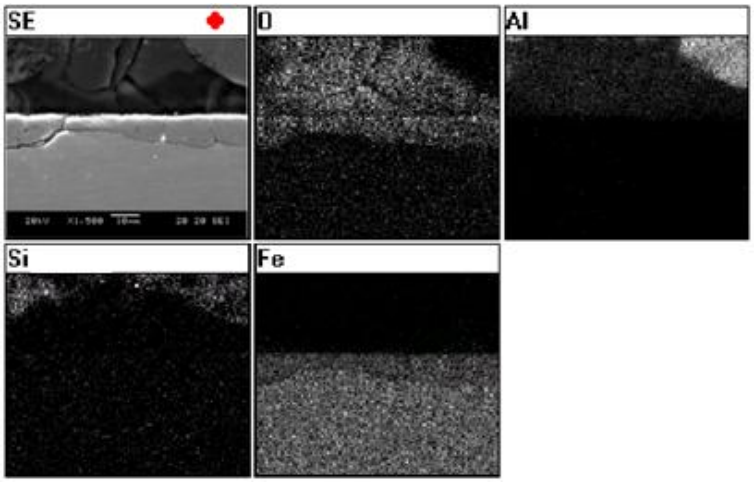

Figure 88. EDS analysis of the reaction zone between raw steel and Al, Fs = 50 %.

The average thickness measured for the interfacial layer has an average thickness of 8 µm. Moreover, the higher forming temperature and therefore lower solid fraction) resulted in an improvement of the spreadability of the aluminum over the oxide surface, as a consequence the gap between steel and aluminum disappeared and the amount of the interfacial crack was reduced. Once again, EDS analysis performed in Figure 88 confirmed the inhibitor effect for the diffusion of metals with an interfacial oxide layer since there was no evidence of intermetallic phases.

In order to get further information of the interface an EDS linescan analysis was performed on the samples. Figure 89 presented the result of the linescan for Al, Fe, Si and O.

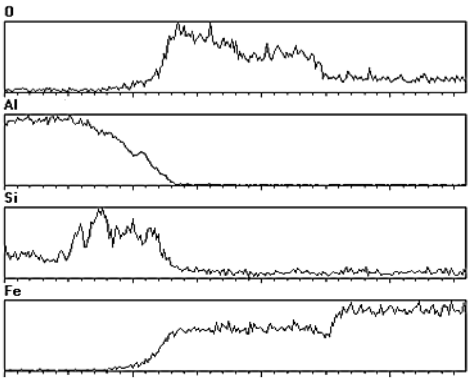

Figure 89. Linescan of the interace formed between raw steel and aluminum.

The results obtained in Figure 89 proved that the sample was composed by three different regions. The right region describes the percentage mass distribution of aluminum, and the opposite side depicts the distribution of iron. In the interfacial area of the sample an overlapped signal between Fe and O corresponding to iron oxides could be observed. Finally it is worth to mention that the results obtained from both sample showed almost no difference, except for the Si concentration near to the interfacial area for low solid fraction samples. This is related to the higher liquid content in the aluminum and the demixing of rich in silicon aluminum phase or eutectic phase due to the segregation phenomena during solidification.

After the heat treatment was applied it was observed that the microstructure of the sample remains equal as showed in the Figure 85 and Figure 87.

6.2.2 Interfacial interaction between aluminum and zinc plated steel tubes

In this section results obtained from the solid/semisolid interdiffusion experiments between aluminum and zinc plated steel tubes are presented. The cross sections of the interfaces obtained at different forming temperatures are given in Figure 90, Figure 94 and Figure 98. SEM micrographs compare the reaction zones obtained at different forming temperatures and the effect of the T6 heat treatment. The first SEM/EDS micrograph corresponds to sample obtained at low forming temperature, T= 565 ºC or Fs= 70 %.

6.2.2.1 T= 565 ºC or Fs= 70 %

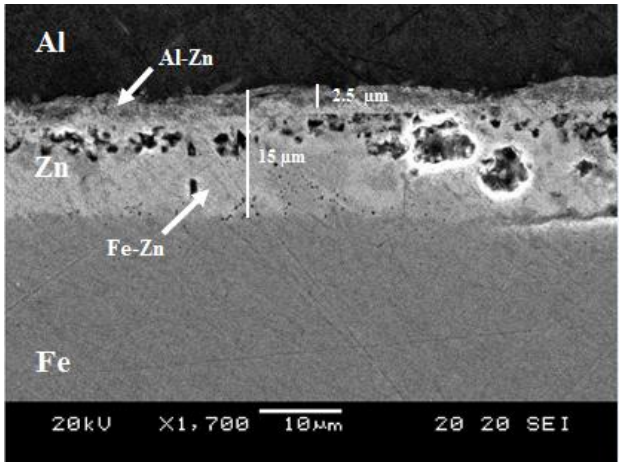

Figure 90. SEM micrographs of the reaction zone between zinc plated steel and Al, Fs = 70 %.

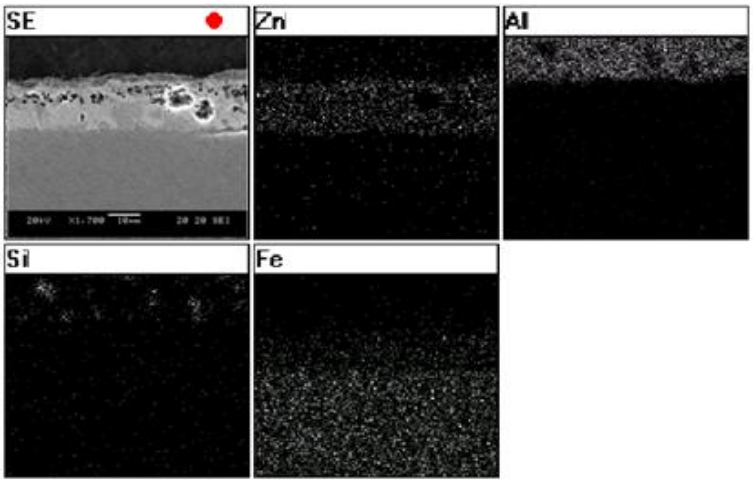

Figure 91. EDS analysis of the reaction zone between zinc plated steel and Al, Fs = 70 %.

Results displayed in Figure 90 revealed the existence of 4 different layers on the interface: the two base metals and two reaction layers one corresponding to steel side and another one corresponding to aluminum side. Developed reaction layer was continuous and its average thickness keeps constant along the base line in 15 μm. Interface presented a 12.5 μm intermetallic layer near the steel interface followed by a 2.5 μm Al-Zn layer adjacent to aluminum. Neither cracks nor oxides were observed at the different interfaces or within the coating itself, however, SEM micrograph clearly shows some small pores (averaging approximately 0.5 μm in diameter) in the intermediate layer attributed to a Kirkendall porosity.

Regarding to its morphology, the reaction layer of Figure 90 exhibited similar characteristics with the reaction layer obtained in the zinc plated steel tubes (chapter 3, Figure 44) where a smooth transition towards Fe and Zn can be observed. The comparison between two interfaces is shown in Figure 92:

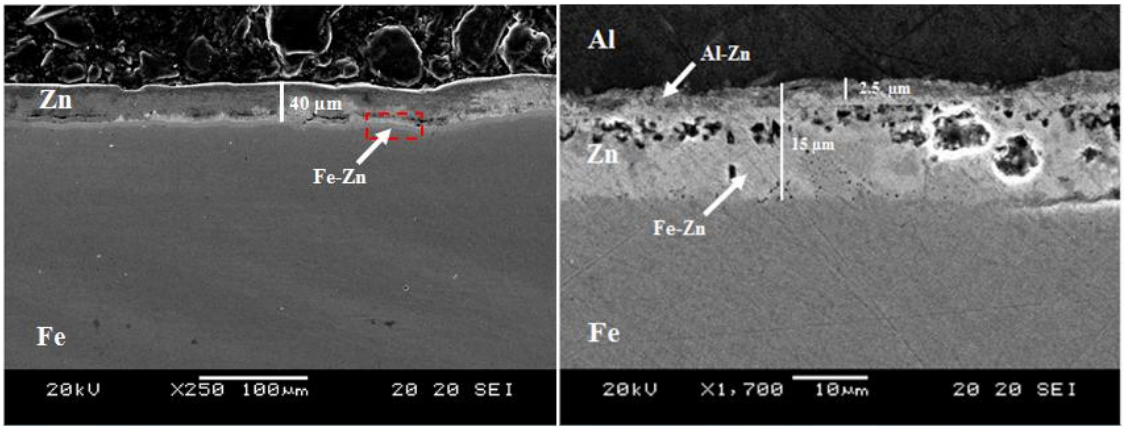

a) b)

Figure 92. SEM micrographs of a) Zn coated steel b) Zn coated steel joined to aluminum.

Compared to Figure 44 the total thickness of the interfacial layer decreased from 40 µm to 15 µm. This comes in a good agreement with the results obtained by Aguado *et al.* [Aguado 2013] where the Zn protective layer was partially dissolved in contact with aluminum melt (Figure 12). Thickness reduction is caused by the diffusion of zinc into semisolid aluminum to form an Al-Zn intermetallic reaction layer.

On the other hand, the elemental mapping of Figure 91 shows superimposed signals of Fe and Zn indicating that the steel interface mainly consists of Fe-Zn intermetallic compounds such as, $FeZn_7$ and $FeZn_{13}$ [Taniyama 2004]. In the same way, the superimposed signals of Zn and Al indicated that the aluminum interface is formed mainly by Al-Si-Zn intermetallic compounds. Additionally, a linescan analysis was performed along the interface as shown in Figure 93:

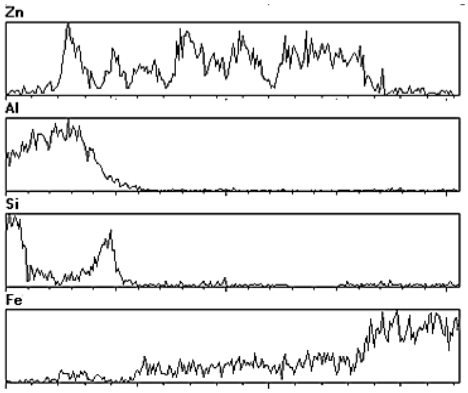

Figure 93. Linescan of the reaction zone between zinc plated steel and Al.

The results obtained in Figure 93 confirmed the existence of 4 different regions. Starting from the right side, the signal of Al-Si corresponding to the aluminum and an overlapped signal between Al, Zn and Si corresponding to aluminum-zinc intermetallic layer could be observed. The following area showed the superimposed signal of Fe and Zn corresponding to thinnest layer formed by Fe-Zn intermetallic compounds and the left side region consistent of steel.

In view of the results obtained, it can be concluded that the bonding is given first among Fe-Zn by electrolysis and in a second step the galvannealed steel is joined to aluminum by diffusion. The formed joint can be described as indirect dissimilar joining as the joint occurred through an intermediate metal, in this case the zinc from the coating.

6.2.2.2 T= 580 ºC or Fs= 50 %

The second micrograph (Figure 94) shows the results obtained at high forming temperature trial Fs= 50 % (580 ºC).

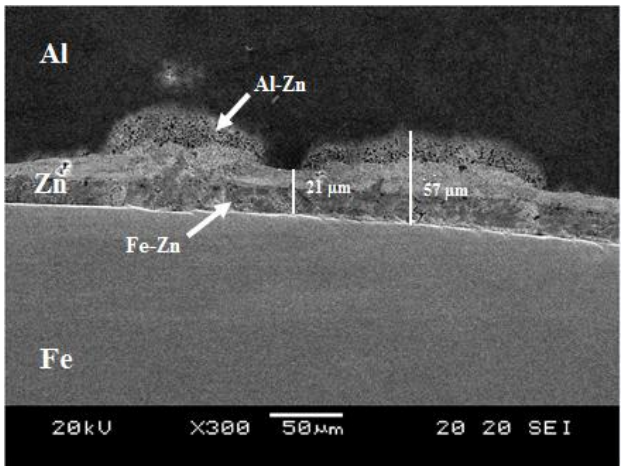

Figure 94. SEM micrographs of the reaction zone between zinc plated steel and Al, Fs = 50 %.

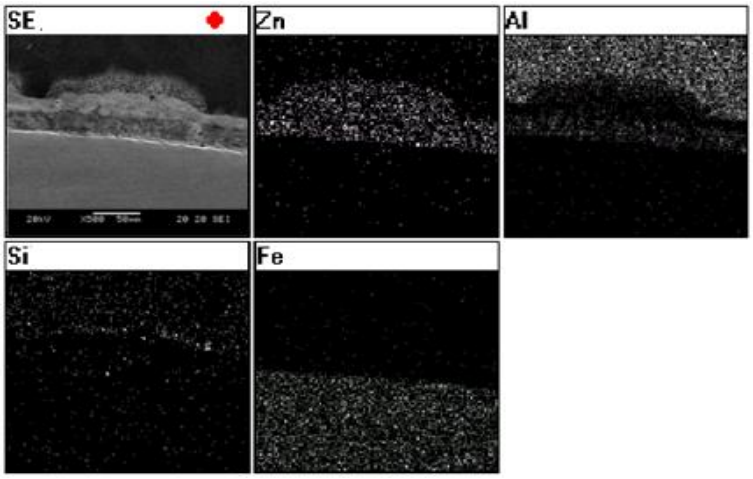

Figure 95. EDS analysis of the reaction zone between zinc plated steel and Al, Fs = 50 %.

Figure 94 revealed the existence of 4 different layers on the interface as in the previous case: the two base metals and two reaction layers one corresponding to steel side and another one corresponding to aluminum side. The reaction layer is continuous although; its thicknesses vary along the base line from 21 μm to 57 μm. This thickness variance probably is caused by the different liquid proportion at the interface. Liquid aluminum atoms have higher energy, its spread reaction ability is bigger and thus the diffusion zone is thicker. In contrast, the solid aluminum atom has lower energy, its spread reaction ability is smaller and therefore the diffusion zone narrower.

Again, neither cracks nor oxides were observed at the interfaces or within the coating itself, however, Kirkendall porosity (with pores averaging approximately 1 to 2 μm in diameter) appeared at the aluminum side. Unlike before, in this case was not possible to clearly discern Fe-Zn reaction layer from the Al-Zn layer.

Regarding to its morphology, the reaction layer of Figure 94 exhibited similar characteristics with the reaction layer obtained in the steel at low forming temperature from Figure 90, where a smooth transition towards Fe and Zn can be observed. In contrast, the Al-Zn interface presented wave-like morphology due to the local thickness increase of the reaction layer. Compared to Figure 41 the total thickness decreased from 40 μm to 21 μm as a result of the diffusion of zinc into aluminum. The comparison between two interfaces is shown in Figure 96.

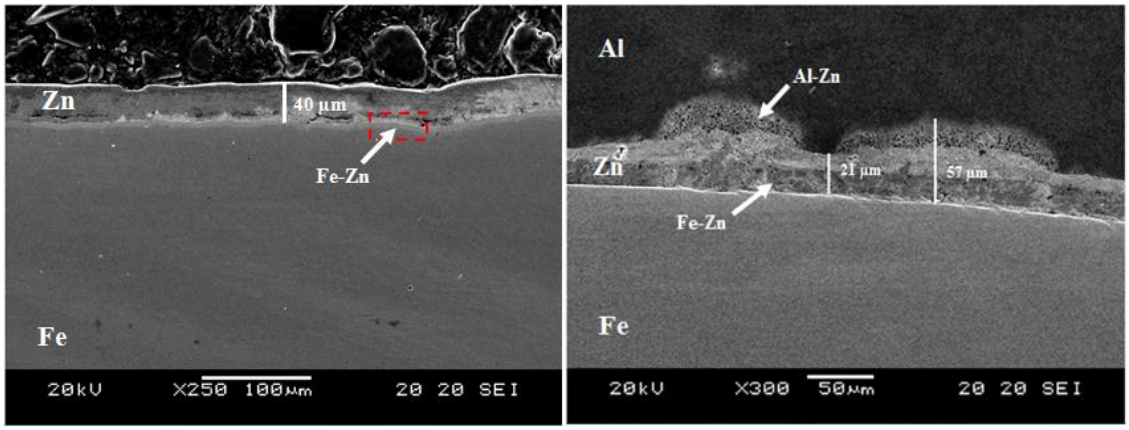

a) b)

Figure 96. SEM micrographs of a) Zn coated steel b) Zn coated steel joined to aluminum.

Elemental mapping performed on the sample (Figure 95) also showed superimposed signals of Fe and Zn indicating Fe-Zn intermetallic compounds, and superimposed signals of Zn, Al and Si indicating Al-Si-Zn intermetallic compounds. Furthermore, it is worth to highlight that there is a higher concentration of Al and Si in the interfacial area. The higher content of aluminum is attributed to the greater diffusion ability of liquid aluminum and the higher content of silicon could be associated to the microsegregation in the aluminum alloy. In segregation phenomena, the parts of rich alloy elements, such as, eutectic aluminum (AlSi12) that have low melting point will be melt first at the effect of surface tension of the liquid phase. These liquid phases possess increased atom mobility and moved by the concentration gradient diffuse through the interface region to form a chemical intermetallic joint.

In order to confirm the composition interface an EDS linescan analysis was performed on the samples. Figure 97 present the results obtained:

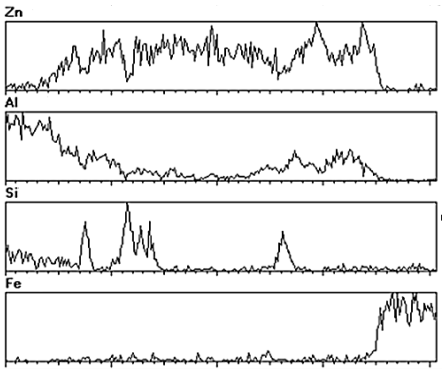

Figure 97. Linescan of the reaction zone between zinc plated steel and Al, Fs = 50 %.

Results obtained in Figure 97 confirmed the existence of the 4 regions with the same distribution showed in Figure 93.

According to the results, a reaction layer between the steel coated insert and AlSi7Mg has been formed. The formed joint can be described as indirect dissimilar joining as the joint occurred through an intermediate metal.

6.2.2.3 Heat treated sample

The following figures show the results found after T6 heat treatment was applied.

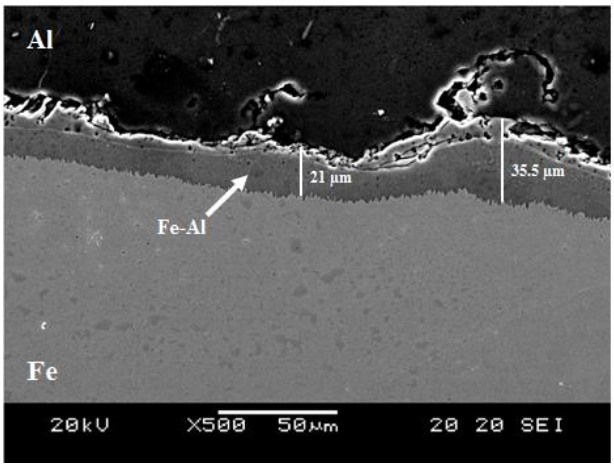

Figure 98. SEM micrographs of the reaction zone between zinc plated steel and Al after T6 treatment.

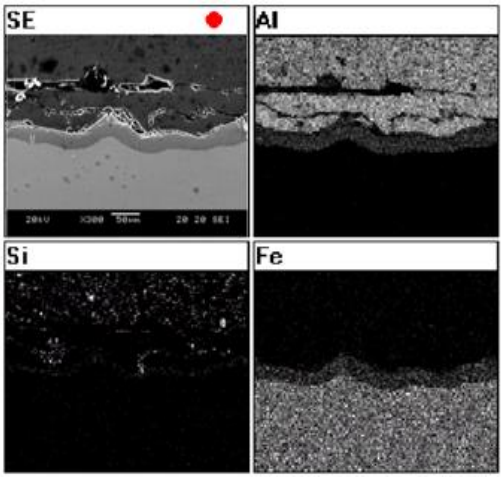

Figure 99. EDS analysis of the reaction zone between zinc plated steel and Al after T6 treatment.

Figure 98 shows that the diffusion zone was composed by 3 layers: the two base metals and the interfacial reaction layer. A continuous intermetallic reaction layer was formed at the interface with variable thicknesses along the section ranging from 21 μm to 35.5 μm. Besides, the diffusion zone at the aluminum alloy side was wider than that of stainless steel side. This means the diffusion ability of Fe in the aluminum alloy is bigger than the diffusion ability of Al in the steel as stated by Liu *et al.* [Liu 2006] and Rathod *et al.* [Rathod 2004]. Nevertheless, the developed reaction zone presented some Kirkendall porosity again in the aluminum side; additionally some cracks appeared on the interface that probably formed during the quenching step of the heat treatment due to the relief of thermally induced interface shear stresses.

Regarding to its morphology, the reaction layer developed after the T6 heat treatment greatly deviates from the layers developed before in sections 6.2.2.1 and 6.2.2.2. In this case the interfacial morphology towards Fe was serrated on a fine scale and the transition towards Al was smooth and wave-like and presented similar characteristics with the layer obtained in the hot dip aluminized steel tube (chapter 3, Figure 47).

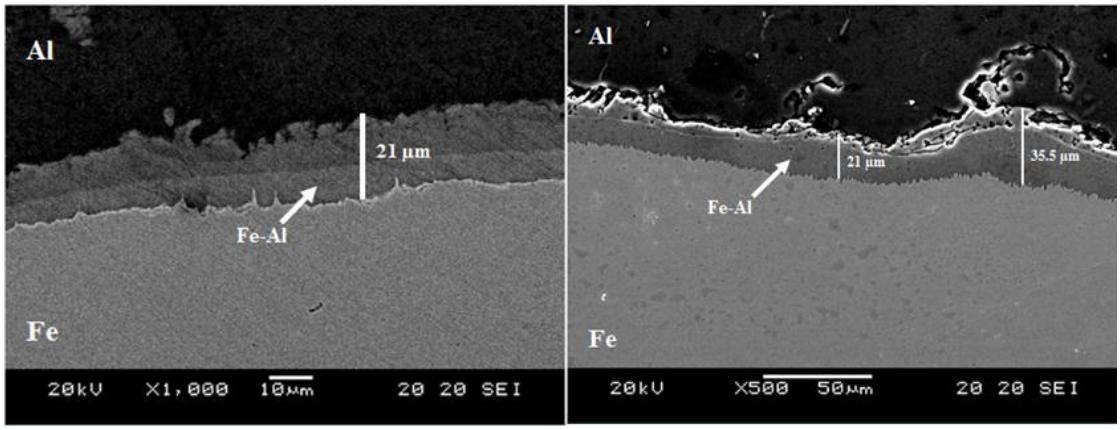

a) b)

Figure 100. SEM micrographs of a) aluminized steel b) Heat treated Zn coated steel joined to aluminum.

Looking SEM micrographs of Figure 90, Figure 94 and Figure 99 it seems that the reaction occurred during the solution stage and it stopped during water quenching. Besides, EDS analysis performed on sample cross section reveals that the interface mainly consists of Fe, Al and Si and no traces of Zn were found. The fact that Zn was not detected in the reaction layer suggests that Zn has been dissolved or evaporated during the solution stage of the heat treatment as stated in section 2.5 of the literature review. On the other hand, the superimposed signals displayed in Figure 99 indicated Fe-Al-Si intermetallic compounds.

In order to get further information on the composition of the interface an EDS linescan analysis was performed on the samples. Figure 101 presented the results obtained:

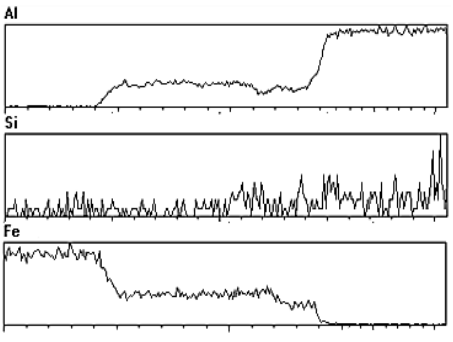

Figure 101. Linescan of the reaction zone between zinc plated steel and Al after T6 treatment.

In the investigated material combination, linescan analysis proved the existence of 3 different layers. Starting from the left side, the signal of Al-Si corresponding to the aluminum and an

overlapped signal between Al, Si and Fe corresponding to aluminum-steel intermetallic layer could be observed. The right side region is mainly composed by steel.

6.2.3 Interfacial interaction between aluminum and aluminized steel tubes

In this section results obtained from the solid/semisolid interdiffusion experiments between aluminized steel tubes and semisolid aluminum are presented. The cross sections of the interfaces obtained at different forming temperatures are given in Figure 102, Figure 105 and Figure 108. SEM micrographs compare the reaction zones obtained at different forming temperatures and the effect of the T6 heat treatment.

6.2.3.1 T= 565 ºC or Fs= 70 %

The first SEM/EDS micrograph corresponds to sample obtained at low forming temperature, T=565 ºC or Fs=70 %.

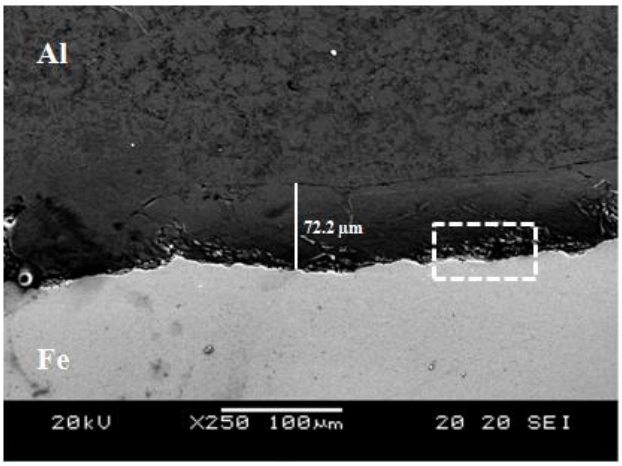

Figure 102. SEM micrographs of the reaction zone between aluminized steel and Al, Fs = 70 %.

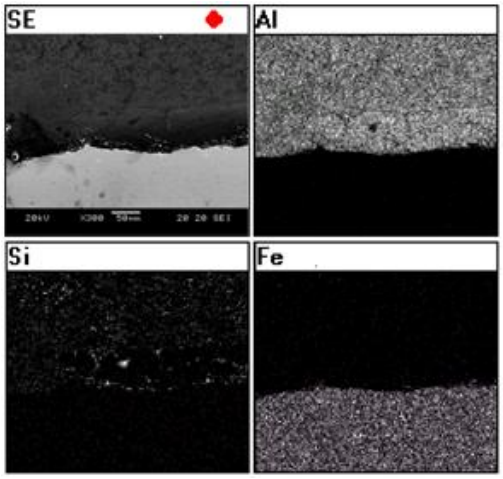

Figure 103. EDS analysis of the reaction zone between aluminized steel and Al, Fs = 70 %.

In Figure 102 the presence of 3 different regions was observed: The two base metals and the interfacial layer. The developed reaction layer was continuous with an average layer thickness of 72.2 μm. Neither oxides nor defects were found at the interface.

Regarding to its morphology, it differs significantly respect to the layer obtained in other cases. The reaction layer presented a smooth transition towards Fe and Al with blocky and needle-shaped intermetallic compounds concentrated mostly nearby the steel side (marked with a dashed square). Moreover, the characteristic globular microstructure of the semisolid formed aluminum is visible on the top layer. Base aluminide layer presented a characteristic irregular morphology associated to $FeAl_3$ and Fe_2Al_5 intermetallic compounds.

EDS analysis revealed that the reaction layer consisted of an aluminum matrix with eutectic Si and small amounts of Fe. Nevertheless, Figure 103 did not reveal evidences of the intermetallic layer associated to these compounds. These results suggest that aluminide layer has been dissolved into the liquid phase of the aluminum and formed a thick intermetallic transition layer. On the other hand, high concentration of Si at the interface suggested that the layer consisted mainly by Fe-Al-Si intermetallic compounds which according to bibliography are probably Fe_2Al_2Si and $Fe_2Al_2Si_2$ [Springer 2011]. Additionally, the blocky and needle-shaped Al4.5FeSi intermetallic compounds were identified.

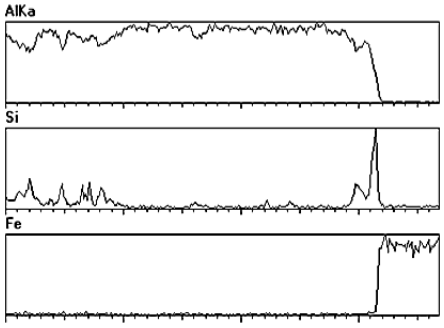

Figure 104. Linescan of the reaction zone between alumized steel and Al, Fs = 70 %.

Figure 104 proved that the sample was composed by 3 different regions. The right region describes the percentage mass distribution of aluminum, and the opposite side depicts the distribution of iron. In the interfacial area of the sample an overlapped signal between Al and Si that cover the widest area of the spectrum and a peak of Si overlapped with the Fe that confirmed the formation intermetallic compounds in the steel side interface.

6.2.3.2 T= 580 ºC or Fs= 50 %

The second micrograph (Figure 105) shows the results of the diffusion reaction obtained at T=580 ºC or Fs=50 %.

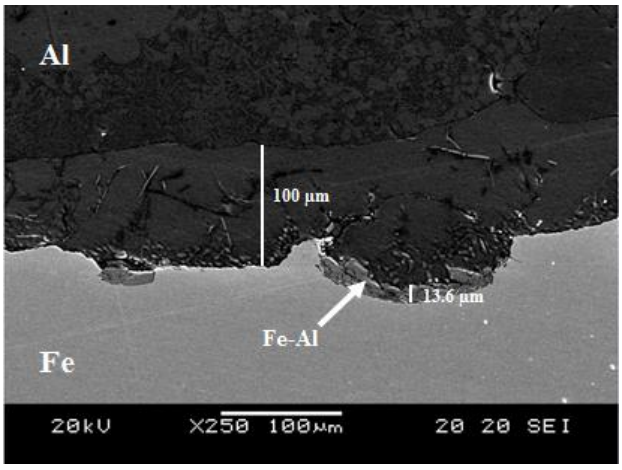

Figure 105. SEM micrographs of the reaction zone between aluminized steel and Al, Fs = 50 %.

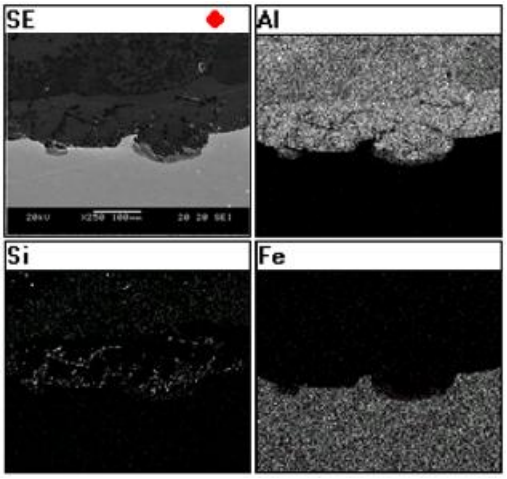

Figure 106. EDS analysis of the reaction zone between aluminized steel and Al, Fs = 50 %.

From the reaction between aluminized steel and aluminum at high forming temperature, 4 different layers were observed on the interface: the two base metals at the top and the bottom respectively and two reaction layers at the interface. It can be seen that the top layer was continuous and with an average thickness of 100 μm approximately. Furthermore, an additional discontinuous layer adjacent to steel was observed with an average thickness of 13.6 μm. The appearance of the discontinuous layer as well as the higher thickness of the reaction layer is due to increased atom mobility associated to the higher forming temperature and its higher reactivity. Cracks neither oxides were found in the reaction layers.

Regarding to its morphology, it can be seen that the developed reaction layer does not differ significantly respect to the layer obtained at lower temperature (Figure 102) except for the discontinuous layer adjacent to steel. The reaction layer presented a smooth transition towards Fe and followed by a thick reaction layer with plenty of blocky and needle-shaped intermetallic compounds and a smooth transition towards Al. Moreover, the characteristic globular microstructure of the semisolid formed aluminum is visible on the top layer accompanied with some dendrites associated to the segregation of the AlSi eutectic phase.

EDS analysis revealed that the reaction layer consisted by Fe-Al-Si intermetallic compounds adjacent to steel (probably $FeAl_3$, Fe_2Al_5, Fe_2Al_2Si and $Fe_2Al_2Si_2$ [Springer 2011]) followed by another reaction layer consisting of an aluminum matrix with eutectic Si and small amounts of Fe. Additionally, high concentration of Si was observed in the interfacial area attributed to the microsegregation of silicon in the aluminum alloy. Due to this high concentration of Si plenty of blocky and needle-shaped Al4.5FeSi intermetallic compounds were formed.

In order to get further information of the interface a linescan analysis was performed on the samples. Figure 107 presented the result of the linescan for Al, Fe and Si.

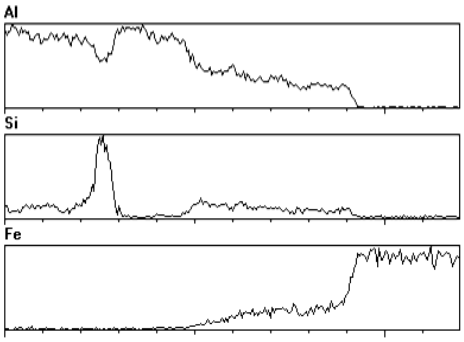

Figure 107. Linescan of the reaction zone between alumized steel and Al, Fs = 50 %.

The results obtained in Figure 107 proved that the sample was composed by 4 different regions. The right region describes the percentage mass distribution of aluminum, and the opposite side depicts the distribution of iron. In the interfacial area of the sample an overlapped signal between Al, Si and Fe that confirmed the formation of congregation compounds of these three different metals.

6.2.3.3 Heat treated sample

In the following image (Figure 108) the micrograph obtained after T6 heat treatment were displayed:

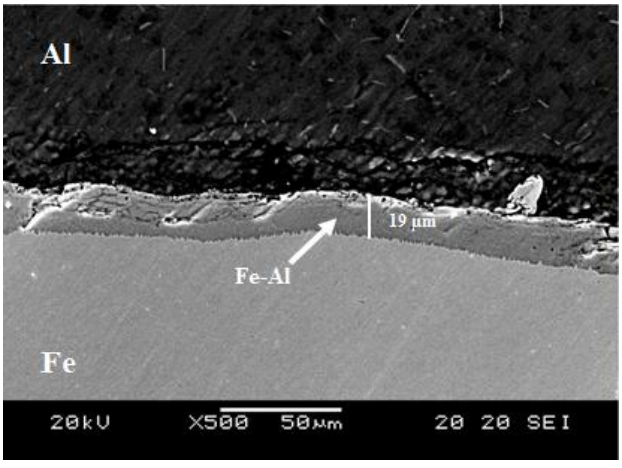

Figure 108. SEM micrographs of the reaction zone between aluminized steel and Al after T6 treatment.

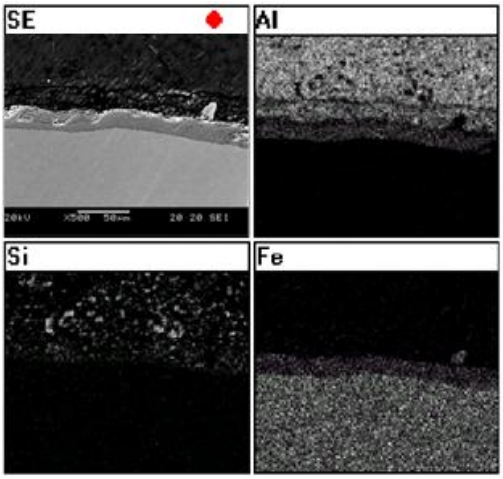

Figure 109. EDS analysis of the reaction zone between aluminized steel and Al after T6 treatment.

The results of Figure 108 revealed the existence of 3 different layers on the interface: the two base metals and the interfacial reaction layer. The developed reaction layer was continuous with an average layer thickness of 19 μm along the base line. The achieved layer was free of cracks and oxides.

Regarding to its morphology, the reaction layer of Figure 108 exhibited the well-known serrated interface adjacent to steel. The interface between the reaction zone and the former liquid Al is also irregular, but on a much finer scale. Such protrusions as are observed in Figure 47 and Figure 98 for the interdiffusion between steel and semisolid Al. The growth mechanism is the same explained in section 6.2.2 with the difference that already existed the contact between the aluminum and aluminum (from the coating) which facilitated the wettability and diffusion among metals.

EDS analysis were carried out in order to determine the phenomena occurred at the interface during the forming process. Results confirmed the formation of intermetallic compound by the superimposed signals of Fe-Al-Si that formed intermetallic compounds. Furthermore, high concentration of Si could be observed in the interfacial area due to the microsegregation of silicon in the aluminum alloy.

On the other hand, Figure 110 shows the linescan analysis performed on the sample:

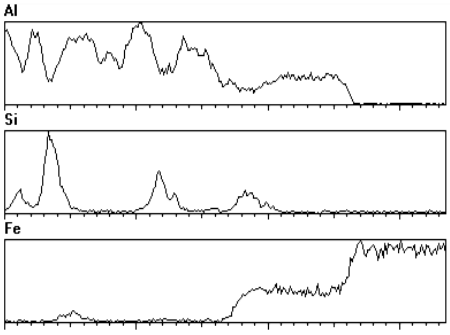

Figure 110. Linescan of the reaction zone between aluminized steel and Al after T6 treatment.

In the investigated material combination, EDS analysis and linescan verify the existence of 3 different layers. Starting from the right side, the signal of Al-Si corresponding to the aluminum and an overlapped signal between Al, Si and Fe corresponding to aluminum-steel intermetallic layer could be observed. The left side region is mainly composed by steel.

6.3 Conclusions

The experiments of section 6.2 tracked the evolution of the reaction zones formed during interdiffusion in the range of 565 ºC to 580 ºC between steel with different surface treatments and AlSiMg aluminum alloys. Investigations were performed under conditions where the steel was solid and the Al alloys were in semisolid state given by a temperature within a two-phase field “mushy zone”. Obtained surfaces have been analyzed by means of SEM/EDS. From the obtained results the following conclusions can be drawn:

Using this type of thixojoining process, there is no need for force or complex equipment. Based on the results of the experiments conducted in this study, the use of this thixojoining technique can create a fine interfacial diffusion along the bonding boundary which properties (thickness, composition and morphology) are dependent on the temperature, the reaction time and the chemical nature of the substrates (the coating and the base material itself). Nevertheless, in the presence of an interfacial oxide layer the diffusion of steel into aluminum was inhibited. Regardless of the forming temperature and pressure used, the oxide layer behaved as a physical barrier impeding the initial contact between metal surfaces and thus preventing the chemical interaction to form an intermetallic phase seam.

Temperature: Increasing the temperature, the proportion of liquid phase is increased. The diffusion ability of liquid phase is much bigger than that of solid phase at the same temperature and. and thus the ability of atomic diffusion at the interface is influenced by solid fraction of aluminum alloy thus the reaction kinetics it is favored and therefore the thickness and growth of the intermetallic layer is favored.

Chemical nature of the materials: one of the keys to achieve the metallurgical joint is the superficial state of the base materials. According to the results obtained, chemical bonding is only achieved in cases where oxide protective coatings were used. Furthermore the combination of materials with different chemical composition resulted in the formation of diverse Fe_xAl_y intermetallic compounds.

Morphology: Different reaction layer morphologies are found that is related, with the nature of the intermetallic compound. As for the interfacial structure, both metals exhibit different reaction and diffusion abilities between solidus and liquidus whereby the base metal is connected to the insert metal along the bonding boundary to achieve what appears to be a good joining at the interfaces of both metals. The liquid aluminum atom has higher energy, its spread reaction ability is bigger and the diffusion zone is thicker. The solid aluminum atom has lower energy, its spread reaction ability is smaller and the diffusion zone is narrower resulting in an uneven layer along the section. Finally a summary of the results is briefly shown in Table 14:

Table 14. Summary of all results obtained in the characterization of steel-aluminum joints.

F_S (%)	**Steel surface**	**Interfacial layer**	**Metallurgical joint**
70	Raw steel	Iron oxide layer	No bonding due to the interfacial oxide layer
50	Raw steel	Iron oxide layer	No bonding due to the interfacial oxide layer
50+T6	Raw steel	Iron oxide layer	No bonding due to the interfacial oxide layer
70	Zn coated steel	Fe-Zn/Al-Si-Zn IMC layers	Indirect bonding through an intermediate metal
50	Zn coated steel	Fe-Zn/Al-Si-Zn IMC layers	Indirect bonding through an intermediate metal
50+T6	Zn coated steel	Fe-Al IMC layer	Bonding by Fe-Al IMC layer
70	Hot dip aluminized steel	Al-Si with Al-Si-Fe IMC layer	No bonding
50	Hot dip aluminized steel	Al-Si/Fe-Al IMC layers	Indirect bonding through an intermediate metal
50+T6	Hot dip aluminized steel	Fe-Al IMC layer	No bonding breakage of the bonding during the T6 treatment

CHAPTER 7

CLOSURE

7.1 Concluding remarks

The current dissertation focuses on design and production of an automotive hybrid left front cradle mount middle. A semi-industrial thixoforming cell has been developed to study the most important aspects of semisolid forging of aluminum on steel. Influence of the main processing parameters such as, solid fraction, mold temperature, compaction time and punch speed are studied. In order to determine the optimum process parameters a thorough mechanical and metallographic analysis of the manufactured components is carried out.

In the first part of this thesis it has been described the manufacturing process of hybrid structures that covers design and modeling the LCM and process parameters. Following conclusions are obtained:

- Surface of raw steel tubes is covered with iron oxides. In order to protect the clean surface from reoxidation protective coatings must be applied.
- An intermetallic layer was developed at the interface between the substrate and the coating layer. The compounds formed are related with the chemical nature of the coating and the thickness with the coating method.
- In Zn coated steel a continuous layer of 40 μm is formed on the surface of the steel. The layer consisted on a 10 μm intermetallic layer of Fe-Zn near the steel interface followed by a 30 μm Zn layer.
- In aluminized steel a continuous intermetallic reaction layer is formed at the interface with an average thickness of 21 μm. The tongue-like morphology found in the iron side suggests that the most probable intermetallic phases that form the layer are $FeAl_3$ and Fe_2Al_5.

In chapter 4, geometry of the component is optimized on the base of the mechanical properties coming from the end use by means of FEM structural analysis whereas the process parameters are defined with the help of thermomechanical simulation. Conclusions extracted are:

- Calculated rigidity of the structure in vertical stiffness test is at least 10.37 kN/mm (>5.5 KN/mm). Furthermore, the resulting distribution of Von Mises stress in permanent deformation test does not exceed the established yield strength so the LCM practically is working within the elastic region.

- To achieve a complete filling of the die the process time has to be below 3.8 seconds other way the aluminum solidifies before forming a joint. Complete solidification of fronts occurs at process time 8.4 seconds.
- When the forming velocity was insufficient, difficulties in the filling process arise; in contrast, increasing the punch speed the process time is reduced and complete filling is achieved.

With the process defined, a set of experiments were carried out. The main conclusions obtained from these works are:

- The reheating cycle of billets is highly reproducible for each alloy. However, measured temperatures evidence a small radial gradient between the surface and the center of 4 ºC in both alloys. In contrary, the axial temperature gradient is almost negligible.
- It is possible to manufacture steel-aluminum hybrid structures in one step through the thixo lateral forging process.
- The comparison of the simulation with the step-shooting experiments shows a good match in reference to the die filling validating the implemented model.

Chapter 5 is devoted to analyze the properties of the semisolid forged left front cradle mount middle. Regarding to a forming process itself, they have been studied the influence of the main parameters which are solid fraction, mold temperature, forming speed, forming load and compaction time in the final properties of the component. Conclusions obtained from the metallographic and mechanical characterization are:

- Sound components are obtained since no discontinuities are appreciated in either the body or the joining zone.
- Pressure exerted in the joining zone generated a severe plastic deformation on the steel insert during the compaction of the material causing an underfilling of the die due to the lack of material.
- Using steel bumpers inside the tube allowed controlling the plastic deformation generated in the tube and therefore the aluminum necessary to fill the gap is always the same.

- Deformation undergone on the steel tube; generates an aluminum accumulation in the cavity. The accumulated material helps to fix the aluminum body in a specific position, avoiding displacements and rotations in service.

On the other hand, it is observed that the forming conditions have a marked effect on the final properties of the component since after the heat treatment, blisters are generated in the surface of the parts due to segregation. The results revealed that high forming speed reduces the segregation. Same way, decreasing the temperature and therefore the solid fraction also reduces this negative effect making blisters disappear.

Mechanical properties obtained are promising, although the produced components have not been able to withstand the number of cycles considered for the complete mechanical validation of the structure. The premature failure is attributed to localized stress concentration or combination of bending stress and moment of inertia of the recessed section. In order to get the desired mechanical behavior under fatigue, the geometry must be redesigned and optimized. It has considered reinforcing the weaker sections component by increasing the thickness of the wall of the aluminum body at the expense of a weight increase.

In chapter 6 the influence of the forming and microstructural parameters which govern the formation and growth of the intermetallic reaction layer were studied. The main conclusions obtained from these analyses are:

- The formation of the intermetallic compounds has high dependence on the temperature and the chemical composition of the joining metals.
- Increasing the temperature, the proportion of liquid phase is increased which promotes the reaction kinetics and therefore the growth of the intermetallic layer is faster.
- Superficial state of the base materials is one of the keys to achieve the metallurgical joint. Chemical bonding is only achieved in cases where oxide protective coating were used as the oxide films restricted metallic contact inhibiting the diffusion of elements to form a chemical joint.
- Different reaction layer morphologies are found that is related with the nature of the intermetallic compounds formed.

Results obtained along the work have demonstrated that it is possible to manufacture near net shape components with promising mechanical properties in a single step. Moreover, this process

allowed joining dissimilar materials in semisolid state at lower temperatures than traditional welding methods, causing a decrease thickness in the reaction intermetallic layer.

Compared to other traditional solutions the fabrication cost of hybrid sub-frames will be reduced by reduction of assembly cost by part integration. Furthermore, the elimination/reduction of assembly joints improves the overall performance of the sub-frame. In addition, the possibility to assemble the hybrid sub-frame separately from the rest of the vehicle facilitates its integration into a steel or mixed material car body.

7.2 Future work

Even if this dissertation demonstrates the viability of semisolid forging of steel, there is almost everything to do yet in the way for industrialization.

Firstly from the material point of view, the semisolid forming of A356, A357 aluminum alloys improves the mechanical properties compared to conventional methods, however, for some specific applications which requires higher strengths, these may not be sufficient. In these cases, nanoparticle reinforced aluminum composites or forging alloys such as the 6XXX and 7XXX series are the considered alternatives.

Continuing with the material but from the insert point of view, it is of interest the use of other high performance materials such as, stainless steel or nickel base super alloys. These material combinations open up unlimited possibilities for modern material science and development in order to produce structures with tailored properties dependent on the application. However, galvanic corrosion is a concern when two different metals of different nature are brought together. The corrosion evaluation as well as the application of new coatings as may be considered.

Regarding the process itself, it is in the pre-industrial phase and ready to take the definitive step towards the desired industrialization. The possibility to heat so different billet dimensions leads to an unoptimized coil geometry and therefore to radial and axial temperature gradients that can be minimized with a proper coil design. An optimized heating device leads to a substantial reduction in the process time as an approach to a pilot plant scale. Furthermore, components must be redesigned in order to obtain all the process advantages and the forming to fight with industrialization and productivity issues. Finally, it is necessary to keep in mind that to ensure a productivity comparable to other forming processes, billets must be heated on a carrousel. In

any case, these are quite affordable issues for the industry to cope with, due to their extensive experience in this area.

Regarding the fundamental role of intermetallic phases in semisolid joining processes understanding of the fundamental reactions governing the phase formation and evolution at the interface between new Al alloys and other materials has to be done.

In any case, at laboratory scale, it would be interesting to be able to validate some more components coming from other sectors interested in the advantages that semi solid forging presents.

CHAPTER 8

REFERENCES

ABAQUS. "Version 6.8 Documentation". *Simulia*-Dassault Systèmes, 2008.

Achar, G.; Ruge, J. and Sundaresan, S. "Joining aluminium to steel, with particular reference to welding". *Aluminium-Verlag*, 1981.

Aguado, E.; Baquedano, A.; Uribe, U.; et al. "Comparative Study of Different Interfaces of Steel Inserts in Aluminium Castings". *Next 6th Int. LMT Conference*, vol. 765, p. 711-715, 2013.

Agudo, L.; Weber, S.; Pinto, H.; et al. "Study of microstructure and residual stresses in dissimilar Al/steels welds produced by cold metal transfer". *Materials Science Forum*, vol. 571, p. 347-353, 2008.

Aguilar-Martínez, J. and Hernández, M. "La infiltración no asistida como una técnica de procesamiento de compósitos Al-Mg-Si/SiC". *Revista Mexicana De Física*, vol. 54, p. 336-340, 2008.

Azpilgain, Z. "Desarrollo y caracterización de aleaciones de aluminio e implementación de un sistema de forja para el conformado en estado semisólido". Ph D Thesis, Mondragon Unibertsitatea, 2006.

Azpilgain, Z.; Ortubay, R.; Blanco, A.; et al. "Servo-mechanical press: a new press concept for semisolid forging". *Solid State Phenomena*, vol. 141, p. 261-266, 2008.

Bach, F.W.; Beniyash, A.; Lau, K.; et al. "Joining of steel-aluminium hybrid structures with electron beam on atmosphere". *Advanced Materials Research*, vol. 6, p. 143-150, 2005.

Bandivadekar, A. "On the road in 2035: Reducing transportation's petroleum consumption and GHG emissions". *Massachusetts Institute of Technology*, 2008.

Bariani, P.; Dal Negro, T. and Bruschi, S. “Testing and modelling of material response to deformation in bulk metal forming”. *CIRP Annals-Manufacturing Technology*, vol. 53, p. 573-595 , 2004

Barreiro, P., Schulze, V. and Löhe, D. “Influence of process parameters on structure and mechanical properties of joints produced by electromagnetic forming and friction stir welding”. *Advanced Materials Research*, vol. 43, p. 47-56, 2008.

Behrens, B.A. and Kosch, K.G. “Development of the heating and forming strategy in compound forging of hybrid steel-aluminum parts”. *Materialwissenschaft und Werkstofftechnik*, vol. 42, p. 973-978, 2011.

Behrens, B.A. and Kosch, K.G. “Influence of different alloying elements on the intermetallic phase seam thickness of compound forged steel-aluminum parts”. *Production Engineering*, vol. 5, p. 517-522, 2011.

Behrens, B.A. and Kosch, K.G. “Production of strong steel-aluminum composites by formation of intermetallic phases in compound forging”. *Steel Research International*, vol. 82, p. 1261-1265, 2011.

Bigham, J.; Fitzpatrick, R.W., Schulze, D.; et al. “Iron oxides”. *Soil Science Society of America Inc*., 2002.

Bouayad, A.; Gerometta, C.; Belkebir, A.A.; et al. “Kinetic interactions between solid iron and molten aluminium”. *Materials Science and Engineering: A*, vol. 363, p. 53-61, 2003.

Candan, E.; Atkinson, H.V.; Turen, Y.; et al. “Wettability of aluminum–magnesium alloys on silicon carbide substrates”. *Journal of the American Ceramic Society*, vol. 97, p. 867-874, 2011.

Chen, Y.C.; Komazaki, T.; Kim, Y.G.; et al. “Friction stir lap joining of ac4c cast aluminum alloy and zinc-coated steel”. *Materials Science Forum*, vol. 580, p. 371-374, 2008.

Cheng, W. and Wang, C. “Microstructural evolution of intermetallic layer in hot-dipped aluminide mild steel with silicon addition”. *Surface and Coatings Technology*, vol. 205, p. 4726-4731, 2011.

Chengand Chaur-Jeng, W.J. “Study of microstructure and phase evolution of hot-dipped aluminide mild steel during high-temperature diffusion using electron backscatter diffraction”. *Applied Surface Science*, 2010.

Choi, C.Y.; Kim, D.C.; Nam, D.G.; et al. “A hybrid joining technology for aluminum/zinc coated steels in vehicles”. *Journal of Materials Science and Technology*, vol. 26, p. 858-864, 2010.

Chrysanthou, A. and Sun, X. “Self-piercing riveting: Properties, processes and applications”. *Woodhead Publishing*, 2014.

Chun, C.K.; Kim, H.J.; Cho, H.J.; et al. “Mechanical and microstructural properties of dissimilar friction spot welded aluminum alloy”, *Materials Science Forum*, vol. 580, p. 389-392, 2008.

Davis, S.J.; Caldeira, K. and Matthews, H.D. “Future CO_2 Emissions and Climate Change from Existing Energy Infrastructure. *Science (New York)*, vol. 329, p. 1330-1333, 2010.

De Figueredo, A. “Science and technology of semi-solid metal processing”. *North American Die Casting Association*, 2001.

Dybkov, V.I. “Reaction diffusion and solid state chemical kinetics”. *Transport Technologies Publications*, 2010.

Ebnesajjad, S. and Ebnesajjad, C. “Surface treatment of materials for adhesive bonding”. *William Andrew*, 2013.

El-Sayed, M.E. and Stawiarski, T. “Multi-Attribute Balancing Process for Automotive Components”. *Transportation Systems; Safety Engineering, Risk Analysis and Reliability Methods*, vol. Volume 9, p. 343-349, 2011.

European Aluminium Association. “The Aluminium Automotive Manual”, 2013.

Eustathopoulos, N.; Nicholas, M.G. and Drevet, B. “Wettability at high temperatures”. *A Pergamon Title*, 1999.

Fan, J.; Thomy, C. and Vollertsen, F. “Effect of thermal cycle on the formation of intermetallic compounds in laser welding of aluminum-steel overlap joints”. *Physics Procedia*, vol. 12, p. 134-141, 2011.

Fan, Z. “Semisolid metal processing”. *International Materials Reviews*, vol. 47, p. 49-85, 2002.

Flemings, M.C. “Behavior of metal alloys in the semisolid state”. *Metallurgical Transactions B*, vol. 22, p. 269-293, 1991.

Gean, A., Westgate, S., Kucza, J. and Ehrstrom, J. “Static and fatigue behavior of spot-welded 5182-0 aluminum alloy sheet”. *Welding Journal*, vol. 78. pp. 80, 1999.

Ghassemieh, E. “Materials in automotive application, state of the art and prospects”, 2011.

Gräf, T.; Jürgens, R.; Gies, J.; et al. Controlled inductive heating for thixotropic materials into the semisolid state”. *International Conference on “Semisolid Processing of Alloys and Composites”*, p. 667-673, 2000.

Harada, Y., Miura, Y. and Takahashi, K. “Formation of Fe-Al intermetallic compound film on carbon steel by shot peening and heat treatment”. *Advanced Materials Research*, vol. 409. p. 802-807, 2012.

Hayat, F. “Comparing properties of adhesive bonding, resistance spot welding, and adhesive weld bonding of coated and uncoated DP 600 steel”. *Journal of Iron and Steel Research*, vol. 18, p. 70-78, 2011.

Hirt, G. and Kopp, R. “Thixoforming: Semi-solid metal processing”. *Wiley-vch*, 2009.

Hks, I. I. ABAQUS ed., *Simulia*-Dassault Systèmes, 2001.

Hu, X.G.; Zhang, F.; He, Y.F.; et al. “Experimental study and numerical simulation on the blistering defect during thixocasting. Experimental study and numerical simulation on the blistering defect during thixocasting”. *Transport Technologies Publications*, vol. 217, p. 144-150, 2015.

Jeswiet, J.; Geiger, M.; Engel, U.; Kleiner, M. et al. “Metal forming progress since 2000*”. CIRP Journal of Manufacturing Science and Technology*, vol. 1, p. 2-17, 2008.

Joo, S.M.; Kim, Y.P.; Bang, H.S.; et al. “Welding of steel and aluminum by Nd-YAG laser. *Key Engineering Materials*, vol. 270, p. 2389, 2004.

Kainer, K.U. “Basics of metal matrix composites”. *Wiley Online Library*, 2006.

Kapranos, P. “Thixoforming wrought al alloys”. *Diecasting & Technology*, p. 44-51, 2004.

Kirkwood, D. “Semisolid metal processing”. *International Materials Reviews*, vol. 39, p. 173-189, 1994.

Kleiner, M., Geiger, M. and Klaus, A. “Manufacturing of lightweight components by metal forming”. *CIRP Annals-Manufacturing Technology*, vol. 52, p. 521-542, 2003.

Kobayashi, S. and Yakou, T. “Control of intermetallic compound layers at interface between steel and aluminum by diffusion treatment”. *Materials Science and Engineering: A*, vol. 338, p. 44-53, 2002.

Kumai, S., Watanabe, M. and Feng, K.; et al. “Microstructure and joint strength of similar-and dissimilar lap joints fabricated by several advanced solid-state welding methods”. *Materials Science Forum*, vol. 654, p. 596-601, 2010.

Kuroda, S., Saida, K. and Nishimoto, K. “Microstructure and properties of directly bonded joint of A6061 aluminum alloy to SUS316 stainless steel-study on diffusion bonding of aluminum alloy to stainless steel (Report 1)”. *Quarterly Journal of the Japan Welding Society*, p. 17-13, 1999.

Laurent, V.; Chatain, D. and Eustathopoulos, N. “Wettability of SiC by aluminium and Al-Si alloys”. *Journal of Materials Science*, vol. 22, p. 244-250, 1987.

Lee, C.; Lee, J.; Ryu, H.; et al. “Design of Hole-Clinching Process for joining of dissimilar materials Al6061-T4 alloy with DP780 steel, hot-pressed 22MnB5 steel, and carbon fiber reinforced plastic”. *Journal of Materials Processing Technology*, vol. 214, p. 2169-2178, 2014.

Lee, K. and Kumai, S. “Characterization of intermetallic compound layer formed at the weld interface of the defocused laser welded low carbon steel/6111 aluminum alloy lap joint”. *Materials Transactions*, vol. 47, p. 1178-1185, 2006.

Lin, S.; Song, J.; Ma, G. and Yang, C. “Dissimilar metals tig welding-brazing of aluminum alloy to galvanized steel”. *Frontiers of Materials Science in China*, vol. 3, p. 78-83, 2009.

Liu, G.; Muolo, M.; Valenza, F.; et al. A. “Survey on wetting of SiC by molten metals”. *Ceramics International*, vol. 36, p. 1177-1188, 2010.

Liu, H.W.; Guo, C.; Cheng, Y.; et al. “Interfacial strength and structure of stainless-steel semi-solid aluminum alloy clad metal”. *Materials Letters*, vol. 60, p. 180-184, 2006.

Lozares, J. “Semisolid forging of steel components for automotive industry”. Ph D Thesis, Mondragon Unibertsitatea, 2014.

Lu, Z.; Pengfei, H.; Wenning, G.; et al. “Arc welding method for bonding steel with aluminum”. *Frontiers of Mechanical Engineering in China*, vol. 4, p. 134-146, 2009.

Malen, D.E. and Reddy, K. “Preliminary vehicle mass estimation using empirical subsystem influence coefficients”. Report Prepared for the FGPC-Mass Compounding Project Team, Auto/Steel Partnership, 2007.

Marciuš, M.; Ristić, M.; Ivanda, M.; et al. “Formation of iron oxides by surface oxidation of iron plate”. *Croatica Chemica Acta*, vol. 85, p. 117-124, 2012.

Mendez, P.; Rice, C. and Brown, S. “Joining using semisolid metals”. Welding Journal, vol. 81, p. 181-S, 2002.

Mendez, P.F. “Joining metals using semisolid slurries”. Master Degree, Massachusetts Institute of Technology, 1995.

Moraes, E.; Graça, M. and Cairo, C.; et al. “Study of aluminium alloys wettability on SiC perform”. *Congresso Brasileiro de Engenharia e Ciência dos Materiais*, vol. 15, p. 4217-4224, 2006.

Murakami, K.; Nishida, N.; Osamura, K.; et al. “Aluminization of high purity iron and stainless steel by powder liquid coating”. *Acta Materialia*, vol. 52, p. 2173-2184, 2004.

Osakada, K.; Mori, K.; Altan, T.; et al. “Mechanical servo press technology for metal forming”. *CIRP Annals-Manufacturing Technology*, vol. 60, p. 651-672, 2011.

Ouyang, Q.B.; Zhou, W.M.; Zhang, G.D.; et al. “Wettability and its improvement at Al/SiC interfaces”. *Key Engineering Materials*, vol. 351, p. 52-57, 2007.

Püttgen, W.; Bleck, W.; Hirt, G.; et al. “Thixoforming of steels- a status report”. *Advanced Engineering Materials*, vol. 9, p. 231-245, 2007.

Qiu, R., Satonaka, S. and Iwamoto, C. “Effect of interfacial reaction layer continuity on the tensile strength of resistance spot welded joints between aluminum alloy and steels”. *Materials & Design*, vol. 30, p. 3686-3689, 2009b.

Qiu, R.; Iwamoto, C. and Satonaka, S. “Interfacial microstructure and strength of steel/aluminum alloy joints welded by resistance spot welding with cover plate”. *Journal of Materials Processing Technology*, vol. 209, p 4186-4193, 2009a.

Qiu, R.; Iwamoto, C. and Satonaka, S. “The influence of reaction layer on the strength of aluminum/steel joint welded by resistance spot welding”. *Materials Characterization*, vol. 60, p. 156-159, 2009.

Qiu, R.; Shi, H.; Zhang, K.; et al. “Interfacial characterization of joint between mild steel and aluminum alloy welded by resistance spot welding”. *Materials Characterization*, vol. 61, p. 684-688, 2010.

Quaak, C.J. “Rheology of partially solidified aluminium alloys and composites”. Ph D Thesis, Delft University of Technology, 1996.

Quadrelli, R. and Peterson, S. “The energy–climate challenge: Recent trends in CO_2 emissions from fuel combustion”. *Energy Policy*, vol. 35, p. 5938-5952, 2007.

Rassili, A. and Atkinson, H.V. “A review on steel thixoforming. *Transactions of Nonferrous Metals Society of China*, vol. 20, p. s1048-s1054, 2010.

Rathod, M. and Kutsuna, M. “Joining of aluminum alloy 5052 and low-carbon steel by laser roll welding”. *Welding Journal-New York-*, vol. 83, p. 16, 2004.

Ryabov, V. “Welding of aluminium alloys to steels”. *Harwood Academic*, 1998.

Sahin, M. “Joining of stainless-steel and aluminium materials by friction welding”. The *International Journal of Advanced Manufacturing Technology*, vol. 41, p. 487-497, 2009.

Sajjadi, S.A. and Ezatpour, H. “Fabrication of A356 composite reinforced with micro and nano Al_2O_3 particles by a developed compocasting method and study of its properties”. *Journal of Alloys and Compounds*, vol. 511, p. 226-231, 2012.

Sajjadi, S.A. and Ezatpour, H. “Microstructure and mechanical properties of Al-Al_2O_3 micro and nanocomposites fabricated by stir casting”. *Materials Science and Engineering A*, vol. 528, p. 8765-8771, 2011.

Sanbao, L.; Jianlin, S.; Chunli, Y.; et al. “Experimental study on dissimilar tig welding-brazing of 5A06 aluminum alloy to SUS321 stainless steel”. *China Welding*, vol. 19, 2010.

Schäfer, R.; Pasquale, P. and Elsen, A. “Material hybrid joining of sheet metals by electromagnetic pulse technology”. *Key Engineering Materials*, vol. 473. p. 61-68, 2011.

Schonbohm, A.; Gasper, R. and Abel, D. “Inductive reheating of steel billets into the semi-solid state based on pyrometer measurements”. *SemiSolid Processing of Alloys and Composits*, p. 734-737, 2006.

Shahverdi, H.R.; Ghomashchi, M.R.; Shabestari, S.; et al. “Microstructural analysis of interfacial reaction between molten aluminium and solid iron”. *Journal of Materials Processing Technology*, vol. 124, p. 345-352, 2002.

Shi, H.X.; Qiu, R.F.; Tu, Y.M.; et al. “Study on the joining characteristics of diffusion welding lap joint with various temperatures between aluminum alloy and stainless steel”. *Advanced Materials Research*, vol. 291, p. 1003-1006, 2011.

Siegert, K.; Wolf, A. and Baur, J. “Thixoforging of aluminium and brass. Production engineering”. *Annals of the German Academic Society for Production Engineering*, vol. 2, p. 1, 2000.

Spencer, D.P.; Mehrabian, R.M. and Flemings, C. “Rheological behavior of Sn15-Pct-Pb in the crystallization range”. *Metallurgical and Materials Transactions A*, vol. 3, p. 1925-1932, 1972.

Springer, H.; Kostka, A.; Payton, E.J; et al. “On the formation and growth of intermetallic phases during interdiffusion between low-carbon steel and aluminum alloys”. *Acta Materialia*, vol. 59, p. 1586-1600, 2011.

Springer, H.J. “Fundamental research into the role of intermetallic phases in joining of aluminum alloys to steel”, Ph D Thesis, Fakultät für Maschinenbau der Ruhr-Universität Bochum, 2011.

Stodolsky, F.; Vyas, A. and Cuenca, R. “World car conference”, Riverside, CA (United States), 1995.

Sun, X. and Khaleel, M.A. “Resistance spot welding of aluminum alloy to steel with transition material-part II: Finite element analyses of nugget growth”. *Welding Journal*, vol. 83, p. 197, 2004a.

Sun, X.; Stephens, E.V.; Khaleel, M.A.; et al. “Resistance spot welding of aluminum alloy to steel with transition material-from process to performance-part I: Experimental study. *Welding Journal*, vol. 83, p188, 2004b.

Taban, E.; Gould, J.E. and Lippold, J.C. “Characterization of 6061-T6 aluminum alloy to AISI 1018 steel interfaces during joining and thermo-mechanical conditioning”. *Materials Science and Engineering: A*, vol. 527, p. 1704-1708, 2010.

Tanaka, Y. and Kajihara, M. “Kinetics of isothermal reactive diffusion between solid Fe and liquid Al”. *Journal of Materials Science*, vol. 45, p. 5676-5684, 2010.

Taniyama, A.; Arai, M.; Takayama, T.; et al. “In-situ observation of growth behavior of Fe-Zn intermetallic compounds at initial stage of galvannealing process”. *Materials Transactions*, vol. 45, p. 2326-2331, 2004.

Temizel, G. and Özenbas, M. “Intermetallic phase formation at Fe-Al film interfaces”. *Turkish Journal of Engineering and Environmental Science*, vol. 31. p. 71-78, 2007.

Thomy, C. and Vollertsen, F. “Laser-MIG hybrid welding of aluminum to steel-effect of process parameters on joint properties”. *Welding in the World*, vol. 56,pp. 124-132, 2012.

U.S. Department of Energy. Http://www.Fueleconomy.gov/feg/atv.Shtml, 2015.

Uggowitzer, P.J., Wabusseg, H. and Kaufmann, H. “New rheocasting-process concept and materials”. Advanced Engineering Materials, vol. 3, p. 65-78, 2001.

Vranakova, R.; Fussel, U.; Zschetzsche, J.; et al. “Arc welding of joints between zinc-coated steel and aluminium”. *Welding in the World*, vol. 49, p. 105, 2005.

Wang, N.; Yamaguchi, T. and Nishio, K. “Effects of welding time and alloy elements on mechanical properties of aluminum/SPCC joint using resistance spot welding”. *Advanced Materials Research*, vol. 602, p. 2123-2129, 2013.

Wang, N.; Yamaguchi, T. and Nishio, K. “Interface microstructure and weld strength of steel/aluminum alloy joints by resistance spot welding”. *Applied Mechanics and Materials*, vol. 117. p. 1895-1899, 2012.

Web, T.; Fuganti, A. and Cupitò, G. “Thixoforming of aluminium alloy for weight saving of a suspension steering knuckle”. *Metallurgical Science and Technology*, vol. 18, p. 19-23 1999.

Zhang, F.; Yang, X.; Wang, H.; et al. “Durability of adhesively bonded single lap-shear joints in accelerated hygrothermal exposure for automotive applications”. *International Journal of Adhesion and Adhesives*, vol. 44, p. 130-137, 2013.

Zhang, P.; Yunhui, D.; Shuming, X.; et al. “Influence of diffusion time on steel-aluminum solid to liquid bonding interfacial structure”. *Journal of Material Science Technologies*, vol. 18, p. 468-470, 2009.